Award: N00014-00-1-0519

MEASUREMENT OF ANISOTROPIC ELASTIC CONSTITUTIVE PROPERTIES AT HIGH TEMPERATURES

2003 Final Report

01-APR-2000 through 30-DEC-2003

Michael L. Peterson, Ph.D.

University of Maine
5717 Boardman Hall
Orono ME 04469-5711

Report Documentation Page

Form Approved
OMB No. 0704-0188

1. REPORT DATE	2. REPORT TYPE	3. DATES COVERED
30 DEC 2003	**N/A**	**-**

4. TITLE AND SUBTITLE	5a. CONTRACT NUMBER
Measurement of Anisotropic Elastic Constitutive Properties at High Temperatures	5b. GRANT NUMBER
	5c. PROGRAM ELEMENT NUMBER
6. AUTHOR(S)	5d. PROJECT NUMBER
	5e. TASK NUMBER
	5f. WORK UNIT NUMBER
7. PERFORMING ORGANIZATION NAME(S) AND ADDRESS(ES) **University of Maine 5717 Corbett Hall Orono ME 04469-5717**	8. PERFORMING ORGANIZATION REPORT NUMBER
9. SPONSORING/MONITORING AGENCY NAME(S) AND ADDRESS(ES)	10. SPONSOR/MONITOR'S ACRONYM(S)
	11. SPONSOR/MONITOR'S REPORT NUMBER(S)

12. DISTRIBUTION/AVAILABILITY STATEMENT
Approved for public release, distribution unlimited

13. SUPPLEMENTARY NOTES
The original document contains color images.

14. ABSTRACT

15. SUBJECT TERMS

16. SECURITY CLASSIFICATION OF:			17. LIMITATION OF ABSTRACT	18. NUMBER OF PAGES	19a. NAME OF RESPONSIBLE PERSON
a. REPORT	b. ABSTRACT	c. THIS PAGE			
unclassified	**unclassified**	**unclassified**	**UU**	**115**	

This page intentionally left blank

Table of Contents

This page intentionally left blank

1 Motivation and Objectives

1.1 Motivation

Knowledge of material properties is one of the key elements in design of advanced aerospace systems. However the measurement of material properties is a difficult task since many, if not most, materials used in aerospace applications are anisotropic. Composite or single crystal materials are used in rockets, engines and vehicle reentry systems. In addition these materials must operate under extreme temperatures and in corrosive or oxidative environments. The measurement of a complete set of material properties at high temperatures is thus necessary for design of systems that must reliably operate under extreme conditions. Knowledge of the complete anisotropic properties of the material allow structural optimization to be performed that can significantly reduce the vehicle mass and improve system reliability.

A particular need is the accurate measurement of elastic and visco-elastic properties of composites at high temperatures in order to design the components used in advanced missile defense systems. Technological advancements such as those proposed in the Atmospheric Interceptor Technology (AIT) program require that the materials in the components operate on high-maneuvering targets in a severe aero-thermal environment. This requirement places a high demand on materials that operate at temperatures up to 3000°C. The length of time that the component must operate reliably may be limited, but reliability is critical. Thus not only are material properties at temperature required, but the effects of time at temperature and dynamic heating effects must be considered. These time dependent characteristics and associated material degradation effects are the focus application for the new sensor that has been developed. Test methods have been demonstrated using new experimental methods that make it possible to measure elastic constants and symmetry planes of materials. The changes in these properties due to changes in temperature and oxidation have also been investigated. Experimental results have been obtained for one high temperature composite material, reinforced carbon-carbon. However, the techniques are applicable to a wide range of anisotropic materials.

While the primary focus of this effort has been development of techniques that are applicable to inspection and monitoring of other high temperature anisotropic materials, the specific results of the work on reinforced carbon-carbon has been the subject of some publicity in the science press [1]. The National Aeronautic and Space Administration Space Transportation System use carbon material similar to that used in this research for the wing leading edges and the nose of the Space Shuttle

Orbiter. The reinforced carbon-carbon components used for the leading edge of the shuttle are the cause of the loss of the orbiter Columbia in 2003 [2].

> The physical cause of the loss of Columbia and its crew was a breach in the thermal protection system on the leading edge of the left wing. The breach was initiated by a piece of insulating foam that separated from the left bipod ramp of the External Tank and struck the wing in the vicinity of the Reinforced Carbon-Carbon panel 8 at 81.9 seconds after launch.

Carbon is a particular design challenge since the material oxidizes quickly at relatively modest temperatures, so oxidation resistant coatings must be used to protect the material. A breech in the coating can reduce the life expectancy of the material dramatically when exposed to an oxidizing environment at temperatures as low as 600°C. More importantly, the fracture toughness of the material can be dramatically influenced by even small losses of the matrix material during these oxidation processes. A small crack in the oxidation protective coating can lead to highly localized and accelerated corrosion of the underlying material. The corrosion of the carbon panels on the shuttle may have been accelerated by contamination by zinc-oxide paint that would lead to a hole in the oxidation resistant coating. The oxidation of the orbiter panels is the same degradation process that has been investigated in this project. The primary motivation has been to enhance the understanding of residual life in carbon-carbon composites. More importantly, these techniques have the potential to allow reinforced carbon-carbon to be inspected in-situ to determine the residual life and even the effect of oxidation on the fracture toughness of the material. Reinforced carbon-carbon is important in spite of its disadvantages, because in many cases it is the only practical material for high temperature applications.

While the application to carbon-carbon is of particular current interest, the new sensor that has been developed is applicable to a number of ultrasonic NDE and monitoring configurations. Several new high temperature materials have been developed that show great promise [3]. Most of these materials have significant anisotropy and may be large single crystals. Since the materials are still under development, they are quite expensive. New materials also require extensive certification prior to use in aerospace applications. This new high temperature sensor and the associated experimental techniques can reduce the time and expense required for flight certification. No other technique is currently available for obtaining full elastic properties of materials at elevated temperatures. The shear modulus is particularly difficult to obtain for materials at elevated temperatures. For monitoring of material degradation, it is particularly helpful to be able to recover the entire material tensor to determine if degradation has occurred along particular diffusion paths. This preferential diffusion

may occur due to variation in density that will allow easier diffusion of oxygen. These experimental techniques also make it possible to obtain damping properties during oxidation or with variation in temperature. Damping measurements are important since damping has been proposed as a key measurand for the detection of the changes in material properties in high temperature materials and ceramics [4].

The work from this project particularly focused on composite materials with more general anisotropy than the more common orthotropic material assumption. This complex anisotropy, or lower symmetry, is possible in reinforced carbon-carbon since it is formed from a three or four-dimensional fiber perform that is densified in a diffusion controlled process. Diffusion controlled processes used include both resin infusion and chemical vapor deposition. General anisotropy also presents opportunities for optimization of the structure. Structural design using composites should exploit the orientation of the material in order to produce a fully optimized structure. However, because the material lay-up is typically designed so that the primary loading is in the fiber direction, it is common in material testing to only test composite materials along the fiber axis. By obtaining more complete properties coupling of the deformation in other axes due to a particular load case can be determined. Coupling of the deformation due to off-axis loading may be desirable in some cases, and may be a natural outgrowth of the material symmetry and composite design in other cases. The knowledge of material symmetry planes was also required for the high temperature-testing program to ensure that the received signal was interpreted correctly.

In order to allow materials to be tested in reasonably straightforward manner, the sample had to be oriented in a principal axis for the high temperature testing. This led to the use of methods where the symmetry planes could be recovered from the full elastic tensor. The measurements were done at room temperature and allowed the sample to be cut in the principal planes. For the high temperature ultrasonic testing, multiple modes would be generated if the material axes were misoriented with respect to the geometric axes of the materials. Instead of generating a single longitudinal mode in the sample, multiple quasi-longitudinal modes were generated which results in a complex received signal. Thus, an effort was undertaken to determine if the material properties could be determined independent of material axes and then based on those results the sample could be reoriented into the principal axes. Using results from a number of experimental investigators a slightly modified technique was developed to obtain the full 21 elastic constants for the material samples used in the studies. Then from those results it was possible to obtain the material symmetry of the sample [5]. The misorientation of the material axes and the geometric axes was thus obtained. The sample was then re-

cut in a plane of material symmetry for the material. The sample was then oriented in the high temperature furnace so that a single longitudinal mode is propagated in the sample.

Additional background work required extensive testing of high temperature ultrasonic coupling materials that then allowed the measurement of in-situ elastic and damping properties at temperatures up to 1200°C. While these tests were performed only at temperatures up to 1200°C, the techniques will facilitate measurement of the elastic properties of anisotropic materials at temperatures up to 2500°C depending on the availability of suitable waveguides to contact the materials. Tests were performed which allowed changes in the elastic properties of a material to be monitored at elevated temperature while changes were made to the atmosphere and temperature. Thus, for the reinforced carbon-carbon material, it was possible to elevate the temperature of the material in an inert atmosphere up above the oxidation temperature of the material. At that point oxygen was introduced into the furnace, and controlled oxidation was monitored in real time by measuring the elastic properties and damping of the sample as the oxidation occurred.

Verification of the results of the new methods was performed using standard high temperature mechanical testing methods. The infrastructure used in this verification has enhanced the capabilities of the University of Maine and has provided resources for high temperature testing in Maine and the upper New England region. This effort is in keeping with the emphasis at University of Maine on composites engineering. In addition to verifying the elastic properties in a limited number of directions in the sample, the mechanical testing will also provide strength information from same samples.

Work on this project was closely coordinated between the University of Maine and Applied Thermal Sciences (ATS) of Sanford, ME. University of Maine had previously been contracted by ATS to perform a "quick-look" into development of techniques to perform high temperature mechanical and thermal property testing of material to be used in the AIT program. At that time they identified a need for a public-sector laboratory in the northeast United States that is capable of performing testing of composites at high temperature. The equipment infrastructure from this project addresses that need.

1.2 Objectives

The primary objective of this work was to develop techniques to measure the material characteristics of composites at very high temperatures. In order to perform the high temperature testing, several key subtasks have been performed. The following objectives were achieved:

1) A new waveguide sensor has been developed

2) Room temperature properties of the material have been fully characterized to ensure that the sample was oriented in a material axis during testing
3) Couplants for coupling the ultrasound into the sample at high temperatures have been identified
4) Waveguide tests have been implemented in a high temperature furnace and compared to mechanical tests when possible.

The background of each of these steps is described below. The following sections describe the work that was performed in the subtasks for each of the steps.

Figure 1 shows a photo of the system with an outline of the tube holding the sample superimposed on the furnace. Figure 2 shows more detail of the configuration of the transducers, waveguides and sample configuration as used for the high temperature testing. In the tube furnace the material sample is placed in the middle of the hot zone. Two ultrasonic transducers are placed outside of the furnace in water-cooled end caps that allow them to remain near room temperature. The ultrasonic wave is transmitted to the sample in the middle of the furnace from the ultrasonic

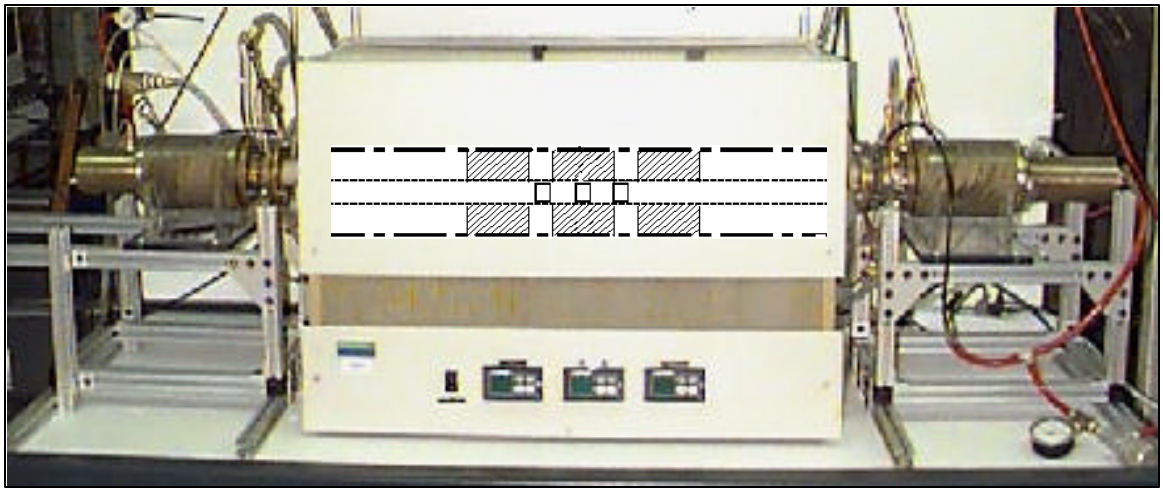

Figure 1: Tube furnace used in testing with outline of sample location superimposed on photo.

transducer using an elastic waveguide made of fused quartz. For higher temperature tests, sapphire was also used. However, alternative materials are still needed because of problems with the thermal shock resistance of sapphire. Testing is then performed using standard room temperature ultrasonic transducers in a contact through transmission configuration. In the case of anisotropic materials, the sample is oriented in a principal material axis in the furnace as described above. Successful testing required that a number of significant barrier issues were overcome. These issues are addressed in the

tasks described below. Additional applications for these results are also described in the specific task sections.

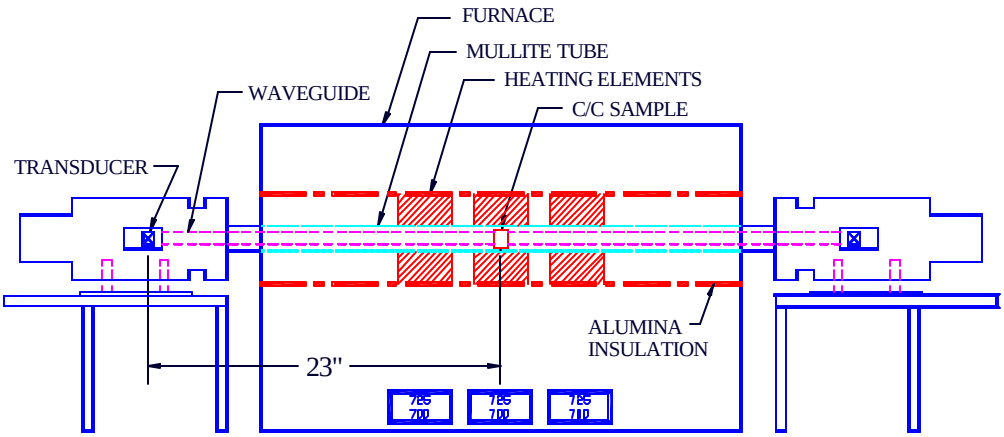

Figure 2: Sketch of system layout showing the sample, waveguides and ultrasonic transducers.

References

1 "It's Not Rocket Science – Or Is It?" *Nature Materials* Vol. 2, No. 6, p. 349.

2 Columbia Accident Investigation Board, 2003, Report Volume 1, August 2003, p. 49, accessed at: http://anon.nasa-global.speedera.net/anon.nasa-global/CAIB/CAIB_lowres_full.pdf on November 10, 2003.

3 A. Sayir and S.C. Farmer, 2000, "The effect of the microstructure on mechanical properties of directionally solidified $Al_2O_3/ZrO_2(Y_2O_3)$ eutectic", *Acta Materialia* 48, 4691-4697.

4 V Birman and LW Byrd, 2000, "Review of fracture and fatigue in ceramic matrix composites" *Applied Mechanics Reviews*, (June) 53(6) 147-174

5 Cowin, S. C. and M. M. Mehrabadi,1987, "On the Identification of Material Symmetry for Anisotropic Elastic Materials", *Quart. J. Mech. Appl. Math*., 40, 451-476.

2 Results of Research

More detailed sections follow a brief overview of each task in the project. Each section of the report includes copies of the publications that resulted form the work, additional narrative is included in cases where publications are still in review or preparation. The graduate students who are primarily responsible for the work are noted in the authorship sections for the publications, and are described below as a part of the educational and infrastructure development aspects of this DEPSCoR funded project.

The waveguide sensor development is a key element of the technique that has been developed for in-situ monitoring of materials at high temperatures. The development of this sensor has also provided an opportunity to address questions of long-standing interest in propagation of elastic waves in multi-mode cylindrical waveguides. This task included the design, development, construction and testing of a waveguide sensor. Because of the high attenuation at the interface between the sensor and the sample due to poor coupling and impedance mismatch, a waveguide that propagates multiple modes must be used to provide sufficient ultrasonic power [1]. These modes consist of a superposition of transverse and longitudinal plane waves. All of the modes are dispersive and many of the modes are not separable in time. Modeling of the propagation of modes in the waveguide has been used to understand the propagation of energy in these multiple overlapping modes and has the potential to recover complete elastic properties of the material. Models are used since the separation algorithm must be sufficiently robust to be able to separate the phase velocities of frequencies contained in both types of modes. The potential for selective mode generation is also explored, using an annular array transducer and narrow band excitation.

Testing of the waveguide sensor in this task showed the ability to predict the shape of the pulse and provided important insight into the attenuation of the leading pulses in the waveguide sensor. In addition to the normal dispersion curve calculation, this work also included a novel transfer function approach to the modeling of waves in solid cylindrical waveguides. The explanation of experimental results in this area has been a topic of controversy for several decades, with experimentalists and theoreticians attributing these changes to different mechanisms [2]. The model of wave propagation in a cylindrical waveguide can also be used as an inversion algorithm or in a time reversal technique. Using model based signal processing it was shown to be possible to generate a simple signal when an elastic wave is propagated through a multi-mode cylindrical waveguide [3]. Thus the work in this task

was able to address a long-standing issue in elastodynamics in cylindrical waveguides, while at the same time providing a model that is directly applicable to the testing of materials at high temperature.

The need to orient the sample in the principal material axes made it necessary to develop methods to recover the full stillness tensor of the composite samples. While a number of references exist in the literature that specifically addresses the recovery of the full stiffness tensor, none of the previous work has included experimental verification for low symmetry materials [4, 5]. This effort has resulted in the recovery of the full 21 elastic constants from an immersion ultrasonic technique, from which it was then possible to experimentally verify the symmetry planes of the material. Additional effort has included significant exploration of the optimization algorithms for the computational effort as well as novel techniques for the measurement of the ultrasonic signals. Significant improvements have been made in the experimental techniques and it has been shown that it is possible to find the relative orientation of the physical axes and the material axes from experimental data. These measurements also allow the assumption of a particular material symmetry, such as transverse isotropy or orthotropy to be tested.

The waveguide modeling, and sample orientation efforts have resulted in a broader understanding of the issues associated with high temperature ultrasonic testing of composite materials. The newly developed test techniques focus on the ability to use ultrasonic measurements in-situ to evaluate the effect of temperature and atmosphere on the properties of the material. The testing included development of coupling materials from the waveguide to the sample for use from 100°C to 1200°C. Improved control of the repeatability of the measurements is a remaining barrier for this type of testing. The effect of proper coupling and the associated signal processing has been important parts of the testing. The ultrasonic testing that was performed can also be verified using traditional mechanical testing. High temperature mechanical testing infrastructure has been developed as a part of this project.

In summary, the specific technical outcomes of the research project include:

- Development of semi-analytical models of the propagation of elastic waves in solid cylindrical waveguides. These models provided insight into a long-standing discrepancy between theory and experiments.
- Development of techniques that allow a simple signal to be generated after propagation of an elastic wave through a solid cylindrical waveguide.

- Techniques to allow the symmetry planes of an anisotropic material to be determined experimentally with no restriction to higher symmetry.
- Identification of coupling materials that allow ultrasonic testing to be conducted up to 1200°C.
- Testing sensitivity and accuracy determined for waveguide sensors at high temperatures.

In addition, as a DEPSCoR project the development of unique capabilities and the training of students is a key element of the effort. During the three and ½ years of the project:

- 2 M.S. Degrees have been awarded, 1 of who is currently working for Portsmouth Naval Shipyard, the second is currently a Ph.D. student in Engineering Science and Mechanics at Virginia Polytechnic.
- 2 M.S. Degrees and 1 Ph.D. Degree will be awarded in December of 2003 or May of 2004 based on funding from this project. Upon graduation the Ph.D. student is most likely to return as a post-doc to Los Alamos National Laboratory where he was previously employed.
- 3 B.S. students in Mechanical Engineering have continued their education based at least in part because of their experience working on this project as undergraduate students.

Finally, dissemination of the results will result in:

- 5 theses or dissertations, all of which will be available electronically [6, 7, 8, 9, 10]
- 2 refereed journal publications in print [11, 12], 2 in review and 3 more in preparation.
- 8 conference publications in print [13, 14, 15, 16, 17, 18, 19, 20] with 1 additional abstract currently submitted and one other in preparation. The proceedings papers include a paper by Anthony Puckett that was awarded second place in the student paper competition at the 2002 Society for Experimental Mechanics Conference [14].

Finally, extensive physical infrastructure for high temperature testing and materials research has been developed over the course of the project. This infrastructure will facilitate future DOD research in Maine.

More detailed technical results for most of the project are available in the following sections, with additional references available from either the thesis web page at the University of Mine or from the PI's web page at http://www.umeme.maine.edu/mick/.

References

1 M.L. Peterson, "A Signal Processing Technique for Measurement of Multi-Mode Waveguide Signals: An Application to Monitoring of Reaction Bonding in Silicon Nitride", *Research in Nondestructive Evaluation*, Vol. 5, p. 239-256, 1994

2 Redwood, M. (**1959**). "Velocity and attenuation of a narrow-band, high frequency compressional pulse in a solid wave guide," J. Acoust. Soc. Am. **31**, 442-448.

3 Anthony D. Puckett, M. L. Peterson, "A time reversal mirror in a solid circular waveguide using a single time reversal element", *Journal of Acoustic Society of America, Acoustics Research Letters On-Line,* Vol. 4, No. 2, April 2003, p. 31-36

4 Aristegui, C., and Baste, S., *J. Acoust. Soc. Am,* **Vol. 101 (2)**, pp. 813-833, (1997).

5 Cowin, S. C. and M. M. Mehrabadi,1987, On the Identification of Material Symmetry for Anisotropic Elastic Materials, Quart. J. Mech. Appl. Math., 40, 451-476.

6 Miao Sun, "Experimental Recovery of General Anisotropic Material Properties", M.S. Thesis, University of Maine, Summer 2002 http://www.library.umaine.edu/theses/.

7 S. Bunker, "In-Situ High Temperature Monitoring of Oxidation of Carbon-Carbon", M.S. Thesis, University of Maine, Summer 2002, http://www.library.umaine.edu/theses/pdf/BunkerSP2002.pdf.

8 Anish Senan, "Visco-elastic Response of Polymeric and Elastomeric Matrix Composites" , M.S. Thesis, University of Maine, Fall 2003, http://www.library.umaine.edu/theses/

9 Amala Mamilla, "High Temperature Couplants for the Characterization of Carbon-Carbon Composite Materials", M.S. Thesis, University of Maine, Expected Spring 2004, http://www.library.umaine.edu/theses/

10 A. Puckett, "Model Based Waveguide Time Reversal Mirrors as a High Temperature Sensor Candidate", Ph.D. Dissertation, University of Maine, Expected Spring 2004, http://www.library.umaine.edu/theses/

11 Anthony D. Puckett and M. L. Peterson, "Technique for determining the pressure distribution on the face of a contact ultrasonic transducer", *Experimental Techniques* Vol. 26, No. 5, 2003

12 Anthony D. Puckett, M. L. Peterson, "A time reversal mirror in a solid circular waveguide using a single time reversal element", *Journal of Acoustic Society of America, Acoustics Research Letters On-Line,* Vol. 4, No. 2, April 2003, p. 31-36

13 M.L. Peterson, A. D. Puckett and S. Bunker, "In-Situ High Temperature Characterization of Carbon-Carbon Oxidation using Time Reversal Mirrors" paper 2023 In *Proceedings of The 14'th International Conference on Composite Materials*, San Diego California, USA, July 14-18, 2003

14 Anthony Puckett and M. L. Peterson, "Time Reversal Mirror Pulse Echo Ultrasonics in a Solid Circular Waveguide", In *Proceedings of Student Paper Competition, SEM Annual Conference and Exposition*, Milwaukee WI, June 10-12, 2002

15 M. L. Peterson, "In-Situ Evaluation of High Temperature Oxidation of Carbon-Carbon Composites" Office of Naval Research, *ONR 334 Composites for Marine Structures*, University of Maryland, College Park, MD 6-8 May, 2002.

16 M.L. Peterson, M. Sun, L. Espinosa , A Sysko, "Stochastic Properties of Anisotropic Materials", *2001 ASME International Mechanical Engineering Congress and Exposition*, New York, Nov. 11-16, 2001

17 M.L. Peterson, Shaun Bunker and Anthony Puckett, "Evaluation of Dynamic Properties of Composites in an Oxidizing Environment" *Review of Progress of Quantitative Nondestructive Evaluation, Vol. 21,* American Institute of Physics , Melville NY, 2002, p. 1038-1045.

18 Miao Sun, Sara Wright and M.L. Peterson "Visco-elastic Tensor Recovery in the Absence of Known Material Symmetry" *Review of Progress of Quantitative Nondestructive Evaluation, Vol21,* American Institute of Physics , Melville NY, 2002, p. 1423-1430.

19 A. D. Puckett and M.L. Peterson, "Fidelity of an Analytical Time Reversal Mirror" *in Review of Progress of Quantitative Nondestructive Evaluation, Vol. 21,* American Institute of Physics, Melville NY, 2002, p. 945-952.

20 Puckett, A.D., Peterson, M.L., Bennett, J.G., Smith, F.W., "Development of a Fidelity Criteria for Finite Element Modeling of a Thick Cylindrical Waveguide", *Canadian Congress of Applied Mechanics, CANCAM 2001,* Memorial University of Newfoundland, Faculty of Engineering and Applied Science, June 3-7, 2001, p. 3-4.

2.1 Task 1 – Waveguide sensor development and testing using ultrasonic techniques.

This tasks focuses on the development of models that will allow effect of the solid cylindrical waveguides to be removed from the measurement system. The models can be implemented in one of to signal processing scheme, either using a time reversal mirrors, or by deconvolving the theoretical input from the received experimental signal. In either case the signal from the furnace will be comparable to that obtained using traditional contact ultrasonic methods. The barriers at that point are well understood and are common to most ultrasonic systems, including such issues as coupling, obtaining proper reference signals and the accurate measurement of time delays. At the same time this portion of the work has addressed a more general problem in elastodynamics.

A number of other investigators have made use of multi-mode waveguides as a high temperature sensor for determining material properties. An early use of multi-mode waveguides was to measure both the Young's modulus and the shear modulus of materials in a single experiment (e.g. McSkimin 1959). Similar techniques were used to obtain single crystal properties. For example, the full elastic coefficients in iron were first measured up to 500°C by Leese and Lord (1968) using ultrasonic pulse methods. The explanation of these experiments was typically framed in terms of a plane wave model that neglects dispersion. When frequency components of the propagating pulse are greater than the cut-off frequency for the second waveguide mode it was consistently observed that the attenuation of the modes is a function of the group velocity (e.g. Mason and McSkimmin 1947, Hughes et al. 1949, Tu et. al. 1955 and McSkimmin 1956). The paper *abstract* by Mason and McSkimin (1947) states "Longitudinal waves show delayed pulses of smaller magnitude that are caused by the longitudinal wave breaking up into reflected longitudinal and shear waves at the boundary". However, the resulting attenuation of the higher modes is not consistent with the accepted waveguide model (Achenbach 1984 and Love 1927). The accepted model does not show a coupling between modes once the pulse has been launched in the waveguide. Redwood (1959) proposed a correction to the Pochhammer-Chree solution for wave propagation in a solid cylinder. Redwood's solution directly accounted for this attenuation by formulating the solution in terms of both Bessel and Neumann functions. The motivation for the modified theory is that the "usual solutions ... fail to predict the observed velocity and attenuation" (Redwood 1959). A monograph by Redwood (1960) further complicates the situation by making a distinction between narrow and wide bandwidth pulses for applicability of the modified solution for a plate. Other explanations for the discrepancy with the accepted model have not been considered in the literature. The result is that experimental discussion

of multi-mode waveguides continues to depend on a model that disregards dispersion (Jen 1990 and Kolsky 1963). The model developed in this work addresses this discrepancy, and a paper is currently in preparation that will better explain the experimental observations using the results from the model.

The papers that follow resulted from the work in this task. The reference to the published paper is shown below the title of each of the sections.

2.1.1 References

Achenbach, J.D., 1984. *Wave Propagation in Elastic Solids*. Amsterdam. North Holland Publishing Company.

Hughes, D.S., W.L. Pondrom and R.L. Mims. 1949. "Transmission of Elastic Pulses in Metal Rods". *Physical Review* 75 (No. 10):1552-1556.

Jen, C.K., Ph. de Heering, P. Sutcliffe and J. Bussiere. 1991. Ultrasonic Monitoring of the Molten Zone of Single-Crystal Germanium. Materials Evaluation 49 (No. 6, June): 701-706.

Jen, C.K., L. Piche and J.F.Bussiere. 1990. "Long Isotropic Buffer Rods". *Journal of the Acoustical Society of America* 88 (No. 1, July): 23-25.

Jen, C.K., Z. Wang, A. Nicolle, J.F. Bussiere, E.L. Adler and K. Abe. 1992. "Acoustic Waveguideing rods with Graded Velocity Profiles". *Ultrasonics* 30 (No. 2): 91-94.

Kolsky, H. 1963. *Stress Waves in Solids*. New York: Dover Publications, Inc.

Leese, John, and A.E. Lord, Jr.. 1968. Elastic Stiffness Coefficients of Single-Crystal Iron from Room Temperature to 500C. Journal of Applied Physics, 39 (No. 8, July): 3986-3988.

Love, A.E.H., 1927. *A Treatise on the Mathematical Theory of Elasticity*. Reprint. New York: Dover. 1944.

Mason, W.P., and H.J. McSkimin. 1947. "Attenuation and Scattering of High Frequency Sound Waves in Metals and Glasses". *Journal of the Acoustical Society of America* 19 (No. 3): 464-473.

McSkimin,H.J. 1956. "Propagation of Longitudinal Waves and Shear Waves in Cylindrical Rods at High Frequencies". *Journal of the Acoustical Society of America* 28 (No. 3): 484 494.

McSkimin, H.J. 1959. "Measurement of Ultrasonic Wave Velocities and Elastic Moduli for Small Solid Specimens at High Temperatures". *Journal of the Acoustical Society of America* 31: 287-295.

Peterson, M.L. 1994. A Signal Processing Technique for Measurement of Multi-Mode Waveguide Signals: An Application to Monitoring of Reaction Bonding in Silicon Nitride. To appear in Research in Nondestructive Evaluation, Springer International.

Redwood, M. 1959. "Velocity and Attenuation of a Narrow Band, High-Frequency Compressional Pulse in a Solid Waveguide". *Journal of the Acoustical Society of America* 31 (no. 4, April): 442-448.

Redwood, M. 1960. *Mechanical Waveguides*. New York: Pergamon.

Tu, L.Y., J.N. Brennan, and J.A. Sauer. 1955. "Dispersion of Ultrasonic Pulses in Cylindrical Rods". *Journal of the Acoustical Society of America* 27, 550-553.

2.1.2 A time reversal mirror in a solid circular waveguide using a single time reversal element

Anthony D. Puckett, M. L. Peterson, "A time reversal mirror in a solid circular waveguide using a single time reversal element", *Journal of Acoustic Society of America, Acoustics Research Letters On-Line*, Vol. 4, No. 2, April 2003, p. 31-36

Abstract: The ability of a single acoustic element to produce a compact time domain signal from a multi-mode solid cylindrical waveguide using a time-reversal mirror (TRM) is considered. Two single element longitudinal contact transducers were used to excite and receive multiple longitudinal modes in a fused quartz waveguide in a TRM experiment. The TRM is demonstrated to be effective with the limited information from a single longitudinal transducer. Experimental results are presented along with a simple interpretation that shows how a TRM with only a single element can be used as a practical sensor.

2.1.2.1 Background

Solid cylindrical waveguides have been used as buffer rods in a number of applications to isolate ultrasonic sensors from hostile environments [Jen *et al*., 1991; Jen *et al*., 1997; Peterson, 1994]. However, due to design constraints it is often not possible to use a waveguide that is sufficiently thin to propagate only a single longitudinal mode. In sensor applications a number of approaches have been taken to eliminate the propagation of multiple modes, including the bundling of thin waveguides, cladding of buffer rods and introduction of surface roughness to eliminate spurious signals [e.g., Thurston, 1978; Jen *et al*., 1990]. However, in some cases design constraints make the use of a multi-mode waveguide necessary [Peterson, 1994]. The propagation of multiple modes causes a signal that is compact in the time domain to have a large time signature after propagating through the waveguide, Fig 1. As a result, if the acoustic signal is propagated through a specimen, as well as a buffer rod, phase velocity and attenuation information about the specimen is harder to extract. A number of approaches have been considered to solve this problem, however the complexity of methods required accommodating the multi-mode signal is high [Peterson, 1999]. A time reversal mirror is proposed in order to eliminate this problem by reducing the complexity of the received signal.

Time reversal mirrors (TRM) have been developed based on the property of time-reversal invariance [Fink, 1997]. A time-reversal mirror experiment consists of three steps. In the case of a cylindrical rod, first, an acoustic signal is excited by a source at one end of the rod. The acoustic signal propagates through the rod, and the altered signal is recorded at the opposite end. Second, the

recorded signal is reversed in time. Finally, the receiver is excited with the reversed signal. The reversed signal propagates through the rod, and a new signal is recorded at the source. If time invariance is satisfied this new signal is the same as the original acoustic signal. This ability of the TRM can be used to produce a compact time signal from a dispersive system. This technique has been shown to be effective in eliminating the dispersive effects of Lamb waves used for plate inspection [Ing and Fink, 1998].

Time reversal in a solid circular waveguide has been demonstrated recently in an application to concentrate acoustic energy at a point in a fluid [Montaldo *et al.*, 2001]. Multiple transducers on the end of a solid circular waveguide were excited by a 1-bit digitized time-reversed signal to create a high amplitude pulse in a fluid near the opposite end of the waveguide instead of the dispersed multi-mode signal. In this application and the applications mentioned previously only the axially symmetric longitudinal modes are excited. Thus, at most, an annular array of transducers would appear to be required to reconstruct the general displacement field on the end of a cylinder. However, a single element cylindrical transducer is most commonly available and is the configuration typically used in sensor applications with cylindrical waveguides [Jen *et al.*, 1991; Peterson, 1994]. The time reversal technique has been shown to be effective when only the first two longitudinal modes are excited in a solid circular waveguide using a single transducer [Puckett and Peterson, 2002]. However, the ability to extend time reversal to a cylindrical waveguide for which a large number of modes propagate using only a single transducer is of interest.

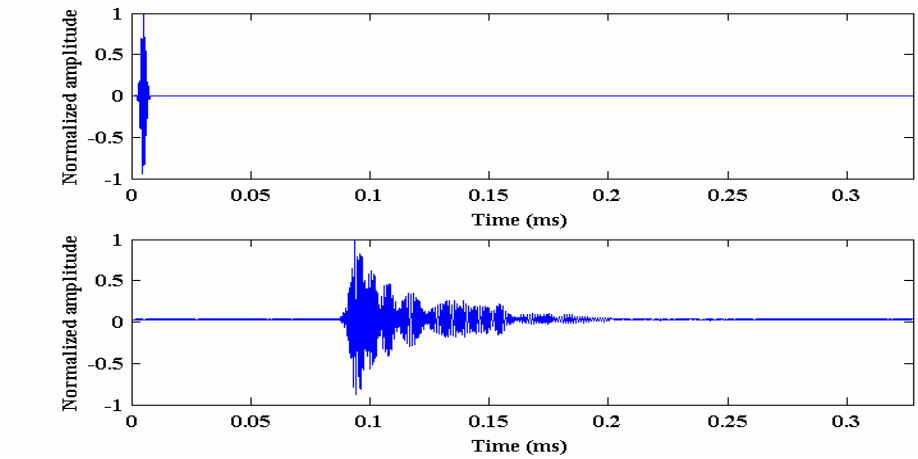

Figure 1. The figure above is an illustration of dispersion in a cylindrical waveguide. The top graph is the original signal with compact time domain. The bottom graph is the original signal after propagating through the cylindrical waveguide used in this research.

The cutoff frequencies for the longitudinal modes in a solid cylinder are determined by two equations. The roots of one equation predict the axial shear modes, which have entirely axial particle displacement at the cutoff frequency. The roots of the other equation predict the radial shear modes, which have entirely radial shear particle displacement at the cutoff frequency [Zemanek, 1972]. For high frequencies the propagating longitudinal modes will consist of both axial shear and radial shear modes. Both the radial shear and the axial shear modes have a normal stress and a shear stress that vary as a function of radius and frequency. The stress in each mode has a component from the superposition of plane dilatational waves and a component from the superposition of plane transverse waves.

It can be shown that a single transducer is capable of exciting multiple longitudinal modes in a circular waveguide. For this research, the diameter of the transducers was approximately 4 times greater than the diameter of the waveguide. This configuration allows the pressure distribution across the face of the waveguide to be considered constant with radius. Although the pressure is nearly constant with radius, all of the modes with cutoff frequencies within the spectrum of the signal will propagate. The propagating modes include axial shear and radial shear modes. These real modes, along with some imaginary modes, and an infinite number of attenuating complex modes are excited in order to satisfy the boundary conditions on the end of the waveguide [Zemanek, 1972]. The multiple propagating modes are evident in the large time signature in the bottom signal of Figure 1. The frequency spectrum of the top signal in Figure 1 and the dispersion curves of the waveguide appear in Figure 2. From Figure 1 and Figure 2 it is evident that multiple dispersive modes are excited and propagated through the waveguide by a single transducer.

The signal from a single transducer should include sufficient information from a multi-mode signal to perform an accurate time reversal. As the signal propagates along the waveguide the modes separate in time and the complex modes attenuate. Thus, the pressure distribution on the receiving end of the waveguide is not constant with radius. The actual pressure distribution on the end of the waveguide at a particular time is the superposition of the normal stress of all of the modes and frequencies present. The transducer does not record the shear stress of any of the modes present. Additionally, the transducer only has the ability to measure the average pressure across the face. It is reasonable though, to assume that the most important information is the frequencies that are present in the received signal and the relative amplitudes of those frequencies. This information is then used when the signal is reversed in time and the time-reversed signal is used to excite the transducer. This novel ability of the TRM with a single transducer invites the use of circular solid waveguides.

To determine if a single transducer is able to provide sufficient information to provide a compact time signal, a TRM experiment was conducted using single element longitudinal contact transducers on either end of a solid fused quartz rod. The original excitation signal was compared to the final signal from the TRM experiment to determine the ability of the TRM to reconstruct the original input signal.

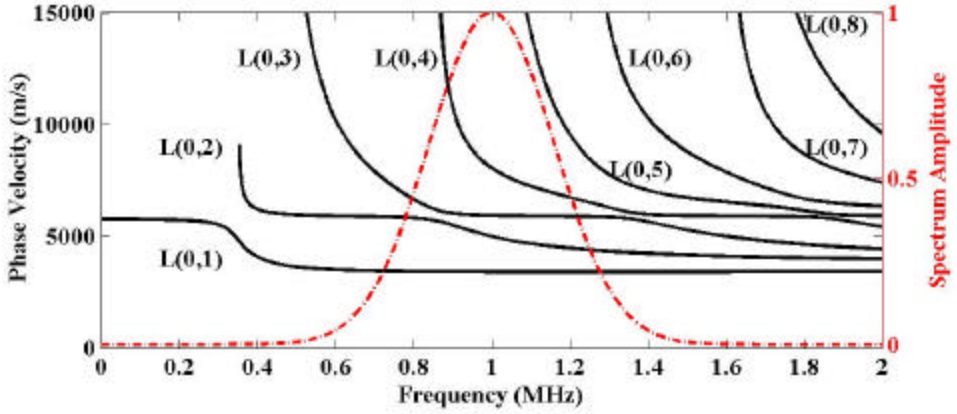

Figure 2. Dispersion curves for the cylindrical waveguide used in the TRM experiments and the normalized frequency spectrum (dashed) of the signal used to excite the waveguide.

2.1.2.2 Methods

The configuration used for the experiments is shown in Figure 3. The waveguide consisted of a 10 mm diameter fused quartz cylindrical rod, 485 mm in length. An amorphous material was chosen for the waveguide because linear elastic and homogeneous assumptions are well satisfied. Fused quartz has a Young's modulus, E, of 73 GPa, a density, ?, of 2200 kg/m^3, and a Poisson's ratio, ?, of 0.14.

Two transducers were used for the experiments. Both transducers were 38 mm diameter, 1 MHz broadband longitudinal contact transducers [Panametrics, model V194, Waltham, MA]. The transducers had a bandwidth corresponding to a 6 dB drop in amplitude between 0.5 MHz to 1.5 MHz. A coupling fluid was used between the transducers and the wave guide [Sonotech, Inc. UT-30, State College, PA].

An arbitrary waveform generator [Agilent 33250A, Palo Alto, CA] produced the signal to drive the transducer. A radio frequency power amplifier [ENI A-300, Rochester, NY] with a gain of 55 dB was used to amplify the signal to the transducer. The received signal was recorded by a digital storage

oscilloscope [Tektronix TDS 520A, Wilsonville, OR] after amplification of the signal by an ultrasonic pre-amplifier [Panametrics model 5660C, Waltham, MA] with a gain of 40 dB.

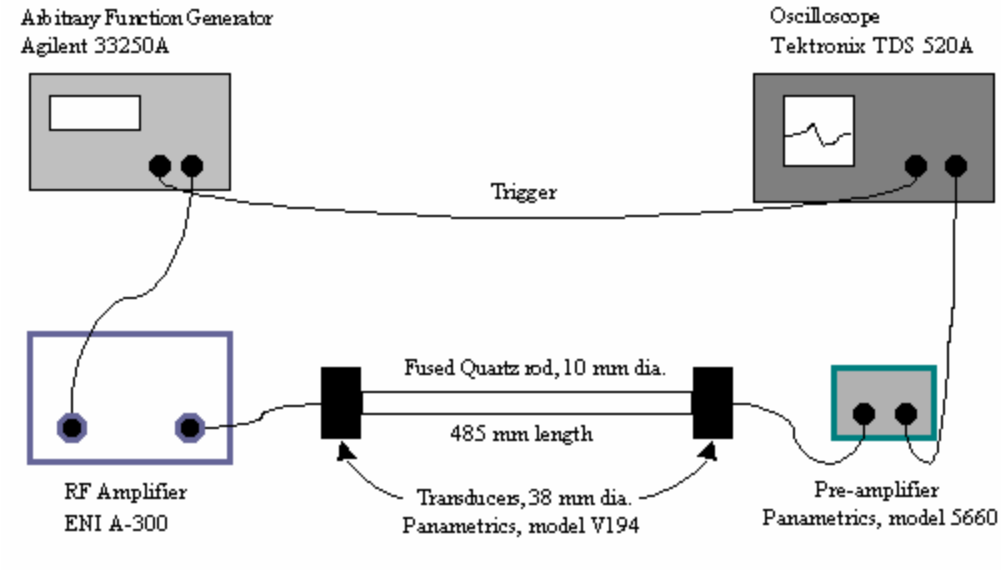

Figure 3. Diagram of the experimental setup.

The acoustic signal used in the TRM experiments was a broadband signal. The signal had a frequency spectrum with a 40 dB drop in amplitude at 0.5 and 1.5 MHz and a central frequency of 1 MHz, Figure 2. For the geometry of the waveguide and the frequency spectrum, six propagating longitudinal modes were excited in the waveguide, with a component of each mode being the superposition of plane transverse waves. Figure 2 shows the dispersion curves calculated for the waveguide used in the experiments.

To ensure the correct signals were recorded the time window was chosen to only include the initial propagated signal and no end reflections. The excitation signals were repeated at a frequency of 10 Hz to ensure that reflections from previous signals were sufficiently attenuated and were not included in the recorded signal. The recorded signals were averaged over 20 signals to remove noise. Finally, since the waveguide is symmetric about its length, the received signal that is reversed can be excited from the source transducer instead of the receiving transducer to produce the same results. So, for the experiments, all signals were sent from the same end of the waveguide using the same experimental set up.

It was necessary to include the experimental frequency response of the apparatus in the comparison of the original excitation signal to the final signal of the TRM, so the ability of the single element TRM in the waveguide could be determined more accurately. The frequency response

includes an amplitude factor and a phase shift for each frequency. However, since the original excitation signal is compared to the final signal of the TRM the phase shift does not need to be known due to the reversal of the signal in the second step of the TRM experiment. For example, if a signal that propagates through the system is altered by a phase shift of f(?), then the reversed signal will have a negative phase shift, -f(?). When the system is excited by the reversed signal, the phase shifts will cancel. Since the signal was always propagated from the same source for the TRM experiments, the phase shift was always the same. Therefore, only the amplitude of the frequency response was required to account for the equipment response.

The frequency response of each piece of equipment (RF amplifier, transducers, and ultrasonic pre-amplifier) was measured. The system response function is the convolution of the amplitude factors of each piece of equipment. The ability of the TRM in the waveguide will be determined by the comparison of the final signal in the TRM experiment with the original excitation signal convolved with the system response function. For this convolution, the system response was squared because the original excitation signal was propagated through the experimental system twice before becoming the final signal.

2.1.2.3 Results and Conclusion

The signals from the TRM experiments are compared in Figure 4. All of the signal amplitudes have been normalized and the signals are plotted with the same time scale. The original excitation signal convolved with the system response function is shown as the top signal of Figure 4. The bottom four signals in Figure 4 are the signals from the TRM experiments in the waveguide. The second signal from the top in Figure 4 is the dispersed signal recorded at the receiving transducer after the excitation signal has propagated through the waveguide. The dispersed signal was reversed in time as shown in the third signal in Figure 4 and was used to excite the ultrasonic transducer. The signal second to the bottom in Figure 4 is the signal recorded at the receiving transducer after the reversed signal is propagated through the waveguide. The bottom signal in Figure 4 is the previous signal reversed in time for comparison to the first signal. A closer comparison of the first and last signals of Figure 4 appears in Figure 5.

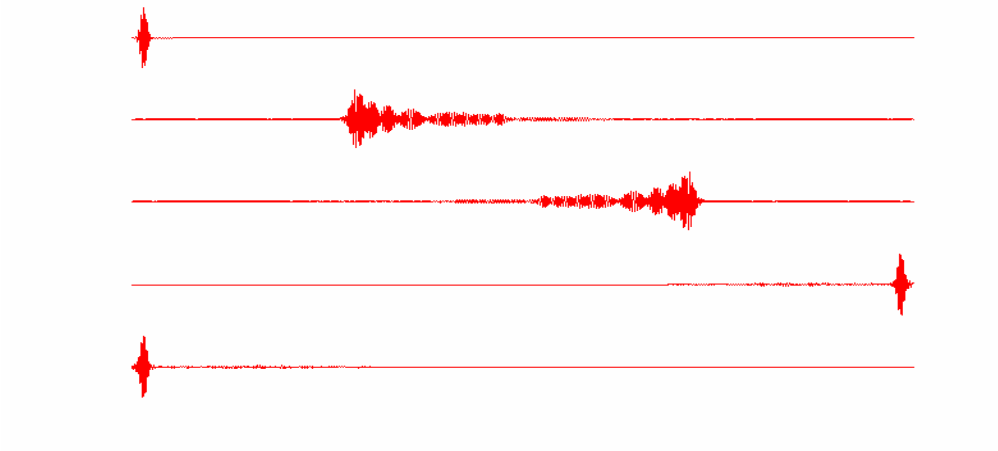

Figure 4. The TRM experiment in a solid multi-mode waveguide. The signals are normalized and plotted on the same time scale. The signals are, from top to bottom, the original signal convolved with the system response, the dispersed signal, the reversed dispersed signal, the final signal created from the propagation of the reversed dispersed signal, and the final signal reversed in time.

The two signals in Figure 5 are very similar with additional noise evident in the experimental signal. The ability of a TRM to reconstruct the original excitation signal using the limited information of a single longitudinal contact transducer appears to be very good. It was shown earlier that a single longitudinal contact transducer excited multiple modes in a cylindrical waveguide, including the longitudinal modes that result from the superposition of plane transverse waves. The experimental signal in Figure 5 implies that a single longitudinal contact transducer appears to be capable of reconstructing a compact time signal from a solid circular waveguide. Thus, the effect of the pressure distribution on the end of the waveguide appears to be minimal.

The most important characteristic of the resulting experimental signal in Figure 5 is the compact time signature. By using the time-reversed signal as the excitation signal, the dispersive properties of the waveguide can be negated. This capability allows the use of a dispersive solid circular waveguide as a low cost sensor. The compact time domain signal greatly simplifies signal analysis that was previously used [Peterson, 1994].

For a practical application with a single waveguide, the signal that will cancel the dispersive effects of the waveguide is easily determined from the TRM experiment. For more complex configurations where significant changes with time are expected [Jen *et al*., 2001] either modeling or more extensive experiments are required. Future work remains to be done to show that measurements can be made in-situ and to develop appropriate models.

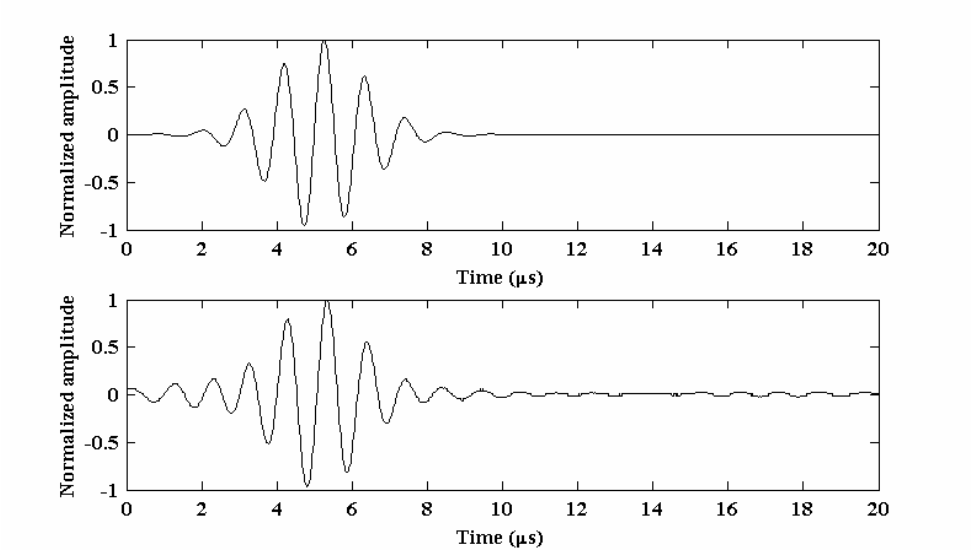

Figure 5. Comparison of the original signal (top) to the final signal from the TRM experiment (bottom). The original signal has been convolved with system response function.

2.1.2.4 Acknowledgement

This research is sponsored by the Ballistic Missile Defense Organization through the Office of Naval research (ONR), Science Officer Dr. Y. D. S. Rajapakse.

2.1.2.5 References and links

Fink, M. (**1997**). "Time reversed acoustics," Physics Today. **50**, 34-40.

Ing, R.K., and Fink, M. (**1998**). "Time-reversed lamb waves," IEEE Trans. Ultrason., Ferroelect., Freq. Contr. **45**, 1032-1043.

Jen, C.-K., Cao, B., Nguyen, K.T., Loong, C.A., and Legoux, J.-G. (**1997**). "On-line ultrasonic monitoring of a die-casting process using buffer rods," Ultrasonics. **35**, 335-344.

Jen, C.K., de Heering, Ph., Sutcliffe, P., and Bussiere, J.F. (**1991**). "Ultrasonic monitoring of the molten zone of single-crystal germanium," Mater. Eval. **49**, 701-705.

Jen, C.-K., Franca, D.R., Sun, Z., and Ihara, I. (**2001**). "Clad polymer buffer rods for polymer process monitoring," Ultrasonics. **39**, 81-89.

Jen, C.K., Piche, L., and Bussiere, J.F. (**1990**). "Long isotropic buffer rods," J. Acoust. Soc. Am. **88**, 23-25.

Montaldo, G., Roux, P., Derode, A., Negreira, C., and Fink, M. (**2001**). "Generation of very high pressure pulses with 1-bit time reversal in a solid waveguide," J. Acoust. Soc. Am. **110**, 2849-2857.

Peterson, M.L. (**1994**). "A signal processing technique for measurement of multi-mode waveguide signals: an application to monitoring of reaction bonding in silicon nitride," Res. Nondestr. Eval. **5**, 239-256.

Peterson, M.L. (**1999**). "Prediction of longitudinal disturbances in a multi-mode cylindrical waveguide," Experimental Mechanics. **39**, 36-42.

Puckett, A.D. and Peterson, M.L. (**2002**). "Fidelity of an Analytical Time Reversal Mirror," to appear in *Review of Progress of Quantitative Nondestructive Evaluation*, (American Institute of Physics, New York), Vol. 21.

Thurston, R.N. (**1978**). "Elastic waves in rods and clad rods," J. Acoust. Soc. Am. **64**, 1-37.

Zemanek, J. (**1972**). "An experimental and theoretical investigation of elastic wave propagation in a cylinder," J. Acoust. Soc. Am. **51**, 265-283.

2.1.3 Technique for determining the pressure distribution on the face of a contact ultrasonic transducer

Anthony D. Puckett and M. L. Peterson, "Technique for determining the pressure distribution on the face of a contact ultrasonic transducer", *Experimental Techniques* Vol. 26, No. 5, 2003

2.1.3.1 Introduction

Contact ultrasonic transducers that generate longitudinal waves in a solid are used in many experimental applications. Typical applications range from determining the elastic properties of materials to locating cracks or inclusions in materials.[1] To accurately interpret the results for these applications, analytical models are often required.[2] In a number of cases analytical models need to include the effects of the transducer on the measurement system. The main attributes of the transducer are the frequency response, which is easily determined experimentally and the pressure distribution across the face of the transducer. It is possible to assume a uniform pressure across the face of the transducer, but often this is not adequate.[3] For example, the beam width of the transducer must be well understood for sizing of cracks, a key nondestructive evaluation task. Therefore, measurement of the pressure distribution across the face of the transducer may be required.[4]

An example of an additional application where the pressure distribution on the transducer is required is in conjunction with a circular cylindrical waveguide sensor.[5] Waveguides are used primarily to isolate contact transducers from a specimen that is at an extreme temperature and/or pressure. However, the relationship between the frequencies required for the experiments and the diameter of the waveguide results in dispersion and the propagation of multiple modes. An analytical model to determine the dispersion of the signal through the waveguide can be developed based on propagating modes. The relative amplitudes of the modes are determined by the boundary conditions on the end of the waveguide.[6] In order to evaluate the boundary conditions, the pressure distribution across the face of the longitudinal contact transducer that is in contact with the waveguide must be known.

The technique described makes it possible to determine the pressure distribution across the face of a transducer using a standard commercial immersion scanning system. This apparatus provides a low cost alternative to laser based methods for verification and testing. The experimental setup and procedure are described. Potential difficulties are discussed as well as the necessary remedies.

2.1.3.2 Technique

The schematic of the system used for the measurement technique is illustrated in figure 1. The apparatus is also shown in a picture in figure 2. The setup consists of two parts, the sensor and the transducer to be characterized (the unknown transducer). The sensor consists of a longitudinal contact transducer (receiving transducer), a stepped waveguide, and a housing fixture to hold the waveguide in contact with the receiving transducer. The stepped waveguide allows a measurement to be performed over a small area of the unknown transducer while still providing sufficient energy to the receiving transducer. The unknown transducer is mounted facing the end of the waveguide. In order to take measurements at multiple locations the sensor is able to move independent of the unknown transducer in two axes of the plane normal to the waveguide.

The ultrasonic signal received by the sensor is indicative of the pressure on the transducer. The unknown transducer is excited by a pulse, a square wave, or an arbitrary function such as a sine burst or chirp. The ultrasonic signal propagates through the air and the sensor receives the signal. The sensor is moved across the face of the unknown transducer and at each point the signal is recorded. The change in amplitude of the signal received by the tip of the waveguide across the unknown transducer is representative of the pressure distribution across the unknown transducer.

This technique takes advantage of the difference in wave speed between the waveguide and the air to isolate the ultrasonic signal received by the tip of the waveguide. Since the velocity of the wave is much higher in the waveguide (aluminum in this case) than in air, the path through the waveguide will represent the first arrival in the signal. The fastest path in this configuration is through the tip of the aluminum waveguide, which is closest to the transducer. The first signal arrival is thus recorded and corresponds to the signal received by the tip of the waveguide. This signal determines the pressure distribution across the transducer. A second signal is received later corresponding to the larger face on the stepped portion of the waveguide. Figure 3 illustrates this phenomenon.

To ensure that the coupling between the waveguide and the unknown transducer is the same at all points across the unknown transducer, air is used as the coupling fluid. Liquid coupling is not possible for contact transducers, and the amplitude is not consistent when using normal contact ultrasonic methods. Air is difficult to use as a couplant, however, since the ultrasonic signal is highly attenuated by the air. The attenuation of the ultrasonic signal in air is highly frequency dependent, changing as a function of frequency.[7] The high attenuation at normal ultrasonic frequencies of 1 MHz to 10 MHz requires that the sensor and face of the transducer be aligned as closely as possible to the plane defined by the two axes of motion. A change in the air gap across the unknown transducer

will change the amplitude of the received signal as the sensor moves across the unknown transducer. However, the distance between the unknown transducer and the waveguide will also change the time delay of the received signal. Therefore, the alignment of the unknown transducer can be verified by the measured time delay, with the accuracy of the time delay a function of the sampling rate of the signal.[8]

2.1.3.3 Results

An example of the pressure distribution measurement is shown for a common transducer. A 28.6 mm (1.125 in.) element diameter 1 MHz longitudinal contact transducer (Panametrics, model v194, Waltham, MA) is presented. The experimental configuration appears in figure 2. The sensor used a 2.25 MHz nominal center frequency, 12.7 mm (0.5 in.) element diameter immersion transducer (Panametrics, model v306, Waltham, MA). Similar results are obtained with matched center frequencies, but the primary requirement is a reasonable amplitude response. The waveguide was made of aluminum with a narrow section 16 mm long and 3 mm in diameter and a wide section 52 mm long and 9 mm in diameter. An ultrasonic pulse generator (Panametrics, model 5072 PR, Waltham, MA) was used to generate the excitation signal to the 1 MHz transducer. Signals were recorded at multiple points along the face of the transducer. An example of a recorded signal and the same signal after filtering appear in figure 4. The filtering was used to remove all of the frequencies above the upper frequency of the 1 MHz transducer, which did not correspond to the ultrasonic signal. For the measurements, the highest peak in the signal after signal processing was picked, and this peak was compared between measurement locations. The amplitude and the time delay were measured for the same peak at each measurement location. The relative amplitude and the difference in time delay appear in figure 5. The difference in time delay can also indicate if there is any misalignment of the transducer by multiplying the difference in time delay by the velocity of sound in air, 330 m/s. The right side of the graph displaying the time delay shows the relative distance.

2.1.3.4 Discussion and Conclusion

Most of the difficulties with the technique are associated with the signal acquired during testing. It is apparent from the signal in figure 3 and figure 4 that the signal to noise ratio is small. This is partially due to the attenuation caused by the air gap between the waveguide and the transducer and in this configuration partially due to the unmatched center frequencies of the transducers.

Appropriate filtering must be used to deal with the noise. The signal to noise ratio can be maximized by using a transducer in the sensor that has the same center frequency as the transducer being measured as well as using narrow band excitation.

In addition to the low signal to noise ratio the signal also contains multiple arrivals, each arrival corresponding to a different cross section of the waveguide. Therefore, care must be taken in analyzing the correct arrival. The second arrival corresponds to the signal received by the larger diameter stepped portion of the waveguide, which has a longer ultrasonic path in air. This arrival has a larger amplitude because the larger area receives more energy.

Since the cross sectional area of the waveguide is directly related to the energy received, the geometry of the waveguide is critical. The waveguide must have a sufficiently small tip so that the measurement can be made over a small area of the transducer. For a more accurate determination of the pressure distribution a smaller waveguide tip would be used. However, the smaller tip will result in a reduction of the amplitude in the received signal. Alternatives, such as narrow band excitation can help overcome these difficulties.

These difficulties are commonly found in other ultrasonic applications, so the difficulties should not be new to most users. This technique is a simple cost effective way of determining the pressure distribution of a contact ultrasonic transducer.

1.1.1.1 References:

1. Krautkramer, J. and Krautkramer, H., *Ultrasonic Testing of Materials*, Springer-Verlag, Berlin, 1983.
2. Schmerr, L.W., Fundamentals of Ultrasonic Nondestructive Evaluation, Plenum Press, New York, 1998.
3. Lerch, T.P., Schmerr, L.W, and Sedov, A., "Ultrasonic beam models: An element edge approach," J. ACOUST. SOC. AM., **104**, pp. 1256-1265, (1998).
4. Bacon, D.R., Chivers, R.C., and Som, J.N., "The acousto-optic interaction in the interferometric measurement of ultrasonic transducer surface motion," ULTRASONICS, **31**, pp. 321-325, 1993.
5. Peterson, M.L., "Prediction of longitudinal disturbances in a multi-mode cylindrical waveguide," EXP. MECH., **39**, pp. 36-42, 1999.
6. Zemanek, J., "An experimental and theoretical investigation of elastic wave propagation in a cylinder," J. ACOUST. SOC. AM., **51**, pp. 265-283, 1972.
7. Pierce, A. D., Acoustics: An Introduction to Its Physical Principles and Applications, McGraw-Hill Book Company, New York, 1981.
8. Peterson, M.L., "A signal processing technique for measurement of multi-mode waveguide signals: an application to monitoring of reaction bonding in silicon nitride," RES. NONDESTR. EVAL., **5**, pp. 239-256, 1994.

2.1.3.5 Figures:

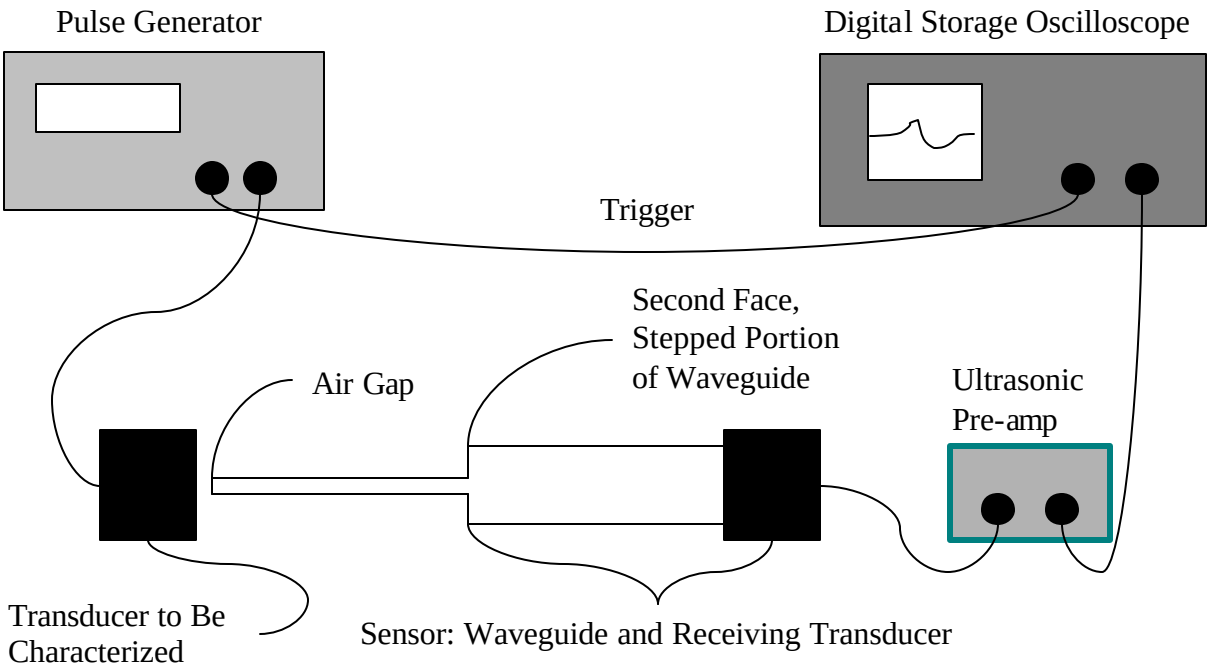

Figure 1. Diagram of the setup for the experimental technique.

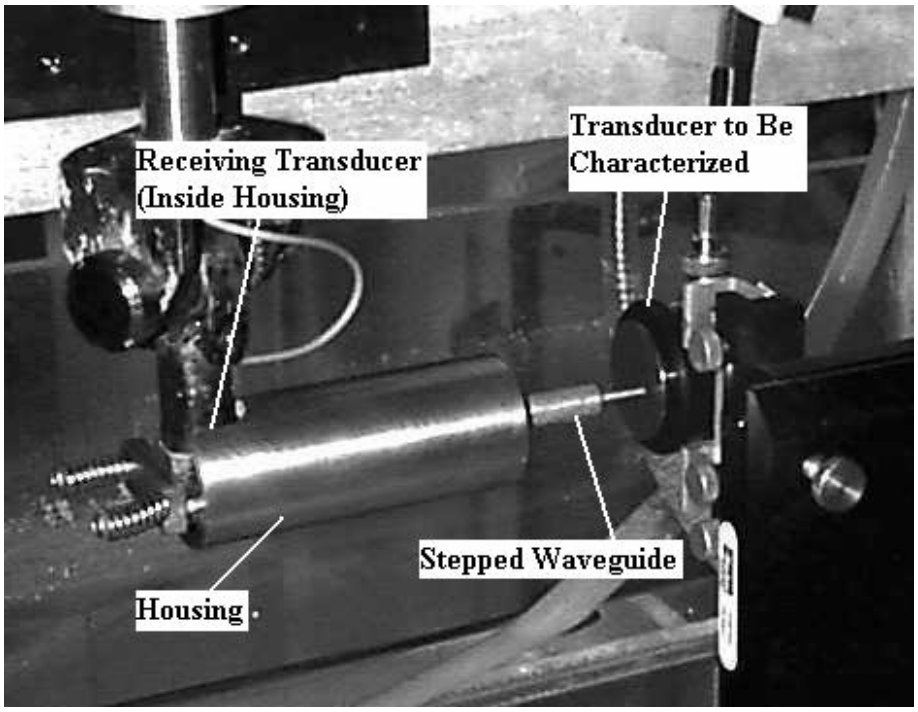

Figure 2. Picture of the sensor and the transducer to be characterized.

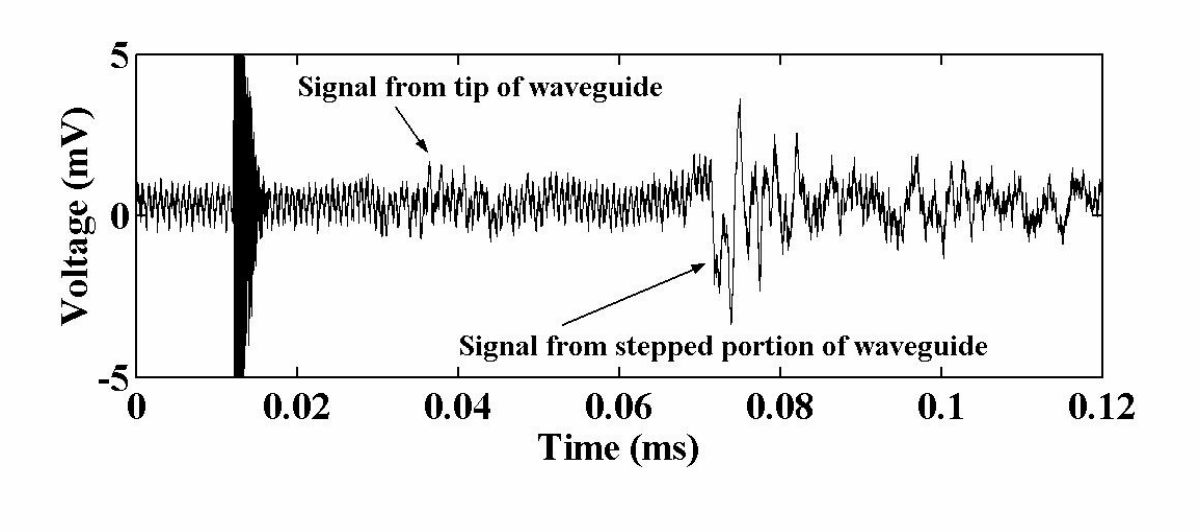

Figure 3. Experimental signal.

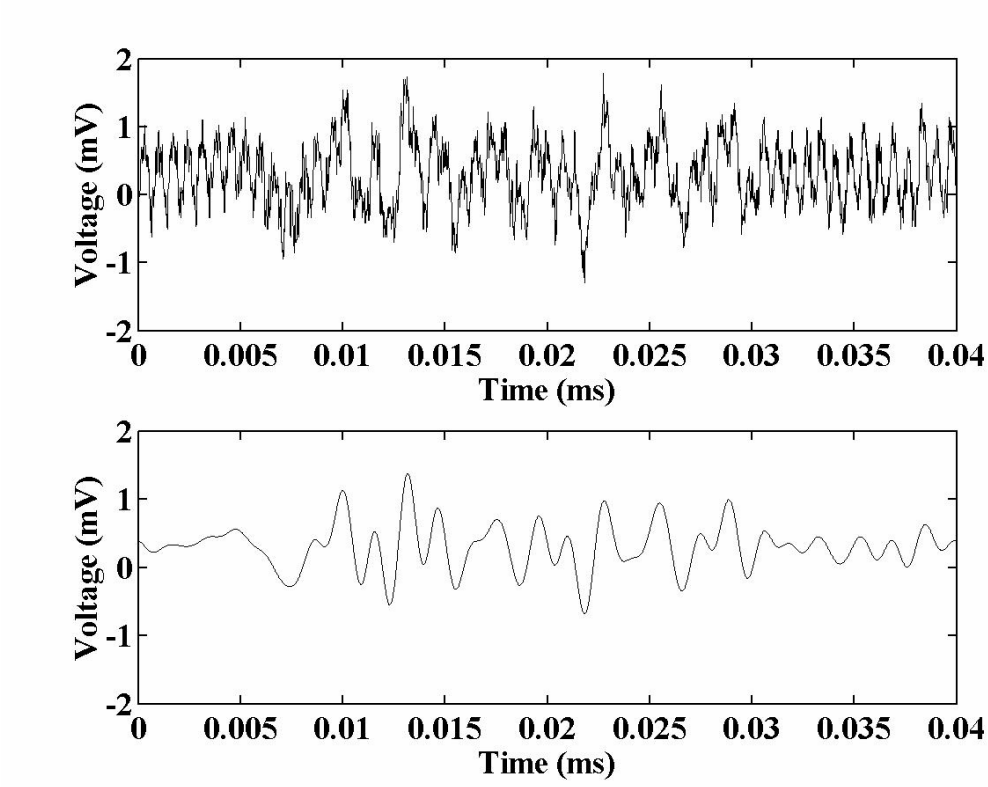

Figure 4. Experimental signal from the tip of the waveguide, before and after filtering.

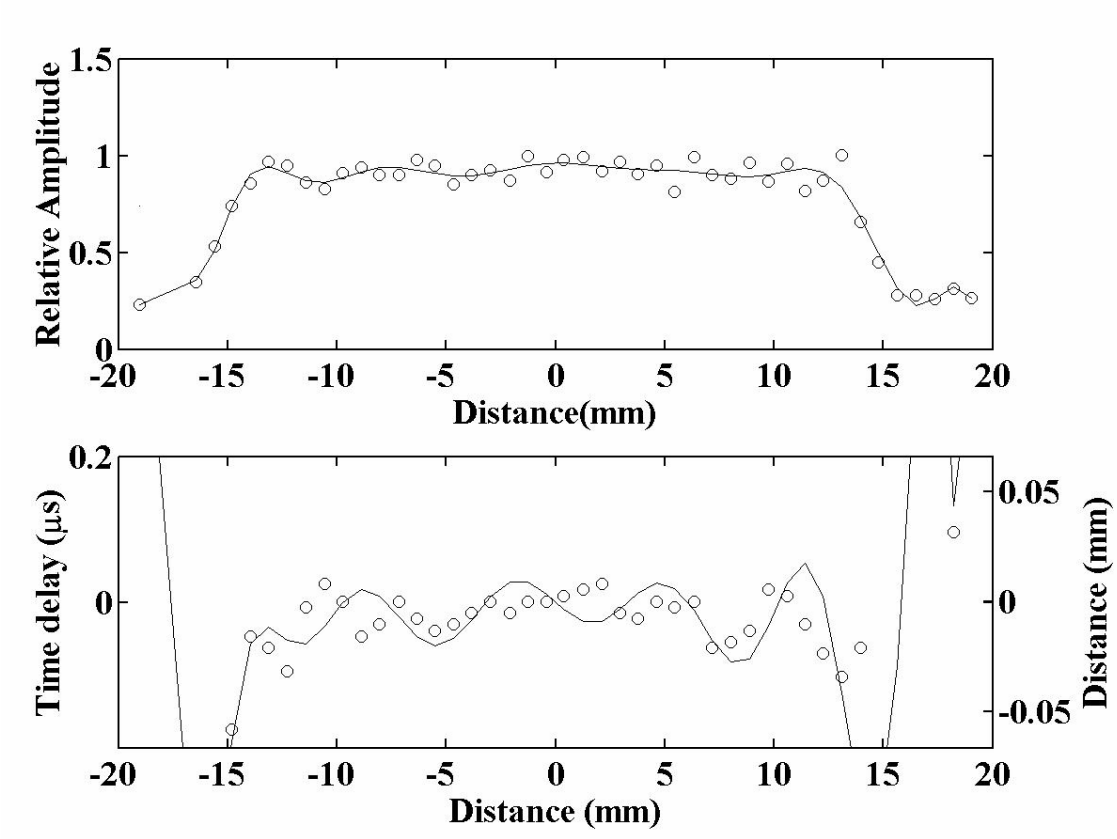

Figure 5. Experimental results.

2.1.4 Fidelity of an Analytical Time Reversal Mirror

A. D. Puckett and M.L. Peterson, "Fidelity of an Analytical Time Reversal Mirror" in *Review of Progress of Quantitative Nondestructive Evaluation, Vol. 21,* American Institute of Physics, Melville NY, 2002, p. 945-952.

Abstract. A time reversal mirror process was used with a solid circular cylindrical waveguide to remove the effects of dispersion. The first three longitudinal modes were considered. An analytic transfer function was developed to predict the time-reversed signal from an input signal. The analytic transfer function was applied to the time-reversed signal to reproduce the original input signal. Experiments were then performed to demonstrate the fidelity of the analytical model. Results of the comparison were reasonable and showed the potential of the approach for use with a high temperature ultrasonic buffer rod.

2.1.4.1 INTRODUCTION

Solid circular waveguides have been used in ultrasonic non-destructive testing and high strain rate testing for over fifty years [1]. For most practical applications the waveguide geometry is combined with appropriate excitation frequencies so that the waveguide approaches one of the two limit conditions: a long thin bar or a disk. However, for a number of applications, the geometry and excitation frequencies are constrained in a manner that one of the limit conditions cannot be satisfied. In those situations multiple dispersive modes may be propagated in the waveguide. One application where these types of waveguides have been used is the determination of material properties at high temperature [2]. Because of the temperature limitations on piezoelectric transducers, waveguides (buffer rods) are used between the transducer and the sample to isolate the transducer from the high temperature. The transmitted ultrasonic signal incorporates the effects of the waveguides as well as the sample.

Using a time reversal mirror the effects of the waveguides can be eliminated from the system response to produce a signal that looks like a transducer that is in direct contact with the specimen. In this paper the time reversal mirror is explored analytically as well as experimentally. Modeling of the dispersion in the cylindrical rod will provide insight in the time reversal process and will make the measurement system more robust.

2.1.4.2 Time Reversal Theory

Time reversal theory utilizes the time reversal invariance of particle physics [3]. When the white particle collides with the black particles they will travel apart (Figure 1). If time is stopped and then reversed the particles will come back to the original configuration with the exception of the white particle traveling away from the black particles. Alternatively, if time is stopped and then the velocity vectors of the particles are reversed, the same scenario will result with the white particle traveling away from the black particles. Thus, reversal of time still obeys the fundamentals of particle physics.

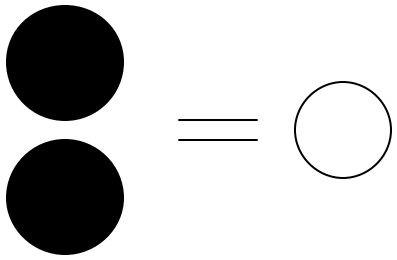

FIGURE 1. A diagram illustrating an impending particle interaction. The white particle is traveling at a velocity towards the stationary black particles. This is a time invariant system.

On a macroscopic scale, modeling particles is not practical due to the shear number of objects. Waves represent a more useful system model on the macroscopic scale. Less information is required to represent the physics of the wave based system. A propagating wave can be described by the frequencies and amplitudes of the frequencies.

The time reversal mirror process consists of three parts that are analogous to the particle example. A source emits an acoustic wave. An alternate location(s) observes and records the wave field versus time. Between the source and the observer reflections, refraction, dispersion and other phenomena alter the wave. The signal of the received wave field is then reversed in time and emitted from the observation point. The original emitted wave field can then be measured at the original source. However, the new wave field is reversed in time compared to the original wave field just like the reversed particle was traveling in the opposite direction in the

previous example. The time reversal mirror process has been demonstrated in different mediums and used in several applications [3-9].

The time reversal mirror can be applied to circular cylindrical waveguides with an added advantage. The rod is symmetric about a plane perpendicular to the central axis at a point half way down the length of the rod. An acoustic signal will be altered identically regardless of the end from which the signal is sent. Therefore, the received signal can be reversed and sent from the source again.

The time reversal mirror may be better understood from a physical explanation. When a bar is excited by a broadband signal at one of its ends the dispersed signal can be measured at the other end. The dispersed signal consists of the frequencies and modes with faster group velocities arriving earlier in time and the frequencies and modes with slower group velocities arriving later in time. By reversing the dispersed signal in time and exciting the bar with the reversed signal the slower frequencies and modes are excited first and the faster frequencies and modes are excited last. Thus, physically the faster frequencies and modes will catch up to the slower ones. As a result of time invariance, the signal will look like the reverse of the original reference signal.

2.1.4.3 Analytical model

An analytical model of a longitudinal wave propagating through an axially symmetric solid circular cylindrical rod must include the change of the signal due to the dispersion in the bar. The dispersion is a function of frequency; therefore, the modeling must be performed in the frequency domain. A similar model was developed previously as an analytical exercise [10].

The dispersed signal can be represented as the inverse Fourier transform of the frequency spectrum of the dispersed signal:

$$x_d(t) = \int_{-\infty}^{\infty} X_D(w) \exp(iwt) dw \,. \qquad (1)$$

where $x_d(t)$ is the dispersed signal in the time domain and $X_D(?)$ is the dispersed signal in the frequency domain. For the geometry and frequencies in question, multiple modes propagate. The term signal will now be used to refer to the signal in the frequency domain, unless otherwise noted. The dispersed signal can be represented by the summation of all of the propagating modes multiplied by a relative amplitude factor, A_i:

$$X_D(w) = \sum_{i=1}^{M} \overline{A}_i(w) X_{Di}(w). \tag{2}$$

Additionally, each of the propagating modes can be represented by the reference signal, $X_R(?)$ times a dispersion function, $\tilde{A}_i(?)$:

$$X_{Di}(w) = \tilde{A}_i(w) X_R(w). \tag{3}$$

The dispersed signal in the time domain is now represented by

$$x_d(t) = \int_{-\infty}^{\infty} \left[\sum_{i=1}^{M} \overline{A}_i(w) \tilde{A}_i(w) X_R(w) \right] \exp(iwt) dw. \tag{4}$$

For the convenience of digital processing, the signal can be represented discretely.

$$x_d(n) = \frac{1}{N} \sum_{m=0}^{N-1} \left[\sum_{i=1}^{M} \overline{A}_i(m) \tilde{A}_i(m) X_R(m) \right] \exp(inm(2p / N)). \tag{5}$$

At this point the discrete dispersed signal in the time domain is represented as the inverse discrete Fourier transform of the sum of the modes, 1 to M. Each mode is represented by the multiplication (in the frequency domain) of the reference signal, the dispersion function for that mode, and the relative amplitude of that mode.

The dispersion function, $\tilde{A}_i(?)$, is actually just a phase term representing the time delay of the signal at that frequency. The time delay can be found from the distance of propagation and the phase velocity of the mode at that frequency. The best way to understand the phase term is to first consider the non-dispersive case. A linear time delay, n_0, results in a phase shift in the frequency spectrum. The delayed spectrum can be represented as the original spectrum times a phase shift.

$$\begin{aligned} &DFT\{x(n)\} = X(m). \\ &DFT\{x(n-n_0)\} = X(m) \exp(-imn_0(2p / N)). \end{aligned} \tag{6}$$

For a phase velocity that is constant with respect to frequency the discrete time delay, n_0, can be represented as the length of the bar, D, divided by the constant phase velocity, c_0, divided by the time interval, ?t.

$$n_0 = (D / c_0) \Big/ \Delta t. \tag{7}$$

For the dispersive case each mode can have a different phase velocity for each frequency. The time delay becomes:

$$n_i(m) = \left[D / c_i(m) \right] \Big/ \Delta t \tag{8}$$

where $c_i(m)$ is the phase velocity, a function of the discrete frequency increment, m, for mode i. The phase term is now of the form:

$$\tilde{A}_i = \exp\left(im \left[D / c_i(m) / \Delta t \right] (2p / N) \right). \tag{9}$$

Each of the modes also has a relative amplitude, A_i, that depends on the frequency. In order to determine the relative amplitudes of the modes, boundary conditions must be applied. The orthogonality relations for a circular cylindrical bar are complex. Rather than expanding directly on the terms of the basis functions, the end conditions can be viewed as n equations with n unknowns. The pressure, P, on the end of the bar that excites the longitudinal waves can be obtained [10]. The normal stress, T_{zz}, associated with each mode can also be calculated. By summing the stresses at a number of points along the radius of the bar and setting the sum equal to the applied pressure at the same points, a set of equations is produced.

$$P_j = \sum_{i=1}^{M} \overline{A}_i \mathrm{T}_{zz}(l_i, r_j). \tag{10}$$

In matrix form the relative amplitudes can be calculated by taking the inverse of the stress matrix. The number of modes determines the number of equations.

$$\{P\} = [T_{zz}]\{\overline{A}\} \Rightarrow \{\overline{A}\} = [T_{zz}]^{-1}\{P\}. \tag{11}$$

The final representation of the dispersed signal is of the form:

$$x_d(n) = \frac{1}{N} \sum_{m=0}^{N-1} \left[\sum_{i=1}^{M} \overline{A}_i \exp\left(im[D / c_i(m) / \Delta t](2p / N) \right) X_R(m) \right] \exp\left(inm(2p / N) \right). \tag{12}$$

This equation represents the dispersed signal obtained for a particular reference signal given a distance of propagation. For the time reversal process a dispersed signal is calculated from the reference signal. The dispersed signal is reversed in time. The reversed signal is then input into the model as the new reference signal. The resulting signal is a mirror image of the original reference signal.

2.1.4.4 Analytical Results

To demonstrate the validity of the model, a reference signal was modeled for a specific rod. The geometry was chosen for comparison to experimental results. The rod was made of fused quartz with a length of 485 mm and a radius of 5 mm. The reference signal was a

Gaussian broadband signal centered at 500 kHz with 6dB defined bandwidth limits of 200 kHz and 800 kHz. For this test three modes were excited. At the highest frequencies the fourth mode was also excited, but for practical purposes only the first three modes were propagated. The first two modes are both dilatational and the third mode is transverse. For all three modes the shear term of the normal stress is several orders of magnitude less than the longitudinal term, so the shear term was ignored for simplicity. For the analytical model the pressure on the end of the bar was set equal to a constant at all points.

Figure 2 illustrates the accuracy of the model. The top signal in Figure 2 is the original reference signal. The middle signal is the dispersed signal calculated by the model from the reference signal. Finally the bottom signal is produced from modeling the dispersion of the reversed dispersed signal. For this paper, this signal will be referred to as the final signal. The signal has been reversed in time again for comparison to the original reference signal and compares favorably to the original reference signal.

2.1.4.5 Experimental Results

For comparison to the analytical results, experiments were also performed. The experiments were performed on a fused quartz rod with properties that were identical to the model. The experimental set up is shown in Figure 3. The configuration consisted of an arbitrary function generator connected to a transducer through a power amplifier. A signal was propagated down the quartz rod to another transducer. This transducer was connected to an oscilloscope through a pre-amp. The transducers were 38 mm in diameter. Signals similar to those from the analytical model were obtained from the experiments. Figure 4 shows the signals. The top signal is the signal used to excite the bar. It is the same broadband Gaussian that was used in the analytical results. The second signal is the dispersed signal measured at the opposite end of the bar from the excitation signal. The bottom signal (final signal) is the signal produced from the dispersed signal reversed in time used as the excitation signal. The final signal was reversed in time again for comparison to the original signal. The fidelity of the signal reconstruction demonstrates the potential utility of the time reversal mirror process for use in waveguides.

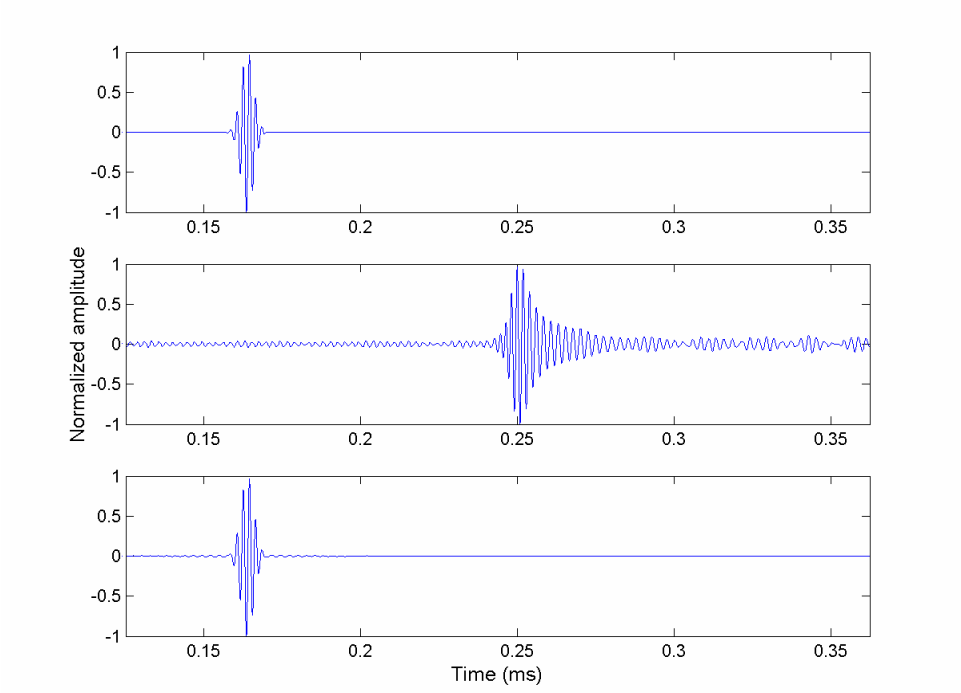

FIGURE 2. Results from the analytic model. Top signal: original reference signal. Middle signal: dispersed signal calculated from the original reference signal and the analytic model. Bottom signal: signal calculated by the model from the dispersed signal reversed in time; this signal has been reversed in time for comparison to the orignal reference signal.

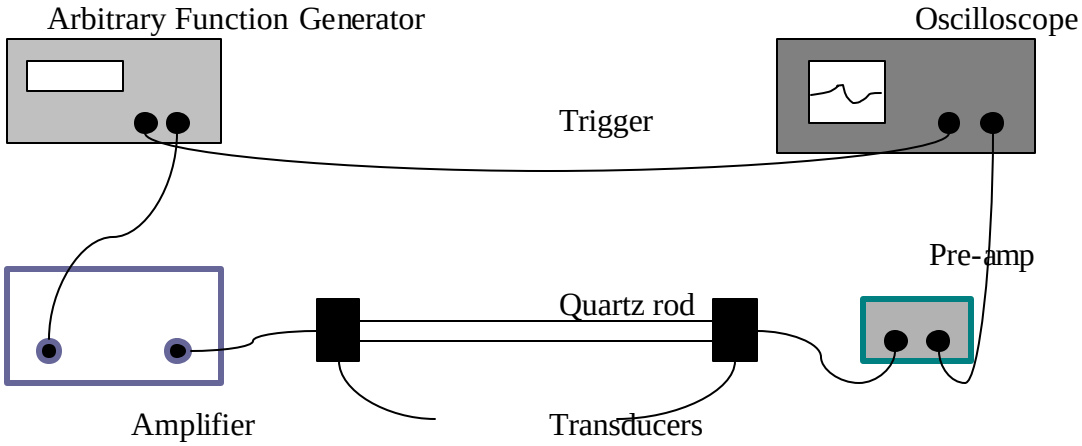

FIGURE 3. Diagram of the experimental setup. The quartz rod is excited by a transducer powered by an arbitrary function generator through a power amplifier. The transmitted signal is measured by another transducer and recorded on the oscilloscope

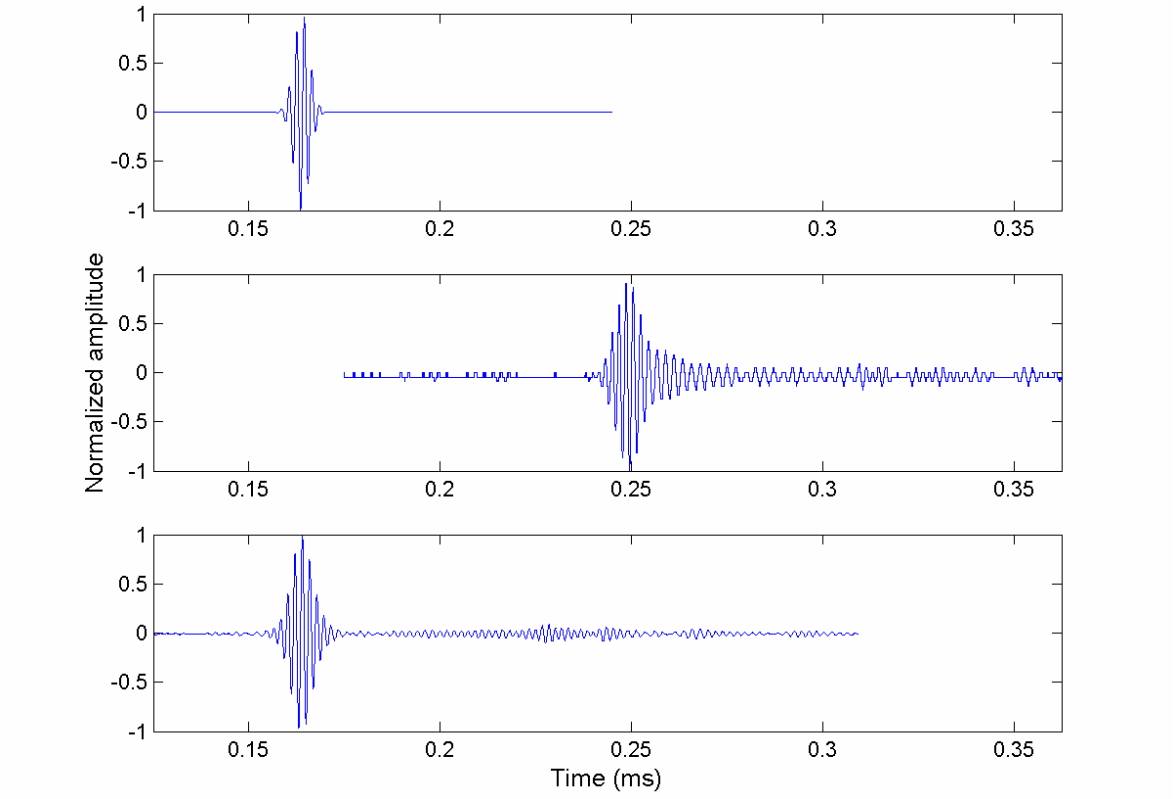

FIGURE 4. Results from the experiments. Top signal: original excitation signal. Middle signal: dispersed signal from the original excitation signal propagated through the bar. Bottom signal: signal recorded from the propagation of the dispersed signal reversed in time; this signal has been reversed in time for comparison to the original reference signal.

For a final validation of the analytical model, the experimental and analytical results were compared. Figure 5 compares the dispersed signal calculated by the analytical model to the dispersed signal measured experimentally. Figure 6 compares the final signals from the analytical model and experiment. The lower signal, representing the experimental signal, has a larger time signature than the analytical signal. This corresponds to a frequency spectrum with a narrower band. The narrower band response is due to the band-limited characteristics of the transducers that are not included in the present analytical model.

CONCLUSIONS

It has been demonstrated that a time reversal mirror process can be used in a solid waveguide with a circular cross-section. Reasonable results are obtained, although inclusion of

the transducer response characteristics is required. Experimentally the reversed signal can be used as an excitation signal to produce a transmitted signal with a compact time signature. The analytical model accurately represents the dispersive effects of the first three longitudinal modes in a solid cylindrical bar. A reasonable comparison to the experimental results was obtained.

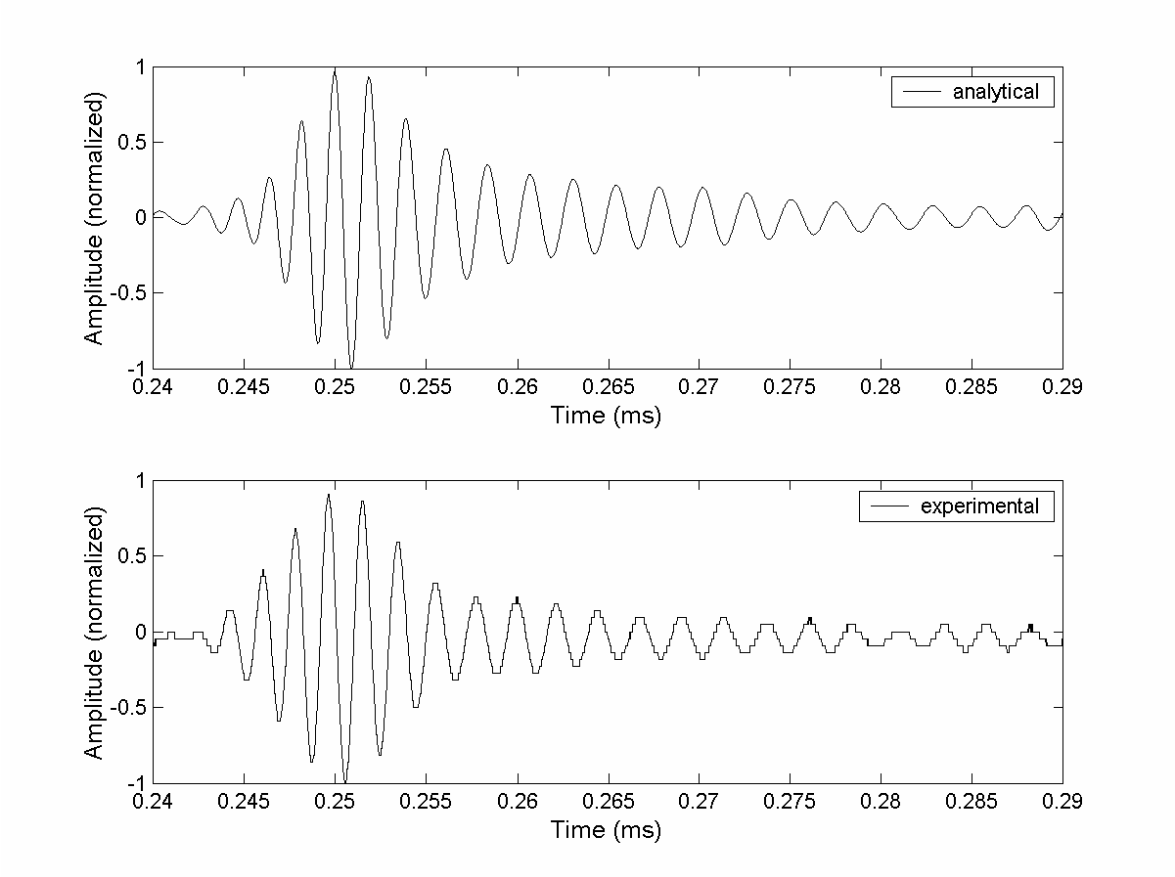

FIGURE 5. Comparison of the dispersed signals from the same reference signal. Top signal: analytical dispersed signal. Bottom signal: experimental dispersed signal.

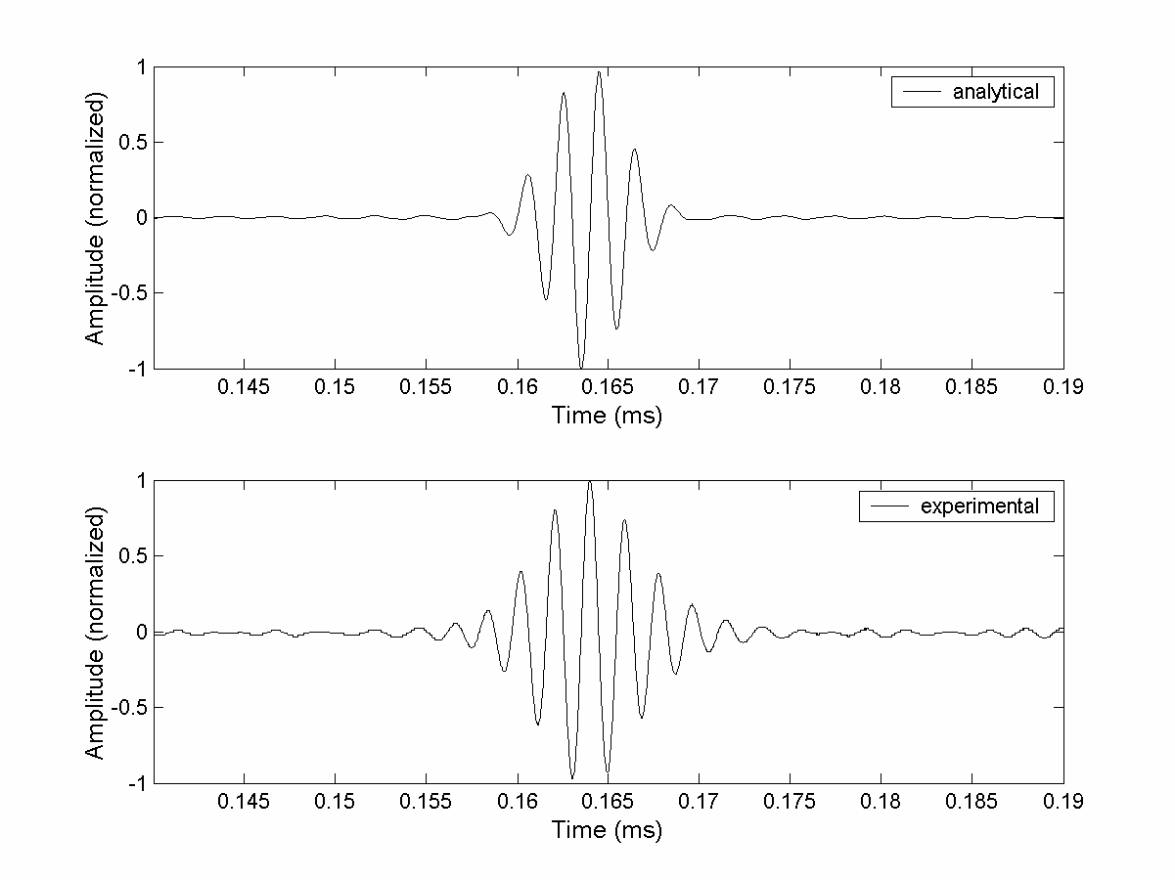

FIGURE 6. Comparison of the final signals. Top signal: analytical final signal. Bottom signal: experimental final signal. Both techniques used the appropriate reversed dispersed signal for the input. Both signals are reversed in time.

2.1.4.6 REFERENCES

1. Davies, R. M., *Trans. Royal Soc. (London)* A240, 375-457 (1948).

2. Schreiber, E., Anderson, O. L. and Soga N., *Elastic Constants and Their Measurements*, McGraw-Hill, New York, 1973, pp. 77-79.

3. Fink, M., *Physics Today* **50**(3), 34-40 (1997).

4. Draeger, C. and Fink, M., *Phys. Rev. Lett.* **79**(3), 407-410 (1997).

5. Draeger, C., Cassereau, D. and Fink, M., *J. Acoust Soc. Am.* **102**(3), 1289-1295 (1997)

6. Ing, R. K. and Fink, M., *IEEE Trans. Ultrason. Ferroelectr. Freq. Control* **45**(4), 1032-1043 (1998).

7. Prada, C. and Fink, M., *Wave Motion* **20**, 151-163 (1994).

8. Chakroun, N., Fink, M. and Wu, F., *IEEE Trans. Ultrason. Ferroelectr. Freq. Control* **42**(6), 1087-1097 (1995).

9. Roux P., Roman, B. and Fink, M., *Appl. Phys. Lett.* **70**(14), 1811-1813 (1997).

10. Peterson, M. L., "A High Temperature Ultrasonic Process Monitoring System Utilizing Signal Processing to Separate Multiple Waveguide Modes", Ph.D. diss., Northwestern University, 1994.

2.1.5 Analytical model for predicting multiple propagating radially symmetric modes in cylindrical waveguides

A. D. Puckett and M.L. Peterson, "Analytical model for predicting multiple propagating radially symmetric modes in cylindrical waveguides" submitted to *Ultrasonics,*

Abstract: An analytical model for multiple mode wave propagation in a finite solid cylindrical waveguide is presented. The analytic model is designed around a general experimental configuration and considers three parts, the excitation of the ultrasonic signal in the waveguide, the propagation of the signal through the waveguide and the reception of the ultrasonic signal. The model uses the eigenvalues (phase velocities) and eigenfunctions (normal stresses) of the longitudinal modes calculated by the Pochhammer-Chree equations to calculate a transfer function for each of the propagating modes. The relative amplitudes of the modes are determined at each frequency by the boundary conditions on the end of the waveguide. Each mode has a phase shift at each frequency based on the length of the waveguide and phase velocities. The amplitude and phase shift determine the transfer function of each mode. The sum of these transfer functions is the transfer function of the waveguide, which can be used to predict the change of a signal. Results are presented from different size waveguides that demonstrate the ability of the model to capture the physics of the experimental configuration.

2.1.5.1 Introduction

Solid cylindrical waveguides have been used as buffer rods in a number of applications to isolate ultrasonic sensors from hostile environments (Jen *et al.* 1991, Jen *et al.* 1997, Peterson 1994). In some cases, design constraints necessitate the use of large diameter waveguides, which propagate multiple modes (Peterson 1994). The propagation of multiple modes causes a signal that is compact in the time domain to have a large time signature after propagating through the waveguide, Figure 1. As a result, if the acoustic signal is propagated through a specimen, as well as a buffer rod, measurement of phase velocity and attenuation information in the specimen are difficult. To help interpret acoustic signals of this nature an analytical model for longitudinal wave propagation in finite solid cylindrical waveguides has been developed.

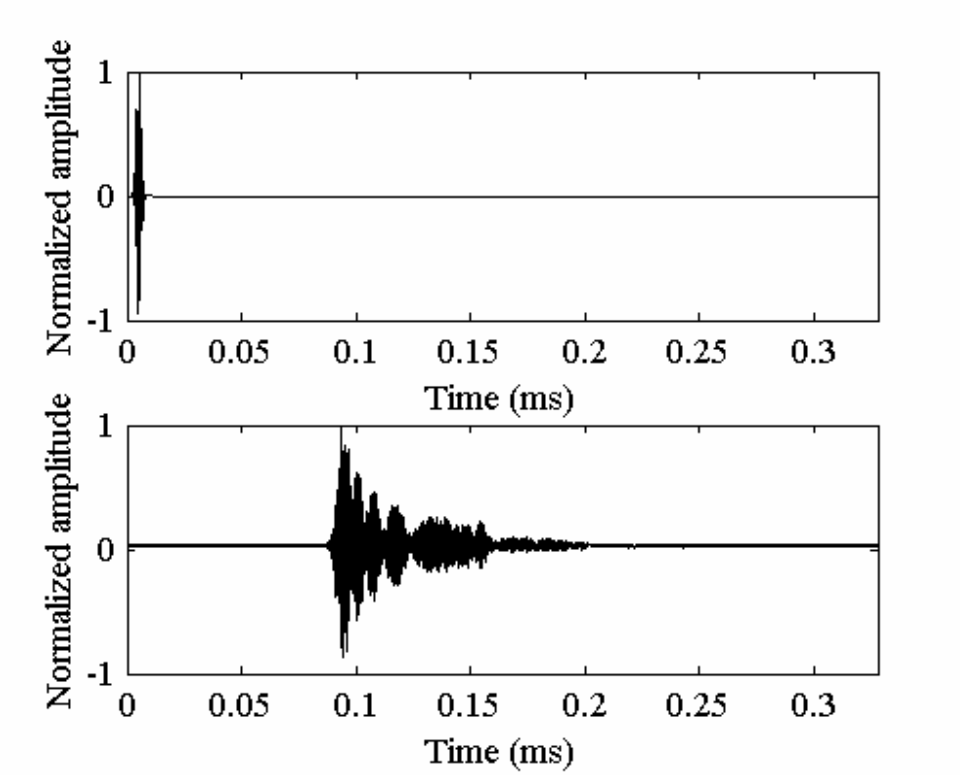

Figure 1. Illustration of dispersion in a cylindrical waveguide. The top graph is the original signal with compact time domain. The bottom graph is the original signal after propagating through the cylindrical waveguide used in this research.

Two methods have been used to develop analytical models for predicting the wave propagation through a finite cylindrical bar. The first method uses the eigenvalues and eigenfunctions of the modes based on the theory developed by Pochhammer (1876) and Chree (1889) for an infinite cylindrical bar. The coefficients in the eigenfunction expansion determine the relative amplitudes of the propagating modes, and the eigenvalues determine the phase shift. The second method solves the boundary value problem for a semi-infinite cylindrical rod subjected to an initial condition. An integral transform technique is used to solve these equations.

The integral transform technique has been used by a number of authors for different initial conditions. Skalak (1957) used the technique to model the collision of two semi-infinite bars. Vales *et al.* (1996) completed the exact solution started by Skalak and extended Skalak's decomposition to the near field with extensive numerical calculations. Folk *et al.* (1958) investigated a single semi-infinite bar with mixed end conditions excited by a step function.

These results compared well at distances greater than 20 bar diameters to experiments conducted by Curtis and Fox (1958) for a cylinder with pure end conditions. The pure-end condition problem was solved by Goldberg and Folk (1993) who extended the method of Folk *et al*. These results also agree well with the experimental work of Curtis and Fox. For large distances the approximate solutions for wave propagation in cylindrical waveguides developed by the integral transform method are representative of experiments.

The method based on the eigenvalues and eigenfunctions of the Pochhammer-Chree theory has not provided as good approximate solutions for wave propagation in cylindrical waveguides as the integral transform method, but it has not been developed as extensively either. Davies (1948) modeled the propagation of a trapezoidal signal (first mode only) in a finite bar using the eigenvalues (phase velocities) predicted by the Pochhammer-Chree theory and a Fourier decomposition. Zemanek (1962) considered multiple modes in an eigenfunction expansion to calculate the reflection coefficients of a continuous train of waves off of the free end of a semi-infinite cylinder. The coefficients in the eigenfunction expansion were determined by solving a system of equations equal to the number of modes considered.

The orthogonality conditions are typically used to determine the coefficients in an eigenfunction expansion; however, the orthogonality conditions for a cylinder with stress free lateral boundary conditions are quite complicated. The orthogonality conditions have been developed for the elastostatic case by Power and Childs (1971) and more completely by Fama (1972). Fraser (1975) extended Fama's solutions to the elastodynamic case. The complexity of the orthogonality conditions makes alternate methods desirable for determining the coefficients.

Peterson (1999) used a system of equations to determine the coefficients for consideration of a finite cylindrical waveguide with a broadband excitation. A Fourier decomposition was used to determine the phase shift of each mode. Peterson's model predicted the shape generally fairly well. Puckett and Peterson (2002) refined the model by calculating the relative mode amplitudes at each frequency; however, the receiving end conditions were still not modeled. Calculated signals were very similar to experimental signals.

Integral transform models predict well the response of a waveguide to a step function excitation. It has been demonstrated that near field calculations can be made that compare well to the understanding of a step wave propagation. Additionally, it was shown that the solutions are independent of the end conditions at large distances. Jones and Norwood (1967), and

Kennedy and Jones (1969) found the difference in peak values was insignificant at distances over 20 diameters, and the difference in average values was insignificant at distances of 5 diameters. They discussed this small difference in terms of a dynamic Saint-Venant's principle. Most of the integral transform solutions and associated experiments looked solely at the response to a step function because of the simplicity of the transforms and of the interest experimentally in modeling the Split Hopkinson Pressure Bar (SHPB). However, an analytical model is needed for acoustic signals used in ultrasonic nondestructive evaluation. These signals are arbitrary broadband signals that are not easily described by analytical functions.

The eigenfunction/eigenvalue technique used by Davies, Zemanek, and Peterson lends itself more easily to end conditions with arbitrary stress functions in both time and space. Additionally, the equations associated with this analytical model are all based on the Pochhammer-Chree theory. Although this technique does not model the pure end conditions associated with the experiments, for large distances the model is also independent of the end conditions as was observed with the integral transform technique. The eigenfunction/eigenvalue technique is the basis for the analytical solution described in this paper. The technique has been refined to more accurately represent the experimental conditions for solid waveguides used for nondestructive testing. Signals calculated by the model are compared to experimental data, and the model is shown to be useful for calculating the necessary time-reversed signal to produce a signal with compact support in the time domain. Additionally, the analytic model provides more insight into the propagation of multiple mode dispersive signals in a cylindrical waveguide and improves the basic understanding of longitudinal wave propagation in cylindrical waveguides.

2.1.5.2 Analytical Model for Longitudinal Wave Propagation

The analytical model presented in this paper is designed as a tool for predicting and interpreting experimental signals, so the model is based on a general experimental configuration. The experimental setup associated with the waveguide consists of an ultrasonic contact transducer that excites the acoustic signal in the waveguide, the waveguide, and another ultrasonic contact transducer for receiving the acoustic signal. The excitation, propagation, and reception of the ultrasonic signal are each described by a part of the model. Therefore, for a given input signal the model predicts the output signal at the opposite end of a specific

waveguide. The model uses the eigenvalues and eigenfunctions of the Pochhammer-Chree theory for an infinite cylinder to predict the output signal.

2.1.5.3 Pochhammer-Chree theory

The Pochhammer-Chree theory describes elastic wave propagation in an infinite isotropic homogeneous solid circular cylinder. The frequency equation is the primary result obtained from the Pochhammer-Chree theory. Using the notation of Achenbach (1999) in standard cylindrical coordinates, it is expressed as:

$$\frac{2p}{a}(q^2+k^2)J_1(pa)J_1(qa)-(q^2-k^2)J_0(pa)J_1(qa)-4k^2pqJ_1(pa)J_0(qa)=0, \qquad (1)$$

where J_0 and J_1 are Bessel functions of the first kind of order zero and one respectively,

$$p^2=\frac{w^2}{c_L^{\,2}}-k^2 \text{ and } q^2=\frac{w^2}{c_T^{\,2}}-k^2, \qquad (2)$$

k is the wavenumber (equal to *?/c*), *?* is the circular frequency, a is the radius of the cylinder, c_L is the velocity of longitudinal waves in an unbounded medium, c_T is the velocity of transverse waves in an unbounded medium, and c is the phase velocity. The roots of the frequency equation define wavenumbers, and these are the eigenvalues. At any frequency there are an infinite number of roots that satisfy the frequency equation. Each real root is associated with a propagating mode. There are also complex and imaginary roots corresponding to complex and imaginary modes, which do not propagate but are excited to satisfy an arbitrary excitation pressure distribution. The roots of the frequency equation are typically illustrated by dispersion curves, which relate the frequency to the eigenvalues/roots in the form of the wavenumber or the phase velocity. Figure 2 shows an example of the phase velocity curves associated with the propagating modes. The frequency dependence of the eigenvalues and the dispersive nature of the modes are apparent.

The eigenfunctions are also dependent on the frequency as well as the eigenvalues and the radius. There are four eigenfunctions associated with each eigenvalue. The eigenvalue $k^{(j)}$ is associated with the eigenfunctions, $s^{(j)}_{zz}$, the normal stress, $s^{(j)}_{rz}$, the shear stress, $w^{(j)}$, the normal

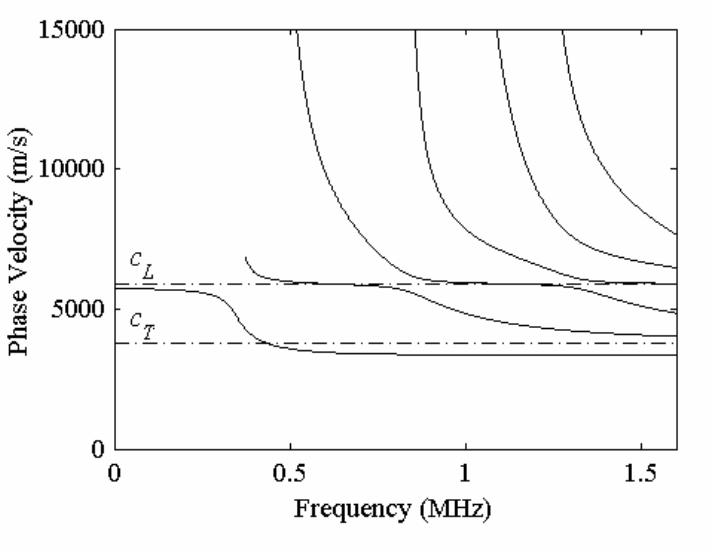

Figure 2. Phase velocity curves for a 10-mm diameter fused quartz waveguide.

displacement, and $u^{(j)}$, the radial displacement (Fraser 1975). The Pochhammer-Chree theory defines the form of the eigenfunctions in cylindrical coordinates as:

$$u^{(j)} = -[pJ_0(pr) + iC^{(j)}k^{(j)}J_1(qr)], \tag{3}$$

$$w^{(j)} = ik^{(j)}J_0(pr) + C^{(j)}qJ_1(qr), \tag{4}$$

$$s_{zz}^{(j)} = -J_0(pr)[l(p^2 + (k^{(j)})^2) + 2m(k^{(j)})^2] + 2mC^{(j)}iqk^{(j)}J_0(qr), \tag{5}$$

$$\text{and } s_{rz}^{(j)} = -[2ik^{(j)}pJ_1(pr) + C^{(j)}(q^2 - (k^{(j)})^2)J_1(qr)], \tag{6}$$

$$\text{where } C^{(j)} = \frac{-2ik^{(j)}pJ_1(pa)}{(q^2 - (k^{(j)})^2)J_1(qa)}, \tag{7}$$

? and μ are the Lamé constants, r is the radial coordinate, and z is the axial coordinate.

The eigenfunctions are also referred to as mode shapes. An illustration of the change in mode shape as a function of frequency is shown in Figure 3. The normalized amplitude of the normal stress is plotted at regular intervals of frequency. The dashed line represents a value of zero stress. The change of the eigenfunctions dictates that an eigenfunction expansion is needed at every frequency in the analytical model.

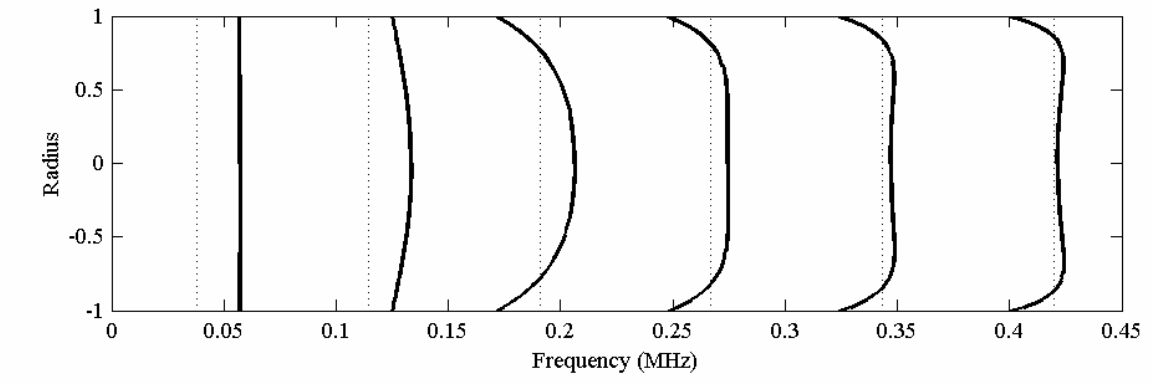

Figure 3. Illustration of frequency dependence of normal stress. The normalized normal stress is plotted at different frequencies. The vertical dashed lines represent zero stress.

2.1.5.4 Parts of the Model

The frequency dependence of the Pochhammer-Chree theory makes it more convenient to perform all of the operations of the analytical model in the frequency domain. All operations are conducted in the frequency domain unless noted otherwise. The time representation of the dispersed signal, $x_d(t)$, that has propagated through the waveguide can be represented as the inverse Fourier transform of the frequency spectrum of the signal, $X_D(?)$, Eq. (8) (Peterson 1999).

$$x_d(t) = \int_{-\infty}^{\infty} X_D(w)\exp(iwt)dw \tag{8}$$

The calculated dispersed signal can be represented by the input reference signal, $X_R(?)$, multiplied by a dispersion function, $F_D(?)$, Eq. (9).

$$X_D(w) = X_R(w)F_D(w) \tag{9}$$

The dispersion function is a transfer function that represents the dispersion in the waveguide, and it is the sum of the transfer functions of the propagating modes. The transfer function of each mode is influenced by the three parts of the experimental setup: the transmission from the exciting transducer to the waveguide, the propagation through the waveguide, and the transmission from the waveguide to the receiving transducer. These three parts describe the propagation of a single mode in a cylindrical waveguide and contribute to the dispersion function, $F_D(?)$, of the waveguide. The transfer function of each mode has a phase shift and an amplitude factor for each frequency, $?$. The phase information is determined from the

propagation of the mode through the waveguide. The amplitude information is determined from the boundary conditions on both ends of the cylindrical rod.

2.1.5.5 Excitation

The distribution of the excitation across the radius of the waveguide is used to determine the relative amplitudes of the propagating modes in the eigenfunction expansion. For this model the excitation transducer exhibits a pressure on the end of the waveguide. The shape of this pressure, P, is the end condition in the eigenfunction expansion, Eq. (10), where the eigenfunctions are defined by the normal stress, s_{zz}, across the radius.

$$P = \sum A^{(j)} s_{zz}^{(j)} \tag{10}$$

where $A^{(j)}$ and $s^{(j)}_{zz}$ are associated with the wavenumber $k^{(j)}$.

There are a number of approaches to calculating the coefficients, $A^{(j)}$, in the expansion. The first choice is to use the orthogonality relations of the eigenfunctions. These relations have been developed by Fama (1972) for the elastostatic case, and Fraser (1975) demonstrated that the relations also applied to the elastodynamic case. The orthogonality condition for a cylinder with stress free lateral surfaces is expressed as:

$$\int_0^a (w^{(j)} s_{zz}^{(l)} - s_{rz}^{(j)} u^{(l)}) r dr = 0 \quad j \neq l \qquad \text{(Fraser 1975, Eq. 17)} \tag{11}$$

For the case of pure stress end conditions with the stresses specified as $s_{zz} = s_0$ and $s_{rz} = t_0$ the coefficients in the eigenfunction expansion are shown to be coupled, Eq. (12) (Fama 1972, Eq. 10).

$$A^{(j)} = \frac{\int_0^a \left\{ s_0 w^{(j)} - t_0 u^{(j)} + \sum_l A^{(l)} \left(w^{(l)} s_{zz}^{(j)} - u^{(l)} s_{rz}^{(j)} \right) \right\} r dr}{2 \int_0^a \left(s_{zz}^{(j)} w^{(j)} - s_{rz}^{(j)} u^{(j)} \right) r dr} \tag{12}$$

This complex relation is not unexpected since the solution for a semi-infinite cylinder with pure end conditions is complicated (Goldberg and Folk 1993). Fama (1972) shows there is a unique solution for the coefficients in the pure end condition problem.

Zemanek (1962) used a much simpler method to solve for the coefficients, a system of equations. At equally spaced points the eigenfunction expansion, Eq. (10), was evaluated to

create a number of equations that were functions of the coefficients. The number of modes being considered determined the number of equations needed to solve the coefficients. This technique works well when a large number of modes are being considered. However, at the lower frequencies there is only one real mode and only one equation. With only one equation, the accuracy of the coefficient is suspect, so complex modes should probably be considered.

The logical compromise between orthogonality and the system of equations is a least squares method, which allows more points to be evaluated and thus the system of equations to be overdetermined. Additionally, the least squares relation can be derived directly from the eigenfunction expansion, Eq. (10), by rewriting the equation to include a residual error, e:

$$P = \sum_j A^{(j)} s_{zz}^{(j)} + e, \text{ or } \quad \{P\} = [s]\{A\} + \{e\}. \tag{13}$$

When the sum of the squares of the residuals is minimized the coefficients can be expressed in matrix notation as:

$$\{A\} = \left[[s]^T [s]\right]^{-1} [s]^T \{P\}. \tag{14}$$

This equation is used to calculate the coefficients for the eigenfunction expansion. These coefficients determine the amplitude of each propagating mode. In the limit as the residual error approaches zero the coefficients are the exact solution.

2.1.5.6 Propagation

The propagation of each mode describes the phase shift for that mode. The phase shift of each mode is entirely determined by the phase velocity of the mode, which is calculated from the Pochhammer-Chree frequency equation. The length of the waveguide divided by the phase velocity is the time for a point of constant phase in a continuous harmonic wave to travel the length of the waveguide. This time delay is a phase shift in the frequency domain. The phase shift is represented as:

$$\Phi^{(j)}(w) = \exp(iwL / c^{(j)}), \tag{15}$$

where $c^{(j)}$ is the phase velocity of mode j at frequency $?$.

2.1.5.7 Reception

The last part of the experiment, the transmission from the waveguide to the receiving transducer, contributes to the amplitude factor of the transfer function of each mode. The

response of the transducer is proportional to the average pressure received over the face of the transducer (Schmerr 1998). The average pressure is calculated by integrating the normal stress over the area of the transducer and dividing by the area. The normal stress is given by the eigenfunction, $s^{(j)}_{zz}$, and is integrated over the area of the waveguide. The average pressure provides additional amplitude information to the transfer function of a mode.

The dispersion function is the sum of the transfer functions of the propagating modes, Eq. (16).

$$F_D(w) = \sum_j A^{(j)}(w) \cdot \Phi^{(j)}(w) \cdot \frac{2}{a^2} \int_0^a r s^{(j)}_{zz}(w, r) dr . \qquad (16)$$

The transfer function of each propagating mode contains a relative amplitude term from the excitation, $A^{(j)}(?)$, a phase shift term from the propagation, $F^{(j)}(?)$, and an additional amplitude term representing the average normal stress. It should be noted that if the phase velocity was constant for all modes and frequencies then the phase shift, $F^{(j)}(?)$, would be a constant, and therefore the dispersion function would reduce to a constant consisting of the phase shift times the average pressure of the excitation. This is the case for a thin bar where only the first mode propagates and the phase velocity is equal to the bar velocity, $c_b = \sqrt{E/r}$.

2.1.5.8 Discretization

The frequency dependence of the Pochhammer-Chree theory makes it useful for the operations of the analytical model to be conducted in the frequency domain. The complexity of the Pochhammer-Chree theory suggests that calculations are best made numerically and thus at discrete frequency intervals. A discrete Fourier transform (DFT) pair, Eqs. (17) and (18), is used to transform between the time domain and the frequency domain. A lowercase letter is used to denote the time domain and an upper case letter is used to denote the frequency domain.

$$F\{x(n)\} \Rightarrow X[m] = \sum_{n=0}^{N-1} x[n] e^{-inm(2p/N)} \qquad m = 0,1,..., N-1. \qquad (17)$$

$$F^{-1}\{X(m)\} \Rightarrow x[n] = \frac{1}{N} \sum_{m=0}^{N-1} X[m] e^{inm(2p/N)} \qquad n = 0,1,..., N-1, \qquad (18)$$

where the index *n* corresponds to time, the index *m* corresponds to frequency, and *N* is the number of points in the DFT.

The substitution of the dispersion function into Eq. (9) and Eq. (9) into the discrete version of Eq. (8) yields the final form of the model,

$$x_d(n) = \frac{1}{N}\sum_{m=0}^{N-1}\left[\sum_j A^{(j)}(m)\cdot\Phi^{(j)}(m)\cdot\frac{2}{a^2}\int_0^a rs_{zz}^{(j)}(m,r)dr\cdot X_R(m)\right]e^{inm(2p/N)}. \qquad (19)$$

The phase shift is represented discretly as:

$$\Phi^{(j)}(m) = \exp(im\lfloor L/c^{(j)}(m)/\Delta t\rfloor(2p/N)), \qquad (20)$$

where $c^{(j)}(m)$ is the phase velocity of mode j at frequency m, and $?t$ is the time step. The operations within the square brackets of Eq.(19) are calculated at each frequency with the eigenvalues and eigenfunctions associated with that frequency.

2.1.5.9 Discussion

Several additional steps help the model perform better. The normal stress eigenfunctions will produce a complex value for most modes at a given radius. If the phase shift is calculated for this complex value and applied to the eigenfunction then the imaginary part will be negligible. The real form of the eigenfunctions simplifies the matrix operations and the integration. Additionally the amplitudes of the eigenfunctions change with frequency; therefore, it is prudent to also normalize the real form of the eigenfunction. For the calculation of the coefficients in the eigenfunction expansion these two steps will simplify the matrix inversion and help prevent the matrix from becoming singular. It is necessary that the same form of the eigenfunctions be used in the eigenfunction expansion and the integration, so that there are no erroneous phase terms added.

The complicated shapes of the eigenfunctions can also cause erroneous calculations in the eigenfunction expansion. It was found that the eigenfunctions of some of the higher modes had similar shapes to other modes near their cutoff frequencies. However, if a mode was not considered until its group velocity was above half the longitudinal wave speed it was found that there were fewer anomalies. From experiments it was observed that the tail end of an ultrasonic signal (i.e. Figure 1) arrives at a time corresponding to approximately one half the longitudinal wavespeed. This corresponds to a phase velocity less than about 1.5 times the longitudinal wavespeed.

The only phase term in the model is determined by the length of the waveguide. Thus the end conditions are the same for any length waveguide with the same diameter and material

properties. Only the calculation of the phase term from the phase velocities is required for a new length waveguide.

2.1.5.10 Experimental comparison of analytical model

Two sets of experiments were performed to validate the analytical model. The signals and the size of the waveguides used in the experiments are representative of ultrasonic NDE experiments (e.g. Jen *et al*. 1997, Peterson 1994). Both sets of experiments considered a through transmission configuration with a pulse excitation. The application of the analytical model is discussed in the description of the experiments.

The experiments used two 38 mm diameter, 1 MHz broadband, longitudinal contact transducers [Panametrics, model V194, Waltham, MA] to excite and receive the ultrasonic signals. The transducers had a bandwidth, corresponding to a 6 dB drop in the peak amplitude of the spectrum, of 0.4 MHz to 1.1 MHz. The transducers have a nearly uniform pressure distribution over the area (Puckett and Peterson 2003). Therefore, the pressure distribution, P, used in the analytical model was prescribed as having a value of unity at all radii and for all frequencies.

Signals were provided by two different sources depending on the experiment. For most of the experiments a pulser/reciever [Panametrics, 5072PR, Waltham, MA] was used to generate a pulse and amplify the received signal. For the time-reversal experiment an arbitrary waveform generator [Agilent 33250A, Palo Alto, CA] was required to generate the complex time-reversed signal to drive the transducer. With this configuration a radio frequency power amplifier [ENI A-300, Rochester, NY] with a gain of 55 dB was used to amplify the signal to the transducer, and the signal generated by the receiving transducer was amplified by an ultrasonic pre-amplifier [Panametrics model 5660C, Waltham, MA] with a gain of 40 dB. For both setups the amplified signal was recorded by a digital storage oscilloscope [Tektronix TDS 520A, Wilsonville, OR].

Waveguides of 10 mm and 25 mm diameter, fused quartz cylindrical rods were used. An amorphous material was chosen for the waveguide because linear elastic and homogeneous assumptions are well satisfied. The properties of the fused quartz rods use in the experiments are a Young's modulus, E, of 72 GPa, a density, ?, of 2200 kg/m3, and a Poisson's ratio, ?, of 0.162. A coupling fluid [Sonotech, Inc. UT-30, State College, PA] was used between the transducers and the waveguide to improve the transmission of the ultrasonic signal.

The transducer excitation in the initial experiments was a pulse. The generated signal is thus primarily a function of the transducers' response. The initial shape of the ultrasonic signal was measured by propagating the pulse through a nondispersive bulk material in place of the dispersive waveguide using the same experimental setup. The discrete Fourier transform (DFT) of this signal is then used as X_R, the reference signal, in the model. The reference signal and its spectrum appear in Figure 4.

2.1.5.11 Long Rod

The first experiment considered a 1.22 m long 10 mm diameter fused quartz waveguide with the pulse excitation of the transducers. At the 1-MHz center frequency the diameter-to-wavelength ratio $d/?_L$ is 1.7, where is $?_L$ is calculated using the longitudinal wavespeed, c_L. For this geometry waveguide the first four modes have cutoff frequencies below the upper 6-dB limit of the frequency spectrum of the signal. The analytical model for this waveguide only considered the real modes. Therefore, at the lowest frequencies only the first mode was considered at each frequency. Additional modes were considered at frequencies above a mode's cutoff frequency.

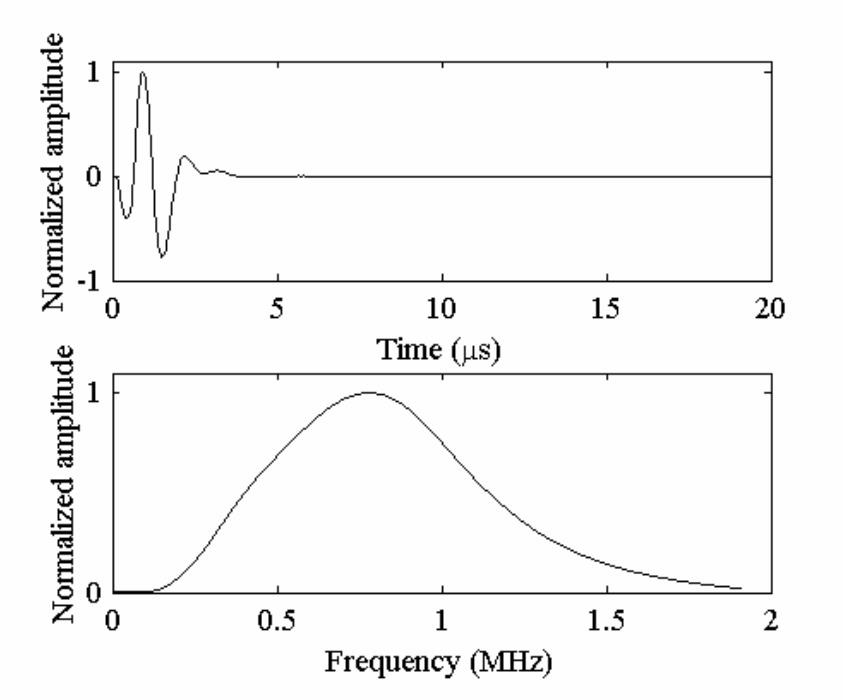

Figure 4. Reference signal used in the experiments. Upper graph is the time domain. Lower graph is the frequency domain.

Dispersion curves (in a wavenumbers vs. frequency domain) were calculated for the real modes at the appropriate frequencies prior to running the model. At each frequency step the eigenvalues and eigenfunctions were used to calculate the complex value of the dispersion function, FD. To evaluate the coefficients in the eigenfunction expansion, A(j), 100 points along the radius were considered. Therefore, in Eq. (14) the pressure, P, is a 100 x 1 column vector, all entries have a value of unity for a constant pressure distribution. The stress is a 100 x j matrix where j represents the number of modes being considered. Each column of the matrix contains the values of the normal stress (Eq. 5) along the radius for one of the modes being considered. For the phase shift, F(j)(?), the length of the rod (1.22m) and the phase velocity is used. The phase velocity is calculated from the eigenvalue by c(j) = ?/k(j). Finally, the average normal stress over the end of the waveguide is calculated for each mode. The coefficient for each mode is multiplied by it's phase shift and average pressure. This product is summed with the products calculated for the other modes to produce the value of the dispersion function for that frequency. These calculations are repeated at each frequency step. The inverse DFT of the dispersion function multiplied by the spectrum of the excitation signal is the calculated dispersed signal.

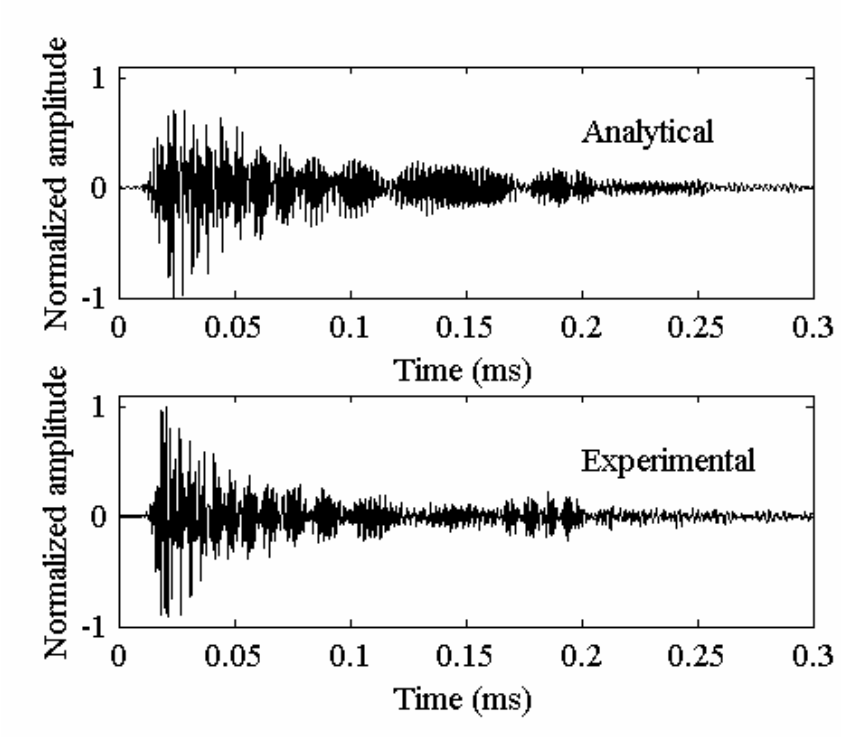

Figure 5. Measured and calculated signals of the reference signal propagating through a 1.22 m long 10 mm diameter fused quartz waveguide.

The calculated dispersed signal is compared to the measured dispersed signal in Figure 5. While the signals have similar shapes some discrepancies are evident. Therefore, it is useful to look at several different domains to compare the accuracy of the model.

One domain in which signals can be compared is a time-reversal mirror (TRM) (Fink 1997). The previously calculated signal was used in place of the experimental signal in a TRM as a means of judging the ability of the analytical model. For a regular TRM all of the signals are exited and measured experimentally. A TRM experiment consists of two steps. In the case of a cylindrical rod, first, an acoustic signal is excited by a source at one end of the rod. The acoustic signal propagates through the rod, and the altered signal is recorded at the opposite end. In the second step of the TRM the recorded signal is reversed in time, and the receiver is excited with the reversed signal. The reversed signal propagates through the rod, and a new signal is recorded at the source. If time invariance is satisfied, this new signal is the same as the original acoustic signal. This ability of the TRM can be used to produce a compact time signal from a dispersive system.

For this experimental setup time invariance has been demonstrated using a TRM, and a compact signal has been produced in a dispersive waveguide (Puckett and Peterson 2003). It is known that the experimentally measured dispersed signal can be used with at TRM to produce a signal with compact support in the time domain. If the analytical model correctly captures the physics of the waveguide then the calculated dispersed signal should also produce a signal with compact support in the time domain. For the experiment, both the experimentally measured dispersed signal and the calculated dispersed signal were reversed in time and used to excite the transducer in the experimental setup. The measured signals are compared in Figure 6. It can be seen that the experimental signal reproduced the original signal. This result is consistent with previously reported experiments. The analytical signal, however, also produces a signal with compact support in the time domain. Again there are discrepancies between the signals, but the general ability of the model to capture the physics is apparent.

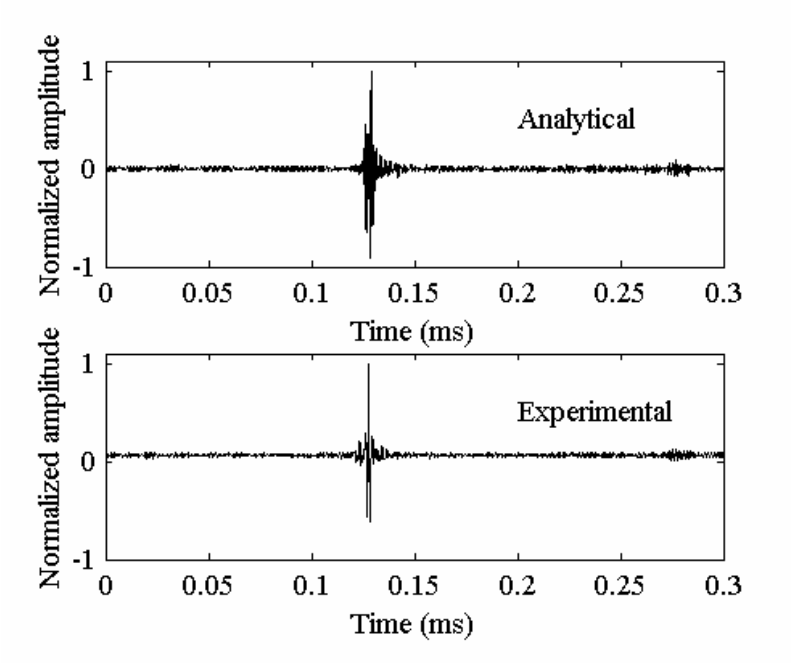

Figure 6. Measured signals recorded in a time-reversal mirror. The top signal represents the signal measured from the excitation of the reversed experimental signal from Figure 6. The bottom signal represents the signal measured from the excitation of the reversed analytical signal from Figure 6.

A second domain for further comparison of the calculated dispersed signal with experimentally measured dispersed signal is the time frequency domain. Time-frequency analysis provides additional evidence that the model captures the physics of the problem. One standard tool to analyze ultrasonic signals is the short-time Fourier transform (STFT) (e.g. Niethammer 2001). The energy density spectrum of the STFT, called a spectrogram, can be used to visualize the results of a STFT. Spectrograms of the dispersed signals appear in Figure 7 and Figure 8 with the analytical curves in black. These curves are the calculated arrival times of the modes based on the group velocity curves. It is reassuring to see that the group velocity curves can be seen in the spectrogram of the analytical signal even though the analytical model uses the phase velocity curves. Despite the discrepancies between the dispersed singles the spectrograms are very similar. The individual modes are apparent in both spectrograms and follow the analytical curves. Additionally, all of the same modes appear in both spectrograms.

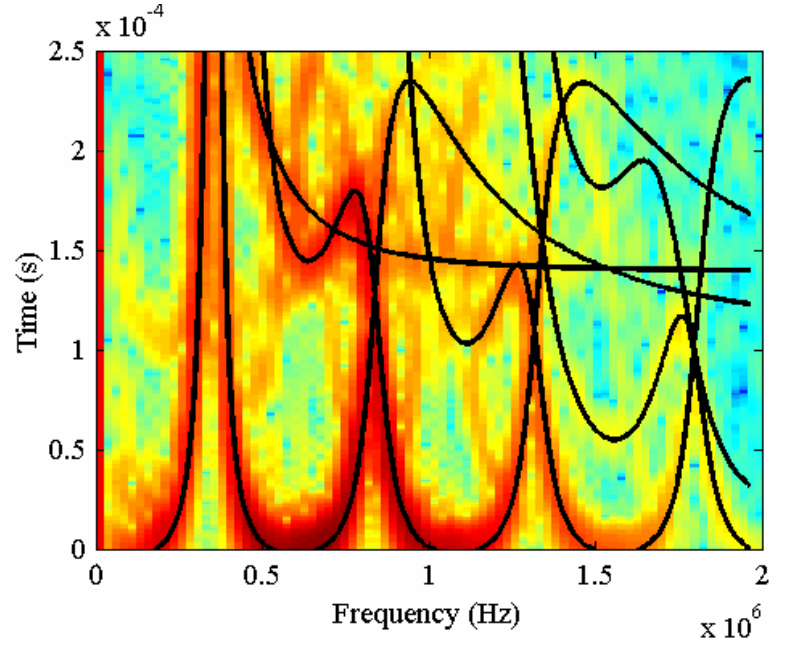

Figure 7. Spectrogram of the measured dispersed signal from Figure 5. Theoretical curves appear in black.

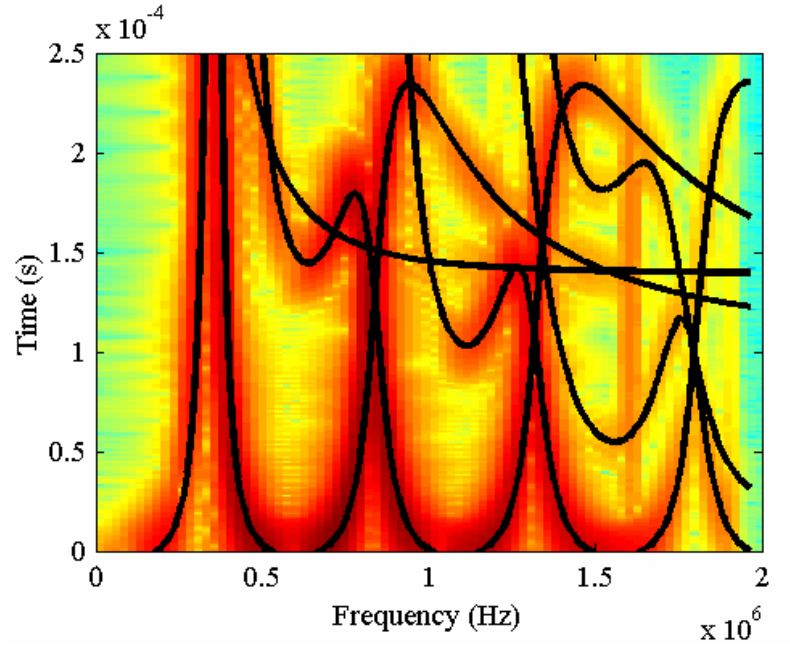

Figure 8. Spectrogram of the calculated dispersed signal from Figure 5. Theoretical curves appear in black.

2.1.5.12 Thick Rod

Another set of experiments considered more closely the ability of the model to predict the dispersed signals. For these experiments a pulse excitation of the transducers was used with different lengths of a 25-mm diameter waveguide. At the 1-MHz center frequency the diameter-to-wavelength ratio $d/?_L$ is 4.2. For the analytical model new dispersion curves were calculated for the larger diameter waveguide. The same procedure was used for the analytical model except 13 modes have cutoff frequencies below the upper 6-dB limit of the frequency spectrum of the signal.

Figure 9 compares the experimental and analytical signals for two different length waveguides. The top graph represents a 0.05 m (2 diameter) long waveguide, and the bottom graph represents a 0.5 m (20 diameter) long waveguide. For this diameter waveguide trailing pulses were observed that are consistent with plane wave theory (Redwood 1960). The general shapes between the analytical and experimental signals for both graphs are very similar. As with the 10 mm diameter waveguide there are some discrepancies between the spacing of the pulses and the arrival times. However, it can be argued that the analytical model captures nearly all of the physics of wave propagation in a cylindrical waveguide.

For these waveguides up to 18 modes were considered at the highest frequencies; however, the results do not change noticeably if only the first 10 modes are considered. An important benefit of the analytical model is the ability to calculate the transfer function for a specific waveguide as well as the transfer function for each mode. The transfer function of the 1^{st}, 4^{th}, and 7^{th} modes are plotted in the lower graph of Fig 10 (other modes are not shown for clarity). It can be seen that the each is dominant over a small frequency range. This is consistent with the observations of Zemanek (1962) who found that the eigenfunctions of a mode are entirely in phase when the group velocity is close to the longitudinal wavespeed. The upper graph in Figure 10 shows the calculated transfer function for a 0.25-m long 25-mm diameter fused quartz waveguide. This transfer function can be used to calculate the dispersed signal for any excitation signal applied to this particular waveguide.

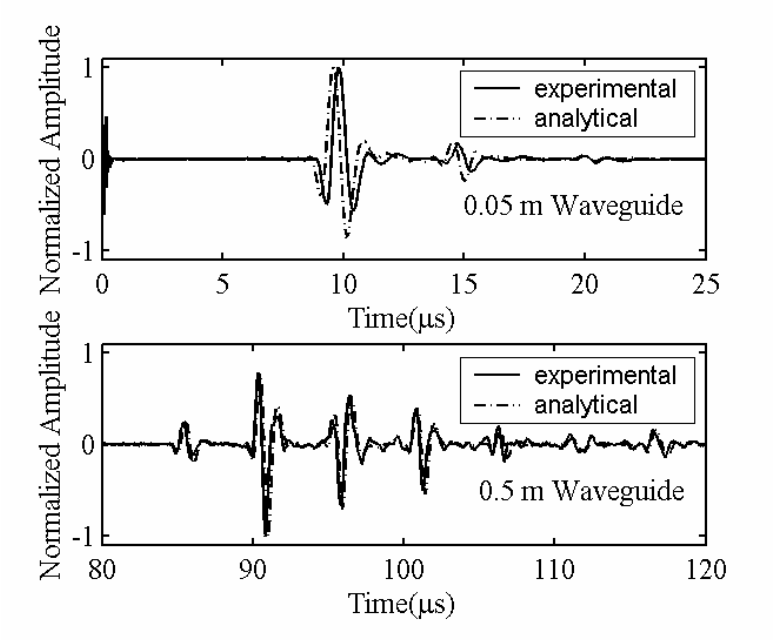

Figure 9. Measured and calculated signals of the reference signal propagating through a 0.15 m long 25 mm diameter waveguide (top) and a 0.5 m long 25 mm diameter waveguide (bottom).

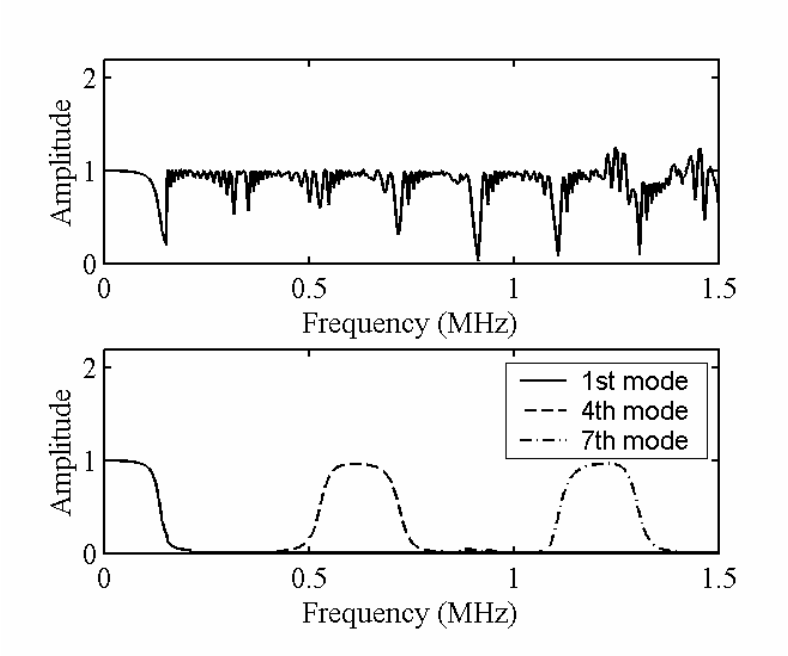

Figure 10. Transfer function of the waveguide (top) and transfer functions of the 1st, 4th, and 7th modes (bottom). Transfer functions of the other modes are not shown for clarity.

2.1.5.13 Conclusions

An analytical model for wave propagation in cylindrical waveguides has been presented. The model uses the eigenvalues and eigenfunctions of the Pochhammer-Chree theory to calculate the dispersed signal measured at the end of the waveguide. The analytic model is designed around a general experimental configuration and considers three parts, the excitation of the ultrasonic signal into the waveguide, the propagation of the signal in the waveguide and the reception of the ultrasonic signal. The relative amplitudes of the modes are determined at each frequency by the boundary conditions on the end of the waveguide. The phase shift is calculated from the phase velocity and the length of the waveguide.

The ability of the model was demonstrated in three different domains. In the time domain the dispersed signals calculated by the analytical model were found to be similar to the experimentally measured dispersed signals for the same waveguide. In the time-reversal domain the calculated dispersed signal was able to produce a signal with compact time domain in a dispersive waveguide using a time-reversal mirror. In the time-frequency domain the spectrograms of the analytical and experimental signals demonstrated the presence of the same modes in each signal. In all three domains it was shown that the model captures the general physics of multiple mode wave propagation in cylindrical waveguides.

The ability of the analytical model to capture the physics of the wave propagation allows the model to be used to explore the behavior of wave propagation in the waveguide. The transfer function of the waveguide has already indicated that different modes dominate over certain frequency ranges. This is consistent with the observation of Zemanek (1962) that the eigenfunctions of a mode are entirely in phase when the group velocity is close to the longitudinal wavespeed. For excitations that are not uniform across the radius a transfer function can be calculated that predicts the ranges of frequencies modes are excited. This allows a frequency to be chosen where only one mode dominates.

This model assumes linear elastic homogeneous isotropic materials. If these criteria are not satisfied calculated signals may not agree well with experiments. An interesting notion

2.1.5.14 Acknowledgements

This research is sponsored by the Ballistic Missile Defense Organization through Dr. Y. D. S. Rajapakse of the Office of Naval Research. Additional support was provided by the National Science Foundation (NSF) GK-12 "Sensors!" grant at the University of Maine. The assistance of S. Vel on the least squares method expansion is also appreciated.

2.1.5.15 References

J.D. Achenbach, Wave Propagation in Elastic Solids, North Holland, Amsterdam, 1999.

C. Chree, The equations of an isotropic elastic solid in polar and cylindrical coordinates, their solution and application, Trans. Cambridge Phil. Soc. **14** (1889) 250-369.

R.M. Davies, A critical study of the Hopkinson Pressure Bar, Phil. Trans. Royal Soc. **A240** (1948) 375-457.

M.E. Fama, Radial eigenfunctions for the elastic circular cylinder, Q. Jl. Mech. appl. Math. **25** (1972) 479-495.

M. Fink, Time reversed acoustics, Physics Today **50** (1997) 34-40.

R. Folk, G. Fox, C.A. Shook, C.W. Curtis, Elastic strain produced by sudden application of pressure to one end of a cylindrical bar. I. Theory, J. Acoust. Soc. Am. **30** (1958) 552-558.

G. Fox, C. W. Curtis, Elastic strain produced by sudden application of pressure to one end of a cylindrical bar. II. Experimental observations, J. Acoust. Soc. Am. **30** (1958) 559-563.

W.B. Fraser, An orthogonality relation for the modes of wave propagation in an elastic circular cylinder, J. Sound Vibrat. **43** (1975) 568-571.

I.S. Goldberg, R.T. Folk, Solutions to time-dependent pure-end condition problems of elasticity: pressure-step wave propagation and end-resonance effects, SIAM J. of Appl. Math. **53** (1993) 1264-1292.

C.K. Jen, Ph. de Heering, P. Sutcliffe, J.F. Bussiere, Ultrasonic monitoring of the molten zone of single-crystal germanium, Mater. Eval. **49** (1991) 701-705.

C.-K. Jen, B. Cao, K.T. Nguyen, C.A. Loong, J.-G. Legoux, On-line ultrasonic monitoring of a die-casting process using buffer rods, Ultrasonics **35** (1997) 335-344.

O.E. Jones, F.R. Norwood, Axially symmetric cross-sectional strain and stress distributions in suddenly loaded cylindrical elastic bars, J. Appl. Mech. **34** (1967) 718-724.

L.W. Kennedy, O.E. Jones, Longitudinal wave propagation in a circular bar loaded suddenly by a radially distributed end stress, J. Appl. Mech. **36** (1969), 470-478.

M. Niethammer, L.J. Jacobs, Time-frequency representations of Lamb waves, J. Acoust. Soc. Am. **109** (2001) 1841-1847.

M.L. Peterson, A signal processing technique for measurement of multi-mode waveguide signals: an application to monitoring of reaction bonding in silicon nitride, Res. Nondestr. Eval. **5** (1994) 239-256.

M.L. Peterson, Prediction of longitudinal disturbances in a multi-mode cylindrical waveguide, Exp. Mech. **39** (1999) 36-42.

L. Pochhammer, Über die Fortpflanzungsgeschwindigkeiten kleiner Schwingungen in einem unbegrenzten isotropen Kreiscylinder, J. Reine Angew. Math. **81** (1876) 324-336.

L.D. Power, S.B. Childs, Axisymmetric stresses and displacements in a finite circular bar, Int. J. Engng. Sci. **9** (1971) 241-255.

A.D. Puckett, M.L. Peterson, Fidelity of an analytical time reversal mirror, in *Review of Progress of Quantitative Nondestructive Evaluation Vol. 21*, edited by D.O. Thompson and D.E. Chimenti, American Institute of Physics, New York (2002) 945-952.

A.D. Puckett, M.L. Peterson, "Technique for determining the pressure distribution on the face of a contact ultrasonic transducer," Experimental Mechanics **27**(4), 37-39 (2003).

A.D. Puckett, M.L. Peterson, A time-reversal mirror in a solid circular cylindrical waveguide using a single, time-reversal element, Acoustic Research Letters Online **4** (2003) 31-36.

M. Redwood, Mechanical Waveguides, Pergamon Press, New York, 1960.

L.W. Schmerr, Fundamentals of Ultrasonic Nondestructive Evaluation, Plenum Press, New York, 1998.

R. Skalak, Longitudinal impact of a semi-infinite circular elastic bar, J. Appl. Mech. **24** (1957) 59-64.

F. Vales, S. Moravka, R. Brepta, J. Cerv, Wave propagation in a thick cylindrical bar due to longitudinal impact, JSME Int. J. **39A** (1996) 60-70.

J. Zemanek, An experimental and theoretical investigation of elastic wave propagation in a cylinder, Ph. D. Diss., University of California, Los Angeles, (1962).

2.2 Task 2 - Recovery of the Compliance Tensor and the Symmetry Axes.

This task considers the problem of finding the symmetry axes of a general anisotropic material. If a specimen is not oriented in the principal axes of the material then the deformation of the specimen will be coupled. For example, axial loading can result in shear deformation in the plane normal to the loading axis. Coupled bending torsion is desirable in some application such as in rotorcraft design, but in most other applications this effect is undesirable and results in complex deformation from simple loading cases. This is also true in dynamic testing. If the ultrasonic wave is not propagated in a principal material axis, more than one wave mode is generated in the sample. The quasi-longitudinal waves will propagate at velocities that are dependent on the properties in the principal material axes that form a basis for the propagation vector of the wave. Thus for either mechanical testing or ultrasonic testing it is important that specimens be used such that the principal material axes are aligned with the geometric axes of the specimen.

For reinforced carbon-carbon it was hypothesized that the direction of the material axes was likely to have significant misorientation with respect to the fiber direction. While the fiber preform is orthotropic for this material, the matrix was likely to also have additional orientation. The matrix is introduced into the fiber preform with multiple steps of either vapor deposition or resin infusion or a combination of the two processes. Therefore, the matrix is introduced in a diffusion-controlled process. A diffusion controlled process will tend to orient any density gradient based on the distance to the free surface, and thus may result in a transversely isotropic matrix superimposed on an orthotropic fiber arrangement. This effect occurs in addition to the normal variation in material axes that results from fiber placement error.

This task is focused on obtaining the full 21 elastic constants for a general anisotropic material. From the full 21 elastic constants the symmetry planes of the material can be determined and the symmetry of the materials can be determined experimentally. From the experimentally determined symmetry it is then possible to calculate the Euler angles and reorient and recut the specimen in principal material axes. The sample is then recut in the principal material axes to produce a specimen that will not exhibit coupled deformation between axes. For the high temperature testing the ultrasonic wave is propagated along a principal material axis.

2.2.1 Visco-elastic Tensor Recovery in the Absence of Known Material Symmetry

Miao Sun, Sara Wright and M.L. Peterson "Visco-elastic Tensor Recovery in the Absence of Known Material Symmetry" Review of Progress of Quantitative Nondestructive Evaluation, Vol21, American Institute of Physics , Melville NY, 2002, p. 1423-1430.

Abstract: In many cases, full knowledge of the material properties is required to facilitate design of a composite structure. Even in cases where the planes of symmetry of the material are nominally well defined, significant variation of these planes can exist due to fiber misorientation and other variation. This paper presents initial results for determining the plane of symmetry of an orthotropic material and a monoclinic material. The concept is extensible to a triclinic material and does not assume *a-priori* knowledge of the material. The experiments are performed using contact ultrasonic measurements of small specimens are easily extended to the visco-elastic properties of the same materials.

2.2.1.1 INTRODUCTION

Extensive research has been directed toward the development of methods for the optimal recovery of elastic properties from ultrasonic measurements. For a number of applications both the elastic and damping characteristics of the materials are required in design. The use of the optimal recovery presents challenges when applied to either man-made or natural anisotropic materials. Variation in material lay-up or growth patterns may result in mis-orientation of the principle materials axes with respect to the geometrical axes. Carbon-carbon composite materials are the considered in this work. The velocities of ultrasonic wave propagated through the material are measured. A procedure is shown that can be used to recover the elastic properties of a material when the material symmetry axes are not known.

2.2.1.2 Theoretical Background

The ultrasonic determination of material elasticity constants has been a subject of interest for quite some time. Aspects of previous work by Van Buskirk, W. C. etc. [1], Norris [2], Aristegui and Baste [3] are used in order to obtain the full set of elastic constants.

2.2.1.2.1 Ultrasonic Velocity in a General Solid

In any given direction, three possible acoustic waves can be generated: a quasi-longitudinal wave and two polarizations of quasi-transverse waves. The phase velocities responding to all of these waves are known functions of the elastic properties and the density of the material [4].

A triclinic solid has at most 21 non-zero and distinct components of elasticity tensor. These 21 components of the elasticity tensor are also the components of the Christoffel's tensor. The three eigenvalues of the Christoffel's equation, which include the three-phase velocity (one quasi-longitudinal and two quasi-transverse velocity) and the density of the material, can be obtained for a known material. The phase velocity, V, of an ultrasonic wave can be measured from the ultrasonic signal. Signal processing is used to measure the phase velocities from the acquired signal. The components of displacement are assumes the form:

$$u_k = A_0 p_k e^{i(k_r x_r - wt)} \qquad (1)$$

where A_0 is a scalar amplitude; the three components of unit displacement vector p_k are the eigenvectors associated with the three eigenvalues; k_r is the wave number.

In order to obtain 21 constants, 21 equations need to be obtained. Since each measurement direction has three wave types, seven directions of wave propagation are required. For the measurements, an appropriate specimen shape was developed by VanBuskisk, Cowin, and Carter [1]. From a Cartesian-coordinate system with axes X_1 X_2 X_3 parallel to the geometric axes of the block of the unknown material, a 1" cube is cut. Opposite edges of the cube are then cut again to form two faces with that are at 45^0 with respect to the original coordinate axes (Figure1 (a)). After cutting two other sets of faces, the specimen is made up of a total six of pair of faces. In order to track the orientation of the sample from the original block, the sample are marked with Arabic numerals 1,2...6 corresponding to each of the opposing faces (Figure1 (b)).

For the first specimen, the ultrasonic wave is propagated through the block for each pair of faces and the signal is acquired. From the velocities measurement from these signals eighteen equations can be set up. Details of the testing method are described below. Since 21unknowns

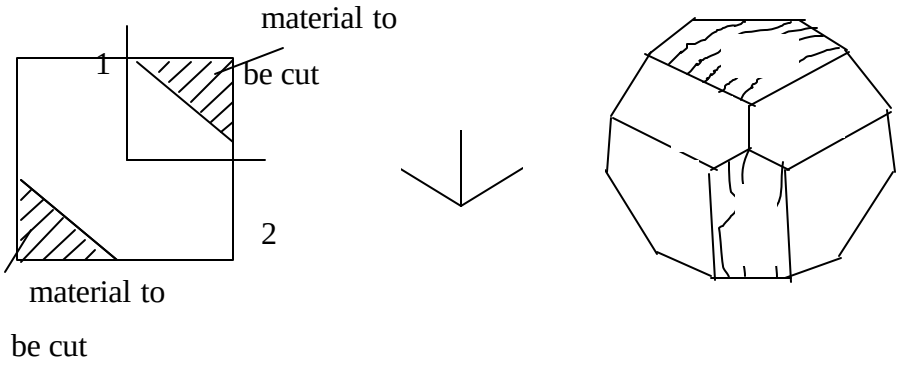

FIGURE 1. (a) The material that must be cut off is shown. (b) The appearance of

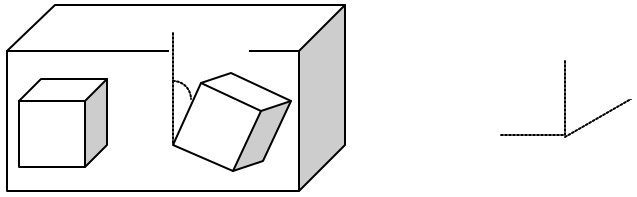

FIGURE 2. Orientation of the specimen with respect to the geometric axes of

are to be determined, one additional direction of wave propagation is required. Figure 2 shows the orientations of a second specimen to be used for the testing. The second specimen is rotated 30^0 with respect to the original coordinate axes X_1, and is simply cut in the shape of a cube.

Since only one more direction of propagation is required. Only one more measurement for each of the three wave types is performed with the direction of propagation normal to each of the two pairs of faces (X_1 or X_3 direction). Combined with three measurements for each of the six other directions from the first specimen, a total of twenty-seven measurements are available for the calculations of the material constants. By solving the equations that are assembled based on the Cristoffel tensor, all 21 components of the elasticity tensor can be determined.

2.2.1.2.2 Elastic Symmetry

The identification of elastic symmetry in an anisotropic material from the elasticity tensor was developed by Cowin and Mehrabadi [5]. The general Hooke's law is:

$$s_{ij} = C_{ijkl} e_{kl} \qquad (2)$$

Rewriting the fourth order tensor C_{ijkl} in a matrix notation, the values of the tensor can be rewritten as:

$$\begin{Bmatrix} s_{11} \\ s_{22} \\ s_{33} \\ s_{23} \\ s_{13} \\ s_{12} \end{Bmatrix} = \begin{bmatrix} C_{11} & C_{12} & C_{13} & C_{14} & C_{15} & C_{16} \\ C_{21} & C_{22} & C_{23} & C_{24} & C_{25} & C_{26} \\ C_{31} & C_{32} & C_{33} & C_{34} & C_{35} & C_{36} \\ C_{41} & C_{42} & C_{43} & C_{44} & C_{45} & C_{46} \\ C_{51} & C_{52} & C_{53} & C_{54} & C_{55} & C_{56} \\ C_{61} & C_{62} & C_{63} & C_{64} & C_{65} & C_{66} \end{bmatrix} \begin{Bmatrix} e_{11} \\ e_{22} \\ e_{33} \\ 2e_{23} \\ 2e_{13} \\ 2e_{12} \end{Bmatrix} \qquad (3)$$

where the rule for simplifying the notation is shown is:

$$11 \Rightarrow 1,\ 22 \Rightarrow 2,\ 33 \Rightarrow 3,\ 23 \text{ or } 32 \Rightarrow 4,\ 13 \text{ or } 31 \Rightarrow 5,\ 12 \text{ or } 21 \Rightarrow 6 \qquad (4)$$

Two second order tensors A_{ij} and B_{ij} are defined from C_{ijkl}. The two tensors are required to determine the elastic symmetry planes of the material [5]. These tensors are defined by:

$$A_{ij} = C_{ijkk}, \quad B_{ij} = C_{ikjk} \qquad (5)$$

They can be given by the following matrices in terms of the components of C_{mn}:

$$A = \begin{bmatrix} C_{11}+C_{12}+C_{13} & C_{16}+C_{26}+C_{36} & C_{15}+C_{25}+C_{35} \\ C_{16}+C_{26}+C_{36} & C_{12}+C_{22}+C_{23} & C_{14}+C_{24}+C_{34} \\ C_{15}+C_{25}+C_{35} & C_{14}+C_{24}+C_{34} & C_{13}+C_{23}+C_{33} \end{bmatrix} \qquad (6)$$

$$B = \begin{bmatrix} C_{11}+C_{55}+C_{66} & C_{16}+C_{26}+C_{45} & C_{15}+C_{46}+C_{35} \\ C_{16}+C_{26}+C_{45} & C_{22}+C_{44}+C_{66} & C_{24}+C_{34}+C_{56} \\ C_{15}+C_{46}+C_{35} & C_{24}+C_{34}+C_{56} & C_{33}+C_{44}+C_{55} \end{bmatrix} \qquad (7)$$

A vector is normal to a symmetry plane of the material if and only if the tensor, which is defined as a specific direction and a specific axis by Cowin, is an eigenvector of the A and B [5]. Once the specific directions and specific axes are obtained by solving the eigenvector problem of A and B, the elastic symmetry of the anisotropic material can be determined.

2.2.1.3 Experimental set up

2.2.1.3.1 Specimen Preparation

As described in the previous section, the objective of this work is the recovery of full elasticity tensor of the carbon-carbon composite material. Two specimens are required for this purpose. The cutting procedures as well as the orientation of the samples were illustrated in the previous section. The carbon composite material used in the tests was cut with an abrasive saw, which was used with fixturing to obtain flat and smooth faces. The final sample was then checked to ensure that the opposite faces were parallel. Accurate dimensions were then taken and recorded for each of the faces.

2.2.1.3.2 Velocity Measurement Method

The longitudinal waves as well as the shear waves were all obtained using a direct contact through-transmission technique. The longitudinal and shear modes are generated using X-Cut and Z-Cut piezoelectric transducers with a nominal 1 MHz. center frequency. A test fixture was designed and built to hold the sample and allow repeatable amplitude measures to be obtained. The experimental set up is shown in Figure 3. The longitudinal wave measurement is straightforward since only a single quasi-longitudinal wave propagates. However, due to arbitrary particle displacement of the transverse components [4], it is necessary to rotate the shear transducer through 180° to find the largest amplitude of transverse component. The maximum amplitude corresponds to X_3-polarization if the ultrasonic wave propagates along the X_1 direction [1]. From the maximum amplitude, the transducer is then rotated 90° to get the orthogonal component that corresponds to the X_2-polarization. Once the particle oscillations and wave velocities for the two models of transverse wave propagation in the X_1 direction have been determined, the same testing procedure is repeated in the X_2 direction.

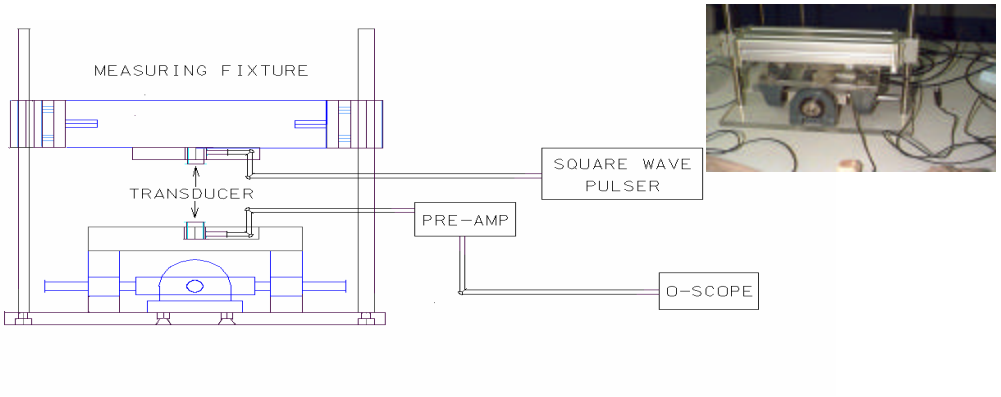

FIGURE 3. Experimental set up for the ultrasonic testing with a photograph

2.2.1.4 Signal processing

To obtain accurate relative time delays, the cross-correlation was used [6]. Cross-correlation algorithms are used to estimate the transit time difference (t) between two signals. In this case a known reference sample of aluminum is compared to the unknown sample of carbon-carbon composite. Windowing of the signal was also required to truncate the additional wave paths that occur because of the small size of the samples.

2.2.1.5 Cross Correlation

The reference signal which was acquired from an aluminum block $x(t)$ and the signal from the block of composite material, $y(t)$, are digitized. The cross-correlation between the two signals is a sequence $r_{xy}(t)$, which is defined as

$$r_{xy}(t) = \sum_{t=-N}^{+N} x(t)y(t-t) \qquad (8)$$

where t is time shift or time delay parameter and the subscript xy indicates the signals used in the cross-correlation.

The cross-correlation provides a measure of similarity between the power in the two signals. The relative time delay between the two signals is the time at which the cross-correlation r_{xy} is a maximum. This time delay t_{max} represents the relative shift. The phase velocity V of the ultrasonic waves propagating through the composite can be estimated by:

$$V = (d \times V_{al}) / (d_{al} + (t_{\max} \times V_{al}) \qquad (9)$$

where V_{al} is the velocity of ultrasonic wave propagating in the reference specimen (aluminum); d and d_{al} are the distances of wave propagation through the aluminum and the unknown samples.

Due to the size of the specimen used, the ultrasonic wavelength is on the order of the dimensions of the specimen. As a result, in addition to the material dispersion that may be evident due to the visco-elasticity of the material, significant geometric dispersion is present. However, the use of the cross-correlation to determine the velocity of the ultrasonic wave results

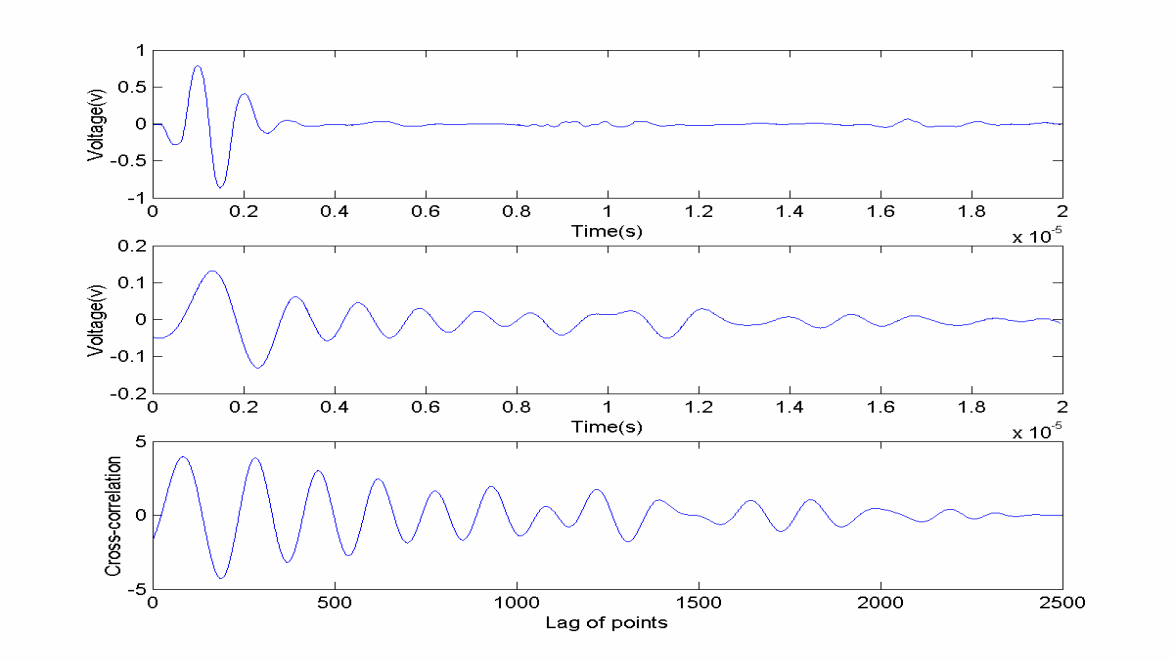

FIGURE 4. A plot of cross-correlation (bottom) between reference signal (top, aluminum) and the tested signal (middle, carbon-carbon).

only in a measure of the relative difference in the velocity between the reference sample (the aluminum block) and the unknown sample. For the range of velocities considered, the only geometrical dispersion that would impact the measurement is the differences in the velocities between the reference sample and the unknown sample [6]. As a result, unlike absolute measurements of velocity, the effect of dispersion even for this size sample can be assumed to be minimal and may be neglected. Figure 4 gives an illustration of the cross-correction between the reference and unknown sample. In the example figure, the ultrasonic wave propagates in the direction of the geometric axis X_1.

2.2.1.6 Signal Windowing

To ensure that multiple reflections are not included in the time signal, a window is used to select the first arrival. The end of the window is located at a point where the wave has traveled two complete passes through the specimen. Since the time delay is not known a-priori, it is necessary to use an adaptive calculation of the window position. To make an initial estimate of the time of flight, a phase velocity is initially estimated based on the reference velocity. For the calculation used the values of the initial estimates were corrected to adjust the time based on the measurement of the two sets of specimens.

A simple truncation of the signal using a rectangular window introduces energy in the high frequencies. The increased energy in the high frequencies is a result of the abrupt transition to zero energy. A triangular window is used as a compromise between simplicity and minimization of the high-energy components. Specifically, if $w(t)$ is defined as a window function, then

$$w(t) = \begin{cases} 1 & (t < 0.8p) \\ (p - t)/(1 - 0.8) & (0.8 \le t \le p) \\ 0 & (t > p) \end{cases} \qquad (10)$$

where p is the time of flight when the wave has made two complete passes through the specimen.

2.2.1.7 Results

Preliminary results for the ultrasonic testing are combined with the tensor relationships to demonstrate the concepts discussed. Extension of the measurements to the configuration shown in figure 2, must be combined with optimization techniques to solve the complete problem [3]. In the initial result the orthotropic elastics constants of carbon-carbon material are obtained. The velocities of the three modes of wave propagation in each of seven directions are measured using the cross-correlation of the signals relative to a block of aluminum reference material. The components of elastic constants are shown in matrix form for the carbon-carbon composite material. The elastic properties are measured for a composite carbon sample with figures shown in GPa as:

$$C = \begin{bmatrix} 47.601 & 44.371 & 46.342 & 0 & 0 & 0 \\ & 18.906 & 20.327 & 0 & 0 & 0 \\ & & 18.839 & 0 & 0 & 0 \\ & & & 3.1112 & 0 & 0 \\ & sym. & & & 5.2180 & 0 \\ & & & & & 4.5369 \end{bmatrix} \quad (11)$$

The orthotropic material constants can then be rotated in order to reduce the apparent symmetry of the constants. With a rotation about the X_3 coordinate axis of 30^0 (in the clockwise direction) the elastic constants obtained are:

$$C = \begin{bmatrix} 47.999 & 36.799 & 39.838 & 0 & 0 & -1.8413 \\ & 33.651 & 26.831 & 0 & 0 & -1.0584 \\ & & 18.839 & 0 & 0 & -1.1265 \\ & & & 3.6379 & -0.9123 & 0 \\ & sym. & & & 4.6913 & 0 \\ & & & & & -3.0346 \end{bmatrix} \quad (12)$$

From the material constants the matrices A and B shown in equations Eqn. (6) and Eqn. (7) are found. These matrices are then used to obtain the unit normals to the planes of symmetry.

$$A = \begin{bmatrix} 124.63 & -23.690 & 0 \\ 0 & 97.281 & 0 \\ 0 & 0 & 85.508 \end{bmatrix}; \quad B = \begin{bmatrix} 49.656 & -13.337 & 0 \\ 0 & 34.254 & 0 \\ 0 & 27.168 & 0 \end{bmatrix} \quad (13)$$

The eigenvectors of A and B are:

$$Vec\_A = \begin{bmatrix} -0.500 & 0 & -0.866 \\ -0.866 & 0 & 0.500 \\ 0 & 1 & 0 \end{bmatrix}; \quad Vec\_B = \begin{bmatrix} -0.500 & 0 & -0.866 \\ -0.866 & 0 & 0.500 \\ 0 & 1 & 0 \end{bmatrix} \quad (14)$$

From this result the unit normals are seen to point in the direction of symmetry that was assumed in the original data set. To demonstrate the same concept in a monoclinic material a case is shown for properties of Aegirine.

Because of the difficulties of making the measurements in a monoclinic material handbook values for the properties of a mineral (Aegirine, $NaFeSi_2O_6$) are used to demonstrate the concept. The elastic material properties for an Aegirine crystal are given as [7]:

$$C = \begin{bmatrix} 193.000 & 48.400 & 76.500 & 0 & -20.100 & 0 \\ & 189.000 & 57.600 & 0 & -14.600 & 0 \\ & & 233.000 & 0 & -18.500 & 0 \\ & & & 58.200 & 0 & -4.400 \\ & sym. & & & 53.100 & 0 \\ & & & & & 46.800 \end{bmatrix} \quad (15)$$

where the units are all GPa. The A and B matrices are then obtained from Eqn. (6) and Eqn. (7) and the eigenvectors of A and B are found as:

$$Vec\_A = \begin{bmatrix} -0.843 & 0 & -0.539 \\ 0 & 1.000 & 0 \\ -0.539 & 0 & 0.843 \end{bmatrix}; \quad Vec\_B = \begin{bmatrix} -0.869 & 0 & -0.4934 \\ 0 & 1.000 & 0 \\ -0.493 & 0 & 0.869 \end{bmatrix}$$

(16)

Eqn. 16 shows that, since only one eigenvector (0,1,0) of A and B are coincident, no more than one symmetric plane can exist. Further, the eigenvector (0,1,0) should be normal to the symmetry plane.

With a rotation about the X_3 coordinate axis of 30^0 (in the clockwise direction), the elastic constants of Aegirine obtained are:

$$C = \begin{bmatrix} 173.625 & 66.775 & 71.775 & 6.063 & -18.122 & -11.475 \\ & 171.625 & 62.325 & 11.288 & -11.930 & 9.743 \\ & & 233.000 & 9.250 & -16.022 & -8.184 \\ & & & 56.925 & 2.208 & -3.096 \\ & sym. & & & 54.375 & 0.963 \\ & & & & & 65.175 \end{bmatrix} \quad (17)$$

where the eigenvectors of A and B are:

$$Vec\_A = \begin{bmatrix} -0.729 & 0.500 & -0.466 \\ 0.423 & 0.866 & 0.293 \\ -0.539 & 0.000 & 0.843 \end{bmatrix}; \quad Vec\_A = \begin{bmatrix} -0.753 & 0.500 & -0.427 \\ 0.434 & 0.866 & 0.247 \\ -0.493 & 0.000 & 0.870 \end{bmatrix}$$

(18)

Comparing with Eqn. 16, Eqn. 18 shows that, after rotated 30^0 with respect to X_3, the orientation of the common eigenvector of A and B shifted from (0,1,0) to (0.5, 0.866, 0), which indicates location of the symmetric plane of the material.

2.2.1.8 Conclusion and Future Work

- A method has been demonstrated for determining the elasticity tensor of an anisotropic material. The approach is based on the wave velocity measurements and theory of polarization transformation of shear wave propagation in a medium.
- The case is theoretically applicable to the most general anisotropic cases, although in this initial case it is shown only for a two somewhat simplified cases.
- Future work can focus on the implication of the existence of planes of symmetry by statistically determining the normals to the symmetry plane of materials. This is a quite simple procedure since it involves solving the eigenvecters of tensor A and B given by Eqn. (6) and Eqn. (7).

2.2.1.9 Acknowledgements

This research is sponsored by the Ballistic Missile Defense Organization through the Office of Naval Research (ONR) Grant N00014-00-1-0519, Science Officer Dr. Y. D. S.

2.2.1.10 References

Van Buskirk, W. C., and Cowin, S. C. and Carter Jr, R., *Journal of Materials Science*, **Vol. 21**, 2759-2762.(1986).

Norris, A. N., *Mech. Appl. Math.,* **Vol. 42**, 413-426. (1988).

Aristegui, C., and Baste, S., *J. Acoust. Soc. Am,* **Vol. 101 (2)**, pp. 813-833, (1997).

Auld, B. A. *Acoustic Fields and Waves in Solids.* (Vol.1), Krieger Publishing Comp. Malabar, FL. 1989, Chapter 3.

Cowin, S. C., and Mehrabadi, M. M., *Quart.J. Appl. Math*., **Vol 40**, pp.451-476.(1987)

Peterson, M. L., *Ultrasonics*, **Vol. 35 (1)**, pp. 17-29. (1997).

Bhalla, A. S., Cook, W. R., Hearmon, R.F.S., Jerphagnon, J., Kurtz, S. K., Liu, S. T., Nelson, D. F. and Oudar, J. L. *Landolt-Bornstein,Numerical Data and Functional Relationships in Science and Technology, New Series,* **Vol. 18,** Supplement to Vol. III/11, Springer-Verlag Berlin, New York, 1984, pp.46.

2.2.2 Experimental Determination of the Symmetry of a Material using an Immersion Ultrasonic Technique

M.L. Peterson , Miao Sun and Anish Senan, "Experimental Determination of the Symmetry of a Material using an Immersion Ultrasonic Technique" To be submitted

Abstract: In many cases, full knowledge of the elastic properties is required to facilitate design of a composite structure. Even in cases where the planes of symmetry of the material are nominally well defined, significant variation of these planes can exist due to fiber misorientation and other variation. This paper presents results for experimentally determining the planes of symmetry from the elastic constants of a trigonal single crystal of aluminum oxide. The concept is extensible to any symmetry group and does not assume *a-priori* knowledge of the material. The experiments for the determination of the elastic constants are performed using an ultrasonic immersion technique. A Newton-Raphson nonlinear optimization is used to reconstruct the elastic constants from the experimental data. From this data the full elastic tensor is recovered which in turn results in data that can be used to determine the symmetry planes in the material.

2.2.2.1 INTRODUCTION

The experimental determination of a misorientation between the geometric axes and the material symmetry axes of a finished part has not been considered extensively. As is the case in other areas, the concepts are firmly established in the more theoretical literature with more limited experimental utilization of the ideas [1, 2] For composite materials, lay-up errors or warpage during manufacturing typically causes the misorientation. In natural materials such as bone or wood, growth patterns may also cause the misorientation. This misorientation and in general the existence of coupling terms in the compliance tensor can cause undesirable coupling of deformation as well as unexpected failure due to excessive matrix loading. In single crystal materials, this misorientation can lead to thermal or elastic properties that are other than that which is assumed. This explores the use of a water ultrasonics for recovery of elastic properties. The ability to determine the symmetry planes from the results is then shown for a single crystal material for which handbook properties can be used for verification.

In this technique, the velocity of an ultrasonic wave that is obliquely incident from a coupling liquid onto the test sample is determined. Water immersion is used in order to maintain

good coupling between the sample and the ultrasonic transducers. Water immersion also makes it possible to generate the range of angles required for the measurement. The elastic constants can be reconstructed from the velocity data by performing a Newton-Raphson nonlinear optimization on the experimental data.

A technique for the identification of elastic symmetries in the material is also described. From knowledge of the symmetry properties, the orientation of the principal axes with respect to its geometric axes are determined. A method for determining the Euler's angles, which transfer the principal coordinate system to an observation coordinate system, is also presented in this work.

2.2.2.2 Theoretical Background

2.2.2.2.1 Ultrasonic Wave Velocity Measurements

A plane wave solution to a second order differential wave equation is an eigenvalue (Christoffel's) equation. 3

$$(\Gamma_{ik} - d_{ik} r V^2) p_k = 0 \qquad 1$$

where $\Gamma_{ik} = C_{ijkl}$ is referred to as Christoffel's tensor, V is the phase velocity of the ultrasonic wave, d_{ik} is the Kronecker delta symbol, p_k are unit displacement polarization vectors.

Wave velocity is measured using an immersion ultrasonic method. The ultrasonic wave is generated by a piezoelectric transducer and then propagates through the water and the testing sample. The signal is received by a second piezoelectric transducer (Figure 1). The transducers and the sample are all immersed in the water that serves as a coupling media for the ultrasonic wave. For convenience a coordinate system, R=($\mathbf{x_1}$, $\mathbf{x_2}$, $\mathbf{x_3}$), is defined such that the origin of R is at the midline of the sample. Unit base vector $\mathbf{x_1}$ is normal to the front surface; unit base vectors $\mathbf{x_2}$ and $\mathbf{x_3}$ follow the right hand rule and lie on the mid-plane of the sample.

For an arbitrary incident angle θ, into an anisotropic plate, three possible wave modes are excited. A quasi-longitudinal wave (QL), a slow quasi-transverse wave (QT1) and a fast quasi-transverse wave (QT2) are generated in the solid (Figure 1). These waves propagate at different phase velocities and their velocity vectors all lie in the incident plane (a plane consisting axis $\mathbf{x_1}$ and the incident wave). If this plane coincides with a plane of the material symmetry, only one transverse wave and one longitudinal wave are generated [1].

To obtain accurate phase velocities of the waves, a cross-correlation algorithm is used to measure the relative time delay. The relative delay is found between a reference signal propagating in a water path without a sample and the sample signal propagating in the water coupling path and through the sample 4,5. In order to find the length of the wave path through the water path and the sample, the Snell-Descartes Law is used [1]. The velocities then can be calculated by the formula [3]

$$V_i(x_1, j) = \frac{V_0}{\sqrt{1 + \frac{V_0 t_i}{d}\left(\frac{V_0 t_i}{d} - 2\cos q_i\right)}} \qquad 2$$

where V_0 is the wave velocity in the water, τ_i is the calculated time delay, θ_i is the incident angle, d is the thickness of the sample, and ($\mathbf{x_1}$, φ) indicates the wave incident plane.

To identify the elastic constants of a general anisotropic material, experimental data is collected from four incident planes ($\mathbf{x_1}$, φ), where $\varphi=0^0$, 45^0, 90^0 and 135^0 are called the azimuthal angles 6. At each incident plane, the measurements were at a range of 0^0 to 24^0 incident angles. This procedure can also be explained by saying the testing plate is rotated through a certain angle ($\varphi=0^0$, 45^0, 90^0 and 135^0) with respect to the $\mathbf{x_1}$ axis. An illustration of the geometric coordinate system R and the incident planes is given in Figure 2. Because the velocity was measured by using the peak of the cross-correlation, only the velocity of the highest amplitude mode was measured. The two quasi-transverse modes in some cases have similar or even identical arrival times at certain angles. Overlapping signals have the potential to complicate the problem. However, since the optimization algorithm does not require that the QL, QT1 or QT2 be distinguished, this problem is eliminated [7].

2.2.2.2.2 Reconstructed Elastic Constants

The elastic constants can be reconstructed if a large number of wave velocity data points are available by performing a Newton-Raphson nonlinear optimization [5, 7]. The secular equation for the optimization is

$$\left|\Gamma_{ij} - d_{ik}\, rV^2\right| = 0 \qquad 3$$

In the general case, three phase velocities corresponding to the three wave modes are three solutions of this non-linear cubic equation. Due to experimental errors, every measured phase velocities V is approximately the solution of:

$$f(V_{\exp}, C_{ij}) = \left|\Gamma_{ij} - d_{ik} r V^2\right| \cong 0 \qquad 4$$

where $f(V_{\exp}, C_{ij})$ is the left hand of Equation 4 and V_{exp} indicates the phase velocities measured from the four incident planes.

Reconstruction of all the twenty-one components of Cij can be performed by minimizing an objective function $F(C_{ij})$, which is the sum of square of the secular equation:

$$C_{ij} = \min\left\{F(C_{ij})\right\} \qquad 5$$

with

$$F(C_{ij}) = \sum_{i=1}^{n}\left[f(V_{\exp}(i), C_{ij})\right]^2 \qquad 6$$

where n =all data points collected from the four incident planes.

This method minimizes the effect of random deviations of experimental data on the results of reconstruction. The wave velocity measurements are included in each objective function to be minimized. There are more experimental data points than the number of the independent elastic constants. Therefore the results are constructed from an over-determined system of the functions $f(V_{\exp}, C_{ij})$ 8. Other methods use direct solutions of Christoffel's Equation 9, However, the minimization technique used in this work requires no mode distinction[7]. Modes do not need to be identified since all of the modes generated are solutions of Christoffel's equation. In order to find all possible 21 elastic constants, velocity data is collected from four incident planes ($\mathbf{x_1}$, 0^0), ($\mathbf{x_1}$, 45^0), ($\mathbf{x_1}$, 90^0), and ($\mathbf{x_1}$, 135^0) for a wide range of incident angles.

2.2.2.3 Determination of Normals to Symmetry Planes

Based on knowledge of the elastic constants C_{ijkl} of an anisotropic material, identification of elastic symmetry possessed by the material was developed by Cowin[10, 11] and Norris [2]. Two tensors A_{ij} (Voigt tensor) and B_{ij} (dilatational modulus) are required to determine the elastic symmetry planes of the material. These tensors are defined by:

$$A_{ij} = C_{ijkk}, \quad B_{ij} = C_{ikjk} \qquad 7$$

A vector is normal to a symmetry plane of a linear elastic material if and only if the vector is an eigenvector of tensor A and B respectively. Theoretically, for an orthotropic material, three eigenvectors of tensor A and B should be coincident. However, due to experimental errors, the eigenvectors of A and B may not exactly line up. This error, is however, quantifiable and can be dealt with by applying a threshold for an acceptable angular definition of the error between the eigenvectors. The orientation of the principal material coordinate frame R^P with respect to an observation coordinate system R can then be specified by a set of Euler's angles $\delta = (\alpha, \beta, \gamma)$.

2.2.2.4 Recovery of Principal Coordinate System

The principal coordinate system R^P is obtained by a successive rotation from an observation coordinate system R. The initial coordinate system R with a set of Cartesian axes $\mathbf{x_1}$, $\mathbf{x_2}$, $\mathbf{x_3}$ is first rotated through an angle α about the x_3 axis. A further rotation through angle β about the *transformed* $\mathbf{x_1}$ brings the body into a coordinate system R'. Finally a rotation γ about the *transformed* $\mathbf{x_3}$ put the system into a coordinate system R^P with a set of Cartesian axes $\mathbf{x_1}^P$, $\mathbf{x_2}^P$, and $\mathbf{x_3}^P$. The rotations are performed as counterclockwise as one looks to the origin **O** along the axis of rotation 12. A set of angles (α, β, γ) is referred to as Euler's angles of the coordinate system R with respect to R^P. Transformations from R to R^P may also be obtained by

$$\{x_i^{\,p}\} = [M]\{x_i\} \qquad 8$$

where

$$[M] = \begin{bmatrix} ca\ cg - sa\ cb\ sg & sa\ cg + ca\ cb\ sg & sb\ sg \\ -ca\ sg - sa\ cb\ cg & -sa\ sg + ca\ cb\ cg & sb\ cg \\ sa\ sb & -ca\ sb & cb \end{bmatrix} \qquad 9$$

$$c = \cos;\ s = \sin$$

In general, two rotations of the coordinate system are enough to characterize the orientation of the principal coordinate system R^P [1.4]. Therefore the transformation matrix [M] in Equation 10, if $g = 0$ as in this paper, can be reduced to

$$[M] = \begin{bmatrix} \cos(a) & \sin(a) & 0 \\ -\sin(a)\cos(b) & \cos(a)\cos(b) & \sin(b) \\ \sin(a)\sin(b) & -\cos(a)\sin(b) & \cos(b) \end{bmatrix} \quad 10$$

2.2.2.5 Experimental System

The experimental arrangement used is shown in Figure 3. Two matched piezoelectric immersion transducers with center frequency of 2.25 MHz (Parametric, Model v306) are placed on each side of the sample. The position of the transmitting transducer is fixed at the center of the sample. The position of the receiving transducer is adjusted manually to a location that corresponds to the peak amplitude of the signal. A disk of the sample material (aluminum oxide, 99.9% pure, Alfa Aesar), with a diameter of 25.4 mm and a thickness of 3.4 mm, is mounted on to a goniometer. The azimuthal angle φ, that characterizes the incident plane, is varied manually by rotating the disk in the fixture. The incident angle θ is controlled by adjusting the goniometer (Figure 4).

The wave is generated by a pulser/receiver, which excites the piezoelectric transmitter. The wave is obliquely incident on to the sample surface and is transmitted through the sample with mode conversion depending on the incident angle. The received signal is amplified by a pre-amplifier (Parametrics, Model 5662, Waltham MA). The received signal is averaged and digitized by a digital oscilloscope (Tektronix, Model TDS 520A, Wilsonville, OR).

Since the immersion ultrasonic through-transmission technique is applicable to any symmetry groups of the materials, the choices of the material for the testing are flexible. Solubility of the material in water, physical size and available geometry of the material represent some of the constraints on the approach presented. The aluminum oxide chosen has a trigonal system with 6 independent elastic constants. Handbook values for the properties of the sample are used as the initial guess for the optimization algorithm as well as for comparison of the final results. For aluminum oxide in the principal coordinate orientation, the elastic constants in GPa are 13

$$C = \begin{bmatrix} 495 & 160 & 115 & -23 & 0 & 0 \\ & 495 & 115 & 23 & 0 & 0 \\ & & 497 & 0 & 0 & 0 \\ & & & 146 & 0 & 0 \\ & sym. & & & 146 & -23 \\ & & & & & 167.5 \end{bmatrix} GPa \qquad 11$$

The reference specimen has a random axis orientation so that the optimization algorithm can be tested as well as the technique to find the misorientation between the measurement axes and the material axes. A photograph of the aluminum oxide can be seen in figure 5.

2.2.2.6 Results and Discussions

Elastic constants are calculated from the velocities found in the experiments. In the observation coordinate system R the results are (in GPa)

$$[C] = \begin{bmatrix} 471.184 & 158.660 & 135.140 & -45.982 & 0.1091 & 0.0010 \\ & 492.222 & 118.221 & 3.444 & 00.4033 & 0.3800 \\ & & 348.080 & 4.033 & 0.6200 & 0.1006 \\ & & & 140.930 & 0.4420 & 0.4801 \\ & sym. & & & 41.410 & -81.340 \\ & & & & & 143.020 \end{bmatrix} \qquad 12$$

These results are for a sample that is randomly oriented. It is thus interesting to note that the value of the C_{14} term is the same order as the C_{55} term and that the C_{56} term is twice the magnitude of the C_{55} term. In the initial guess, the C_{14}, C_{24}, and C_{56} term were all equal. However, while the magnitude of some of the off-diagonal terms, and one of the diagonal terms are different, the general structure of the terms is the same and thus suggests a trigonal symmetry with a small change in sample orientation.

To find the principal orientation of the sample, the eigenvectors of A (Voigt tensor) and B (dilatational modulus) are

$$[eig\_A] = \begin{bmatrix} -0.0074 & -0.9996 & -0.0275 \\ 0.2137 & 0.0254 & -0.9766 \\ 0.9769 & -0.0128 & 0.2162 \end{bmatrix}, [eig\_B] = \begin{bmatrix} -0.0096 & -0.9999 & -0.0040 \\ 0.2674 & 0.0013 & -0.9636 \\ 0.9635 & -0.0101 & 0.2673 \end{bmatrix} 13$$

As noted previously, the eigenvector pair that exhibits a sufficiently small angular deviation is considered to be a good estimate of a normal to a symmetry plane. Three angular deviations between each pairs of eigenvectors are

$$q_1 = 3.03^0, q_2 = 1.40^0, q_3 = 3.35^0 \qquad 14$$

Equation 7.3 shows that all three angular deviations are small enough that it would be reasonable to conclude that three symmetry planes exist in the material. Recall that the original values from the material handbook shows that three perpendicular symmetry planes exist in a trigonal material. The average of the two vectors V_i^{ave} (i=1, 2, 3) associated with the eigenvector pairs is used as an estimate of the normals to the symmetry planes. Thus, the three unit vectors of the normals to the symmetry planes with respect to the observation coordinate system R are

$$\begin{aligned} e_1 &= -0.0087x_1 + 0.2405x_2 + 0.9702x_3 \\ e_2 &= -1.0000x_1 + 0.0134x_2 - 0.0115x_3 \\ e_3 &= -0.0158x_1 - 0.9701x_2 + 0.2404x_3 \end{aligned} \qquad 15$$

where $\mathbf{x_1}$, $\mathbf{x_2}$, $\mathbf{x_3}$ are unit base vectors of the observation coordinate system R. Figure 6 shows the orientations of the normals to the symmetry planes.

The orientation of the sample with respect to the material axes remains to be seen. The principal coordinate system R^P with respect to the observation coordinate system R can be located by determining a set of Euler's angle unknowns $\delta=(\alpha, \beta, \gamma)$ with at least one of the unknown is zero [1, 4]. e3 was used to extract the Euler's angles.

$$\begin{aligned} e_3 &= -0.0158x_1 - 0.9701x_2 + 0.2404x_3 \\ &= \cos(a)x_1 - \sin(a)\cos(b)x_2 + \sin(a)\sin(b)x_2 \end{aligned} \qquad 16$$

Thus, a set of Euler's angles are

$$a \cong 90.9^0; \; b \cong 14.0^0; g = 0 \qquad 17$$

Figure 7 shows the rotations associated with the corresponding Euler angles α and β.

The elastic constants C^P referred to its principal coordinate system R^P determined from the Euler's angles:

$$
\left[C^{P}\right] =
\begin{bmatrix}
478.5(495) & 178.9(160) & 121.9(115) & -1.882(-23) & -23.54(0) & 0.801(0) \\
 & 471.9(495) & 114.9(115) & 2.063(23) & 35.02(0) & 0.910(0) \\
 & & 354.5(497) & 0.210(0) & -13.33(0) & 0.110(0) \\
 & & & 91.70(146) & 2.139(0) & 47.87(0) \\
 & \textit{sym.} & & & 144.5(146) & -1.681(-23) \\
 & & & & & 175.3(168)
\end{bmatrix} \quad (18)
$$

The numbers in the parenthesis in Equation 21 are the elastic constants obtained from a material handbook [12]. Reconstructed values C_{11}, C_{13}, C_{16}, C_{22}, C_{23}, C_{26}, C_{34}, C_{36}, C_{45}, C_{55}, C_{66} are within ± 5 % of the handbook values. C_{12} is within 11.5 %.

The reason for the large difference for the remaining may be explained by the following. For a trigonal material, in addition to the three perpendicular symmetry planes, a symmetry axis also exists. Any of the $\vec{x}_1, \vec{x}_2, \vec{x}_3$ coordinate axes can be symmetry axis. The handbook value shows that the $\vec{x}_1$ is the symmetry axis. However the result in Equation 21 indicates that $\vec{x}_2$ may potentially be the symmetry axis in this coordinate system setup.

The result shown in Equation 21 can be verified by finding the normals to the symmetry planes with respect to the constructed R^P. The closest of eigenvectors of the tensor A and B determined from the components of C^P should be the unit base vectors of R^P itself. The unit vectors of the normals to the symmetry planes in coordinate system R^P determined by C^P are

$$
\begin{aligned}
e_1 &= -0.014 x_1{}^P - 0.000\, x_2{}^P + 0.999 x_3{}^P \\
e_2 &= -0.016 x_1{}^P + 0.999\, x_2{}^P - 0.000 x_3{}^P \\
e_3 &= -0.999\, x_1{}^P - 0.016 x_2{}^P - 0.014 x_3{}^P
\end{aligned} \quad (19)
$$

If the experimental errors are taken into count, the e_i (i=1,2,3) in Equation 20 actually line up with the three unit base vectors x_i^P (i=3, 2, 1) of R^P, respectively.

2.2.2.7 Conclusions and Future Work

From this work, several conclusions can be drawn.

A water immersion method to optimally recover the elastic constants for a general anisotropic material has been demonstrated. The approach is based on wave velocity measurements and a Newton-Raphason nonlinear optimization.

Identification of material symmetries and the corresponding principal coordinate system has been introduced.

Numerical as well as experimental results show the method introduced in this work is effective and applicable.

Future work should focus on the stability of the optimization algorithm. This involves applying some random scatter on the initial guess and on the measured velocity data. Another extension to this work is to investigate the sensitivity of this elastic constant determination for weak and strong anisotropies. This can be done by using both numerical and experimental data from various materials that possess different symmetry classes.

Many materials have not been challenged completely by a method such as the one shown. For specimens ranging from wood to composites, many interesting results are expected. Further work will also consider extending the determination of symmetry class to non-Cartesian samples. This is an interesting problem and is with relevance to a range of natural and man-made materials.

2.2.2.8 Acknowledgements

This research is sponsored by the Ballistic Missile Defense Organization through the Office of Naval Research (ONR) Grant N00014-1-0519, Science Officer Dr. Y. D.S.

2.2.2.9 Reference

1 Cowin, S. C. “The structure of the linear anisotropic elastic symmetries.” J. Mech. Phys. Solids. Vol. 40, No. 7. pp.1459-1471. 1992.

2 Norris, A. N. “On the acoustic conditions for the existence of symmetry planes.” Q. J. Mech. Appl. Math. Vol. 42. pp. 412-426. 1989.

3 Auld, B. A., *Acoustic Fields and Waves in Solids.* Vol.1, Chapter 3, pp.57-82. Krieger Publishing Comp. Malabar, FL. 1990.

4 Peterson, M. L., “A Method for Increased Accuracy of the Measurement of Phase Velocity.” Ultrasonic. Vol. 35 (1), pp. 17-29. 1997.

5 Hosten, B., “Ultrasonic Through-Transmission Method for measuring the complex stiffness moduli of composite materials.” *Handbook of Elastic Properties Solids, Liquids, and Gases*. Chapter 3, pp. 67-70. Academic Press. New York. 2001.

6 Aristegui, C. and Baste, S., “Determination of the elastic symmetry of a monolityic ceramic using bulk acoustic waves.” J. Nondestructive Evaluation. Vol. 19, pp. 115-126. 2000.

7 Aristegui, C. and Baste, S. “Optimal determination of the material symmetry axes and associated elasticity tensor from ultrasonic velocity data.” J. Acoustic. Soc. Am. Vol. 102 (23). Pp. 1503-1521. 1997.

8 Every, A. G. and Saches, W. "Determination of the elastic constants of anisotropic solids from acoustic-wave group-velocity measurements." Physics Review. Vol. B42. pp. 8196-8205. 1990

9 Rokhlin, S. I. and Wang, W. "Double through-transmission bulk surface wave method for ultrasonic phase velocity measurement and determination of elastic constants of composite materials." ." J. Acoust. Soc. Am. Vol. 91. pp. 3303-3312. 1992.

10 Cowin, S. C. and Mehrabadi, M. M. "On the identification of material symmetry for anisotropic elastic materials." Q. J. Mech. Appl. Math. Vol. 40. pp. 451-476. 1987.

11 Cowin, S. C. "Properties of the anisotropic elasticity tensor." Q. J. Mech. Appl. Math. Vol. 42. pp. 249-266. 1989

12 Shames, I. H., *Engineering Mechanics*. Vol. II. Dynamics. Chapter 19, pp. 653-655. Prentice-Hall, Inc. New Jersey, 1966.

13 Hellwege, K. H., (chief) Editor. *Numerical Data and Functional Relationships in Science and Technology*. Chapter 3, pp. 44-47. New Series. Springer-Verlag Berlin. 1979.

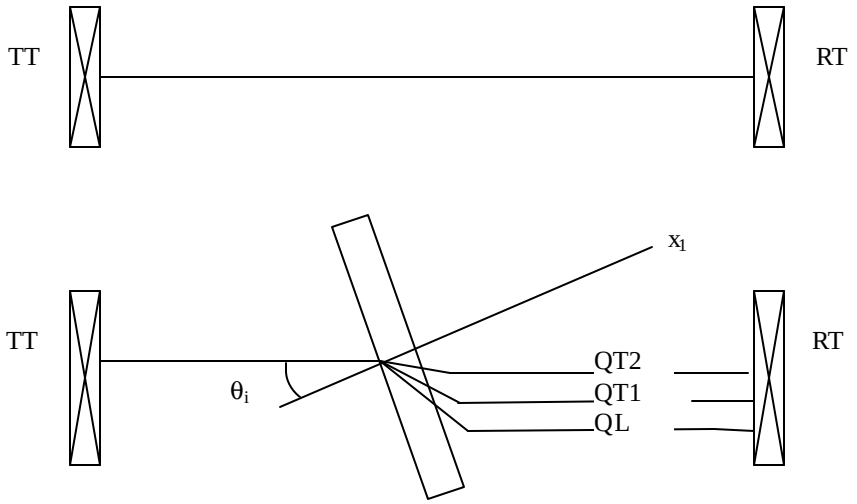

Figure 1. Illustration of ultrasonic wave propagation through a reference media (Top) and through an anisotropic sample with incident angle θ_i (Bottom).

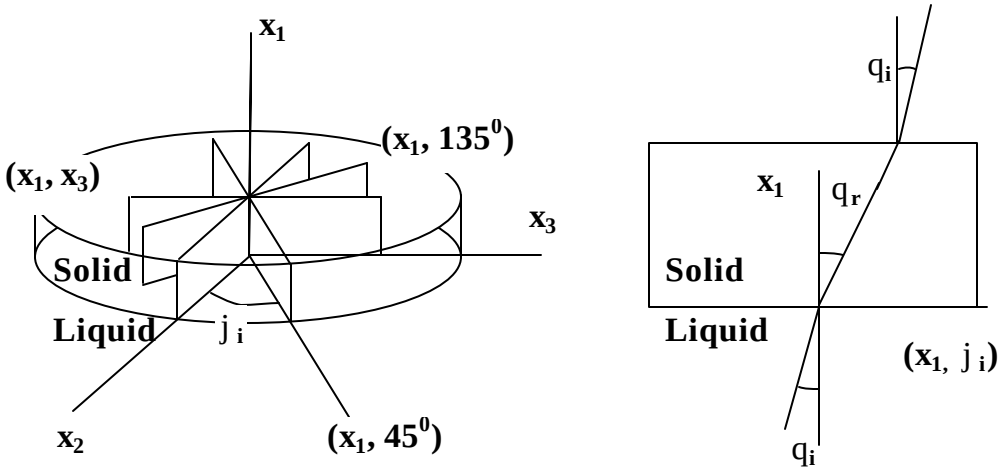

Figure 2. Diagram of the coordinate system R=(x_1, x_2, x_3) and incident angle associated with the sample (Left). Wave propagation in the incident plane (x_1, φ_i) (Right).

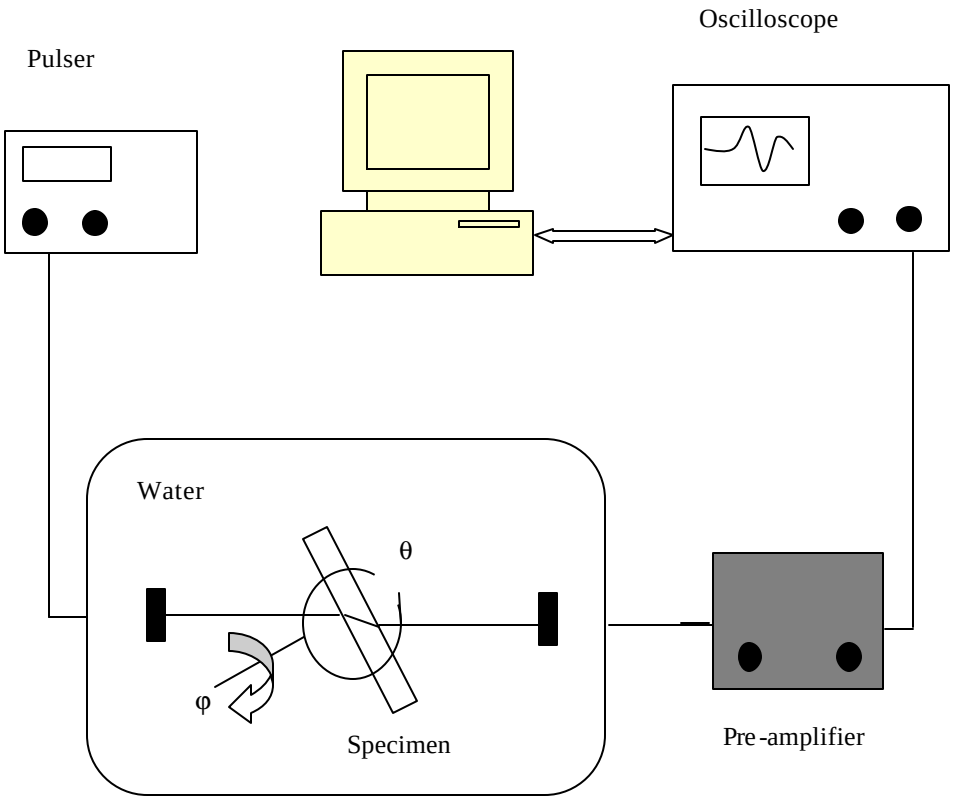

Figure 3. A schematic drawing of the experimental system for measuring elastic constants with immersion method.

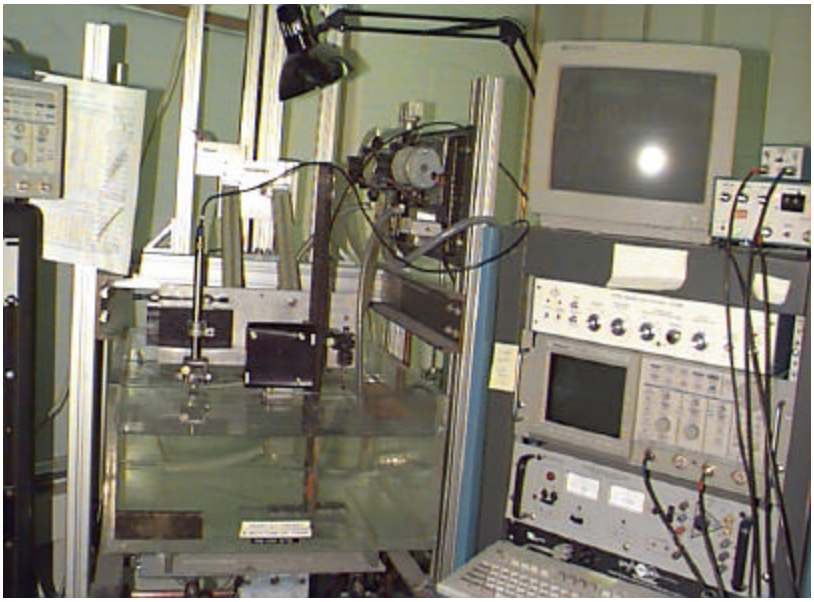

Figure 4. A photograph of the experiment setup.

Figure 5. A photograph of the testing material, single crystal of aluminum oxide.

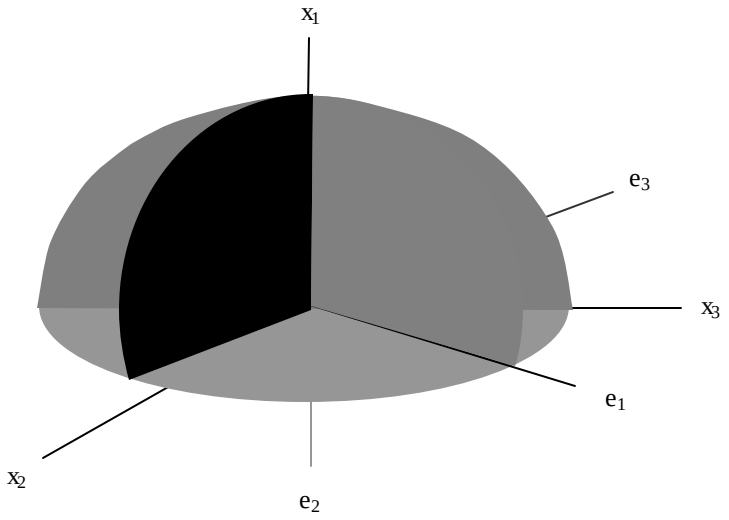

Figure 6. An illustration of normals to the symmetry planes for a single crystal of aluminum oxide in an observation coordinate system R.

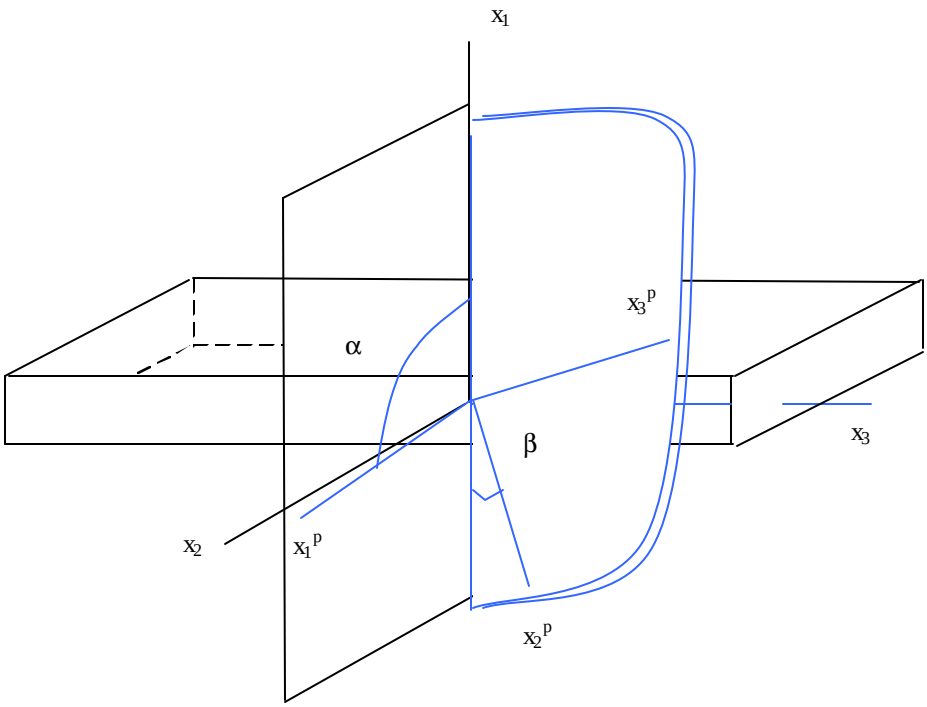

Figure 7. Location of the principal coordinate system R^p (x_1^p, x_2^p, x_3^p) with respect to the observation coordinate system R associated with the Euler angles $\alpha=90.9^0$ and $\beta=14^0$.

2.3 Task 3 – Elevated Temperature Testing.

This portion of the effort includes the work of two M.S. students, Shawn Bunker, M.S. "In-Situ High Temperature Monitoring of Oxidation of Carbon-Carbon" who graduated in summer 2002 and Amala Mamilla M.S., "High Temperature Couplants for the Characterization of Carbon-Carbon Composite Materials", who is expected to complete her work in spring 2004. In addition to the results shown, significant high temperature test infrastructure has been developed at the University of Maine. These resources build on the research capability of the institution and can support future work for the DOD in high temperature materials. Because of the delays in the experimental work, the complete results of Ms. Mamilla's thesis are not included in this report. However, the complete text of both theses is available at http://www.library.umaine.edu/theses/.

The techniques developed in this task show promise for monitoring of processes and as a tool to assist in the development of new materials. However, significant barriers remain so that non-specialists may use these techniques in the course of their research. The signal to noise ratio for the contact ultrasonic technique remains low. This is particularly driven by variation of the coupling between the waveguide and the sample. A number of alternative approaches exist such as laser excitation and narrow band excitation of piezo-electric transducers. In all cases the primary challenge remains the development of improved and more consistent coupling of the ultrasonic wave to the sample when testing at high temperatures. A number of candidate coupling materials have been identified including thin layers of glasses and metal foils. More work remains because of the effect of both temperature and the furnace atmosphere on the couplant. However, as seen in the in-situ testing of reinforced carbon-carbon, unique information about the materials is available using in-situ techniques. Using in-situ techniques it becomes practical to investigate the degradation with time at a range of temperatures for these materials. Engineers of high temperature systems can then design based on residual strength and stiffness properties, the minimizing excess material in non-payload applications. Using these tests it is not only possible to obtain this information for reinforced carbon-carbon, but for any of the other new materials that are being developed for use at high temperature.

2.3.1 In-Situ High Temperature Characterization of Carbon-Carbon Oxidation using Time Reversal Mirrors

M.L. Peterson, A. D. Puckett and S. Bunker, "In-Situ High Temperature Characterization of Carbon-Carbon Oxidation using Time Reversal Mirrors" paper 2023 In Proceedings of The 14'th International Conference on Composite Materials, San Diego California, USA, July 14-18, 2003

2.3.1.1 Abstract

The development of methods for in-situ monitoring of high temperature composites materials during oxidation is important in a number of technological applications. This work is the development of methods that make use of solid cylindrical multi-mode waveguides to monitor the oxidation reaction in carbon-carbon composites.

A time reversal mirror process was used with a solid circular cylindrical waveguide to remove the effects of dispersion. The first three longitudinal modes were considered. An analytic transfer function was developed to predict the time-reversed signal from an input signal. The analytic transfer function was applied to the time-reversed signal to reproduce the original input signal. Experiments were then performed to demonstrate the fidelity of the analytical model.

Results of the comparison were reasonable and showed the potential of the approach for use with a high temperature ultrasonic buffer rod. Results are shown for preliminary coupling studies that will be used to help in characterization of ultrasonic attenuation and the increase in the accuracy of the time reversal mirror. A signal obtained during an oxidation of carbon composites is also shown. Future work will focus on the better integration of the time reversal technique to obtain quantitative information from the experimental apparatus described. Applicability to other material systems and measurements will also be discussed.

2.3.1.2 Motivation

The primary objective of the work described is the development of techniques to measure the in-situ characteristics of composites at temperatures above 1000°C. A number of important civilian and military applications for composites exist in these high temperature regimes. However the cost effectiveness depends on highly optimized design and durability models for the material. Of course the anisotropy must be exploited in order to achieve the desired performances as well in a number of these applications. However, while the room temperature

design process is reasonably well understood and has shown great progress in recent years, the degradation of the matrix and the selective diffusion of oxygen in many of these materials are less well understood. At least a portion of this lack of understating is due to the absence of in-situ sensing techniques that can allow the process dynamics of the degradation to be monitored. Optimization for complex composite structures where load paths may vary requires knowledge of the off-axis elastic and strength properties as well as the changes in these properties during oxidation processes. Applications for these methods would include evaluation of carbon-carbon and other materials for use in oxidizing environments that exist in missile defense applications and developing increased understanding of the durability of these materials for the civilian space program. The technique is not specific to carbon systems, since similar mechanisms may also exist in other emerging materials for high temperature applications. The emphasis is placed on methods that can be used to recover the full constitutive tensor [C] as well as the changes that would occur during oxidation. In-situ methods will allow repeatability studies to be performed to assess sample-to-sample and test-to-test variability without creating an unreasonable test matrix for the material.

2.3.1.3 Background

In a number of applications a need exists for techniques to determine a complete set of elastic anisotropic material properties at high temperatures. A particular application is for high accuracy measurements of the elastic properties as a function of temperature and as a function of the rate of temperature change. However, because of limitations in the size and quantity of specimens available and limitations in the availability of testing equipment, significant obstacles remain. New methods need to be developed where appropriate and the results of the methods should be compared to other documented results.

Elastic waves have the advantage of providing a non-destructive method of evaluating the elastic properties, in particular the modulus and density, of an anisotropic material. The number of propagating modes and the shape of the dispersion curve can be used to simultaneously determine a number of the material properties for an anisotropic material. The proposed method differs from other efforts in this area in the use of a reconstruction algorithm for the characterization of dispersive modes. By making use of the dispersion of the modes along with the changes in the group and phase velocity, as well as the attenuation of the modes, fully

anisotropic, linear visco-elastic characterization of materials is possible in-situ. Shear and Young's modulus measurements are possible in-situ from the evaluation of a single received signal [1]. This approach has been shown in previous studies to yield extensive information on the nature of a disturbance that has propagated through either a dispersive material or through a dispersive geometry [2, 3]. Additional applications in this area have shown the potential for waveguide sensors to provide real-time information in process sensing and materials research applications [4, 5, 6].

The determination of the elastic properties of a material is attractive because of the potential of this method to characterize the degradation of properties of a composite after time at an elevated temperature or the change in material properties as a function of temperature. IN particular damping changes (attenuation of the elastic wave) are quite sensitive to small levels of change in the matrix of the composites. The approach that has been taken is elastic waveguide monitoring. While acousto-optical methods are attractive for some applications, elastic waveguides are useful in some cases because of the insensitivity of the technique to changes in surface reflectivity. However, acousto-optic sensing has shown promise in some applications where this is not an issue. For example, acousto-optics has been successfully applied to the monitoring of the sintering of zinc oxide [7].

Multi-mode waveguides are a low cost and effective method of providing an acceptable signal to noise ratio at high temperatures [6]. Dry coupling of the buffer rods to the sample has been shown to be possible by a slight modification of the standard technique. While the complexity of the received signal is high (the waveguide propagates multiple waveguide modes which are not separated in time) the signal to noise ratio is reasonable. High temperature waveguide buffer rods not only show great promise for overcoming the limitations on cost and complexity, they also have the potential to provide important additional information which would be difficult to acquire using acousto-optical methods. By exploiting the dispersive nature of higher order waveguide modes, and using multiple waveguide modes, it is also possible to separate out the geometrical changes from the changes in material properties. Using the waveguide modes could also produce an image of the cross sectional density gradient of the sample. Reconstruction of an in-situ cross-sectional image of the material would make it possible to track the effects of the diffusion controlling parameters versus time at temperature. Heat flux controlled degradation of a composite would be an example of such a process. For

simple elastic property measurements below the material degradation temperature, elastic properties can be measured at a range of temperatures without risk of damage to the specimen.

By generating more data during each test run, the effect of sample dependent conditions can also be significantly reduced, further reducing the number of measurements required. This real-time data could either be used to determine times at which the samples need to be removed for strength testing or to determine if the bulk properties of the sample have been affected by holding the sample at a high temperatures for shorter time periods.

Related work considers applications for waveguides for the monitoring of die casting [8] as well as the previously mentioned work in reaction bonding of silicon nitride [6]. The other work suggests that the sensor developed in this work may applicable to the monitoring of related problems in ceramic processing as well as in the monitoring of physical and chemical vapor deposition processes. Cross-sectional density gradient monitoring is of particular importance in applications such as the production of carbon-carbon composites as well as in filling of high aspect ratio vias in chemical vapor deposition processes in the electronics industry.

2.3.1.4 Experimental Apparatus

The basic apparatus used in this work consists of a tube furnace with long multi-mode cylindrical waveguides that isolate the piezo-electric transducers for the high temperature environment in the furnace. The entire apparatus is controlled so that a cooling system protects the transducers and the environment can be modified to move the sample from an inert to an oxidizing environment. The furnace employed for this work is a conventional tube type furnace (Lindberg Model 55346, Watertown WI) with heating elements capable of producing sample temperatures of approximately 1100°C. The furnace used is a 3-zone furnace, however for the experiments performed the outer zones were not observed to differ significantly from the central zone regardless of settings. The furnace is evacuated using a medium vacuum pump (Marvac Scientific, Model #R-10, Concord CA) that is attached to the sealed furnace tube. The apparatus is also supplied with an inert gas atmosphere (argon) from bottled source. Nitrogen is used to purge the furnace prior to performing the tests in an oxidizing environment. The system was purged with the vacuum pump and then back filled with nitrogen. This process was repeated several times in each experiment to eliminate oxygen from the furnace environment. Argon is then used during the heating of the sample. Finally, once the sample is at equilibrium at

temperature medical air is flowed through the furnace to provide a controlled oxidizing environment. All experiments are performed at a slight pressure about atmospheric. The pressurized furnace maintains the atmosphere even in the presence of leaks. A gas flow meter is used on the output of the pressure tank to monitor leakage from the system. Simultaneous measurement of the furnace temperature profile on the buffer rods is also possible for up to eight channels using a switchable thermocouple system.

The ultrasonic system used is a conventional pulser with standard low temperature transducers. The initial waveguide experiments were carried out using a spike pulser (Panametrics Model 5072PR, Waltham MA). For the higher amplitude required for monitoring samples in the furnace a square wave pulser is used (Ritec SSP-801, Warwick, RI). The receiving transducer uses a separate pre-amp (Panametrics 5660C) to improve the signal isolation due to low signal to noise ratio in the received signal. The transducers used are broadband nominal 1 MHz. central frequency units (Panametrics V103, Waltham MA) that are coupled to the end of the waveguides using High Vacuum Grease (Dow-Corning, Midland MI). Standard room temperature transducers are used since most "high temperature" transducers are significantly past their Curie temperatures at the temperatures of interest in these experiments. High temperature transducers are also significantly less efficient than the room temperature counterparts. In this application large signal amplitudes are required because of the attenuation that occurs in the sample, in the coupling between the buffer rods and the sample, and in the coupling between the buffer rods and the transducer. The cooling system associated with the waveguides is then sized to maintain the transducers at the lower temperature.

Thus the key to the apparatus is the design of the end-caps used in the system. The end cap configuration is shown in an exploded view in Figure 1. The ultrasonic transducer is designed to maintain continuous contact with the end of the waveguide. The waveguide and the transducers are withdrawn when measurements are not being made on the specimen in the furnace. Small, one-inch diameter air cylinders, that are operated using the inert gas, are used to retract and extend the waveguides. A series of water-cooling coils are wrapped around a double set of ball bearings. These ball bearings are the only contact between the furnace frame and the waveguides. This design allows the waveguides to be retracted as well as being cooled by the water jacket. The entire system is air tight, with the only penetrations of the furnace end caps

used for the ultrasonic cable and the thermocouples and other wiring. A spring-loaded fixture that holds the transducer provides constant pressure between the transducer and the waveguide.

Unlike the intermittent contact between the buffer rods and the sample, the buffer rods and transducers can be in continuous contact. In order to restrict movement of the transducers, they are clamped along with the buffer rods in a cylindrical housing. Set screws are used to secure the transducer and buffer rod into place. The quartz buffer rods however prove to be a bit more difficult due to the brittle nature of the quartz. Minimal pressure applied to the setscrews along with the use of a Nylon tip will decrease the chance of damaging the buffer rods.

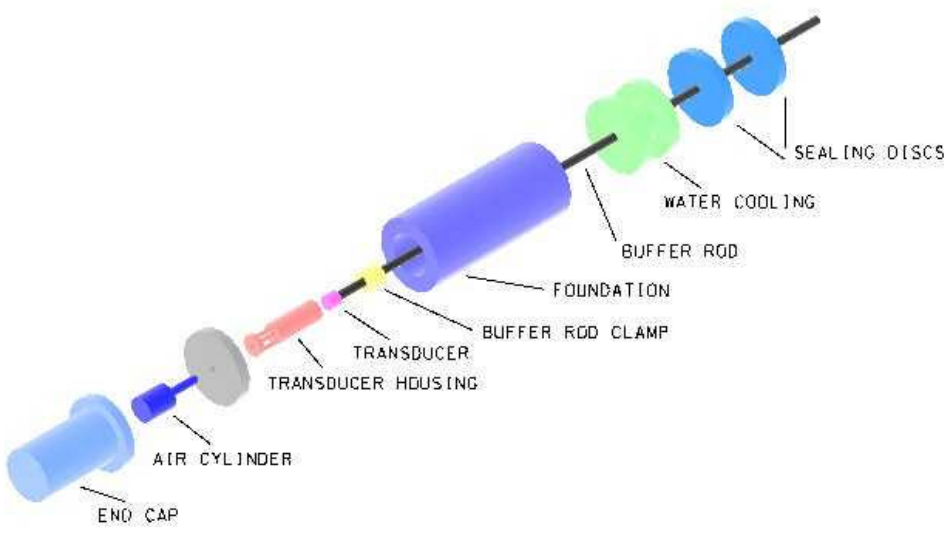

FIGURE 1. An exploded view shows the end cap and frame for housing the transducer, air cylinder, and buffer rod. The cooling system is also shown.

2.3.1.5 Experimental Furnace Results

Intermittent contact between the sample and the buffer rods is used for several reasons. First, the buffer rod inhibits the flow of the atmosphere around the sample during the testing. When the buffer rod is withdrawn the influence on the atmosphere is reduced and any cooling associated with the contact of the buffer rod with the face of the sample is eliminated. Withdrawing the buffer rod also reduces contamination of the end of the buffer rod by material from the sample. Even heating of the end of the buffer rod is also ensured. At the higher temperatures used in this testing the fused quartz buffer rods approach their softening point, which significantly changes the properties of the material. The softening may increase the

coupling between the buffer rod and the sample. Finally, the buffer rod is withdrawn so that the ultrasonic signal from the free of the buffer rod may be acquired. This signal is used in the deconvolution of the signal. The effects of changes in the rest of the system make it necessary to obtain a number of signals in order to extract the material response of the sample (Peterson, 1994).

The configuration of the carbon samples and the alumina support tooling is shown in Figure 2. This configuration allows gas flow around the sample and withdrawal of the buffer rods during times at which measurements are not being taken. The buffer rods are shown in both a contact and a withdrawn configuration. An example of a signal that has been propagated through a carbon sample at 1000°C is shown in Figure 4. The signal to noise ratio in the signal is quite good and shows the effects of the complex signal which results from propagation through waveguides that propagate multiple modes.

2.3.1.6 Time Reversal Mirrors

As is evident from figure 3, the significant complexity of the signal makes measurements of arrival time quite difficult. While this is true for the through transmission configuration, it is even more true for the reflected signal that is used in the deconvolution [6]. Thus, a method is desirable that would allow a simpler signal to be used in the processing of the data.

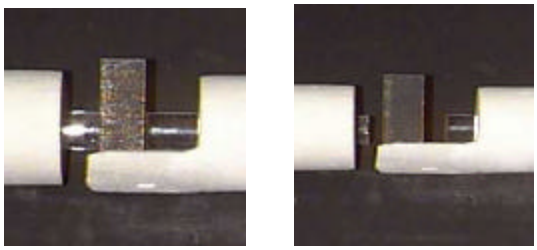

FIGURE 2. Photographs show the intermittent contact between C/C sample and Quartz buffer rods.

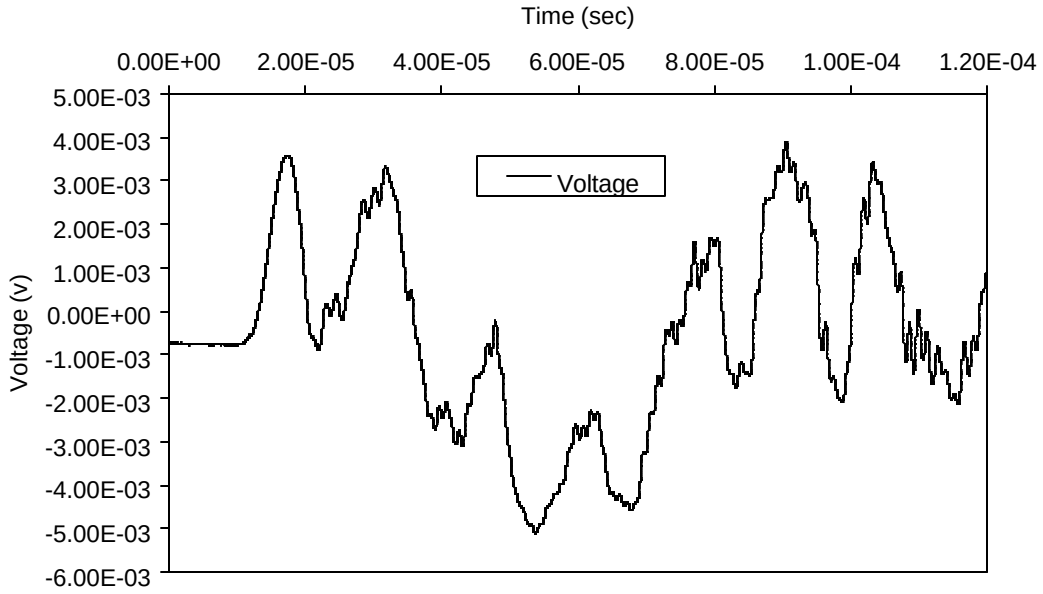

FIGURE 3. Received signal after propagating through the Quartz buffer rods at 1000^{o}C.

In a thick waveguide the acoustic signal propagates along multiple paths that superpose to create propagating modes in the waveguide. The propagation of multiple modes causes a signal that is compact in the time domain to have a large time signature after propagating through the waveguide, Figure 4 shows both the input and the transmitted signal for the a solid waveguide used similar to that use in the furnace application. As a result, information obtained from changes is harder to extract. A number of approaches have been considered to solve this problem, however the complexity of accommodating the multi-mode signal is high [1]. A time reversal mirror (TRM) has been shown to eliminate this problem in a through transmission configuration in a cylindrical waveguide by removing the complexity of the signal [9].

The use of a TRM in a pulse-echo configuration with a solid cylindrical waveguide is shown as an example. This corresponds to one of the six signals used in the deconvolution for the data from the furnace. Signals were recorded both with and without a sample on the end of the waveguide. The TRM was able to produce a signal with a compact time signature in both cases. Information about the aluminum sample was obtained in a comparison between the two signals.

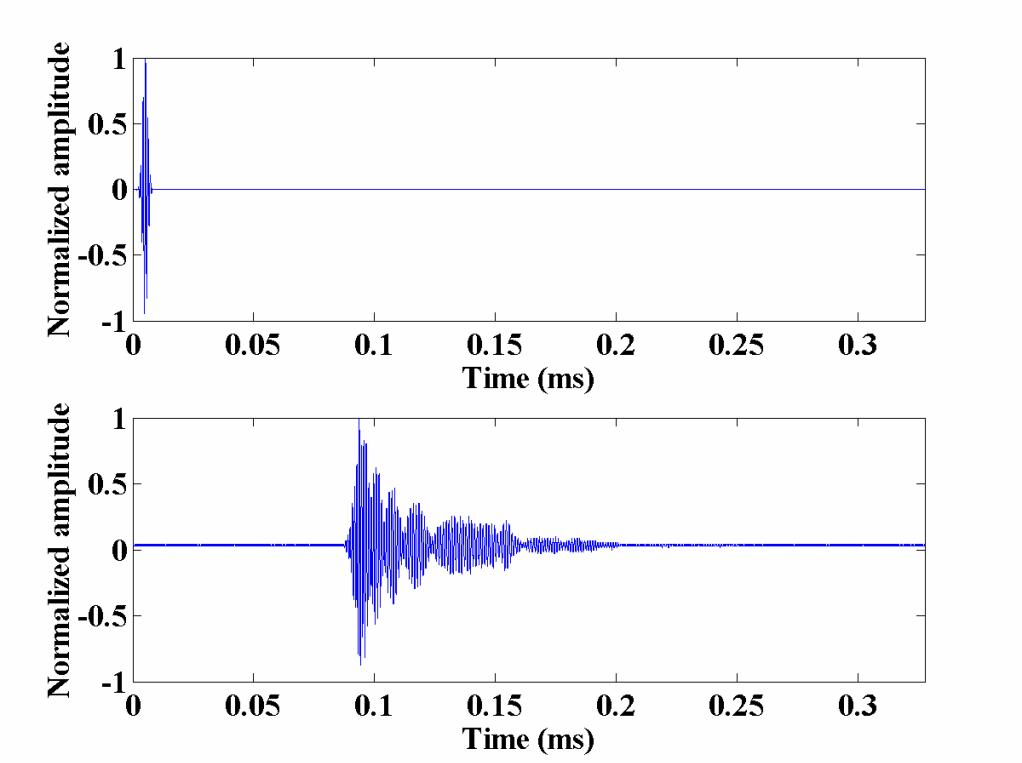

Figure 4. Illustration of dispersion in the cylindrical waveguide showing the loss of compact support.

2.3.1.7 Time Reversal Mirrors

A time-reversal mirror experiment consists of three steps. In the case of a cylindrical rod, first, an acoustic signal is excited by a source at one end of the rod. The acoustic signal propagates through the rod, and the altered signal is recorded at the opposite end. Second, the recorded signal is reversed in time. Finally, the receiver is excited with the reversed signal. The reversed signal propagates through the rod, and a new signal is recorded at the source. If time invariance is satisfied this new signal is the same as the original acoustic signal except reversed in time. The ability of the TRM to determine the input signal needed to produce a desired output signal can produce a compact time signal from a dispersive system.

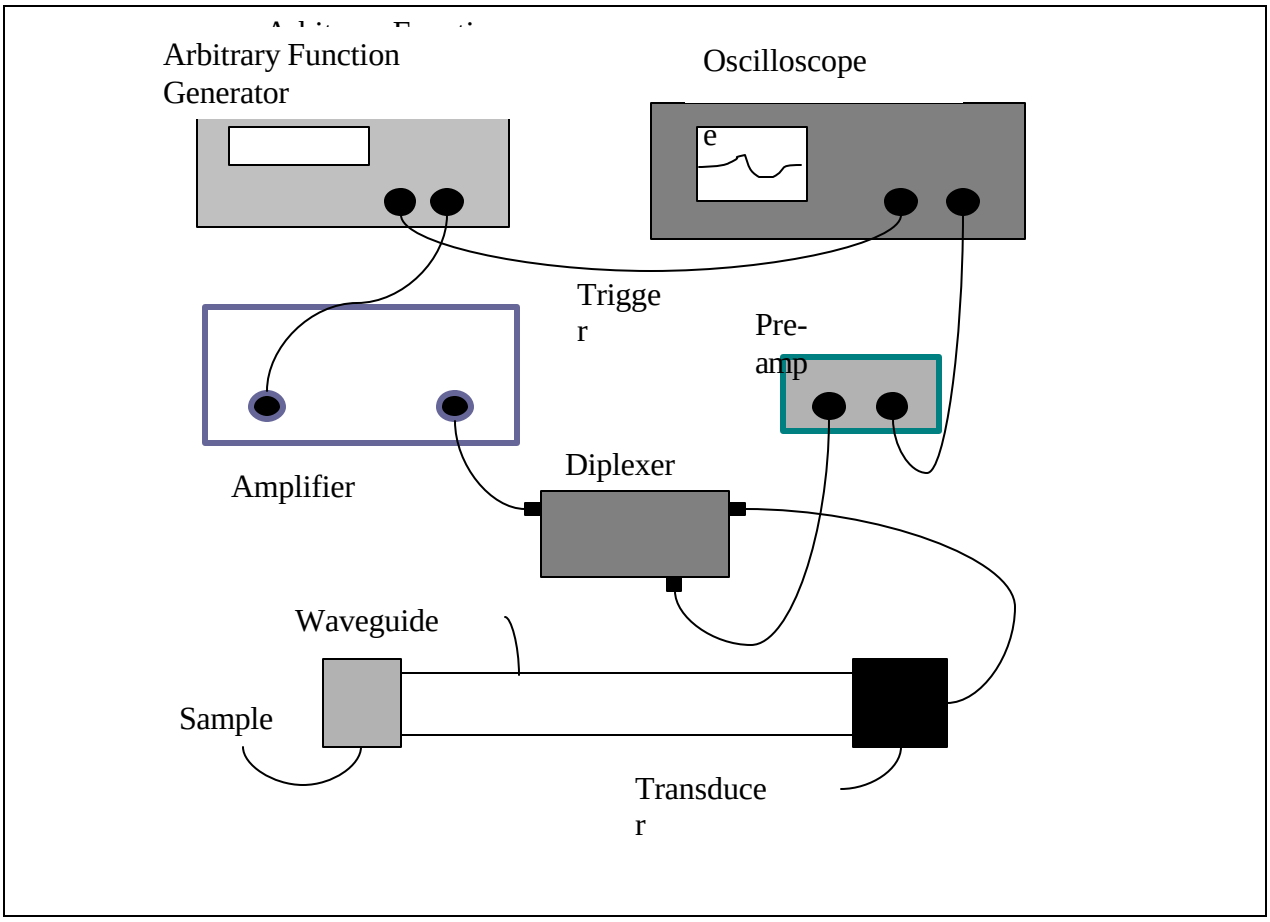

Figure 5. Diagram of the experimental setup for time reversal mirror.

The pulse echo configuration used for the experiments is shown in Figure 5. The waveguide consisted of a fused quartz cylindrical rod, 228 mm in length. Fused quartz has a Young's modulus, E, of 73 GPa, a density, ?, of 2200 kg/m^3, and a Poisson's ratio, ?, of 0.14. The data shown is for a waveguide that is larger than that which is used in the furnace, however the technique is applicable to the smaller diameter waveguide as well.

The pulse-echo configuration uses a single transducer that acts as the source and the receiver. The transducer used in the experiment was a 38 mm diameter, 1 MHz broadband longitudinal contact transducer [Panametrics, model V194, Waltham, MA]. A coupling fluid was used between the transducer and the waveguide and between the waveguide and the sample [Sonotech, Inc. UT-30, State College, PA]. A pulser [Panametrics, 5072PR, Waltham, MA] was used to generate a pulse to the transducer. The dispersed signal was recorded and reversed in time. An arbitrary waveform generator [Agilent 33250A, Palo Alto, CA] produced the time-reversed signal to drive the transducer. A radio frequency power amplifier [ENI A-300,

Rochester, NY] with a gain of 55 dB was used to amplify the signal to the transducer. The received signal was recorded by a digital storage oscilloscope [Tektronix TDS 520A, Wilsonville, OR] after amplification of the signal by an ultrasonic pre-amplifier [Panametrics, model 5660, Waltham, MA] with a gain of 40 dB. In order to use the transducer in pulse-echo mode with the arbitrary waveform generator a transformer diplexer [Ritec Inc., model RDX2, Warwick, RI] was placed between the transducer, the ultrasonic pre-amp, and the power amplifier.

The TRM proved to be effective in the pulse echo configuration. The time-reversed signal was used to excite the transducer, and the echoed signal received by the transducer was a pulse, top graph in Figure 3. The most important characteristic of this experimental signal is the compact time signature. By using the time-reversed signal as the excitation signal, the dispersive properties of the waveguide can be negated. This capability allows the use of a dispersive solid circular waveguide as a low cost sensor. The compact time domain signal greatly simplifies signal analysis that was previously used [6].

To explore the ability of this technique as a sensor a 25.4 mm aluminum cube was placed at the free end of the waveguide. The same time-reversed signal was used to excite the transducer. The received signal includes both front and back wall reflections from the aluminum cube, bottom graph Figure 3. The first peak corresponding to the reflection at the end of the waveguide was attenuated compared to the peak from the reflection from the free end of the waveguide. The attenuation results from transmission into the finite impedance material. Also a second peak was generated from the reflection of the back wall of the sample. The time delay between the two peaks correlates to the bulk wave speed in aluminum and the thickness of the cube.

From these experiments the technique is promising as a means to detect changes in impedance or wave speed in an actual application. For a practical application with a single waveguide, the signal that will cancel the dispersive effects of the waveguide is easily determined from the TRM experiment. For more complex configurations where significant changes with time are expected either modeling or more extensive experiments are required [10]. Future work remains to be done to show that measurements can be made in-situ and to develop appropriate models.

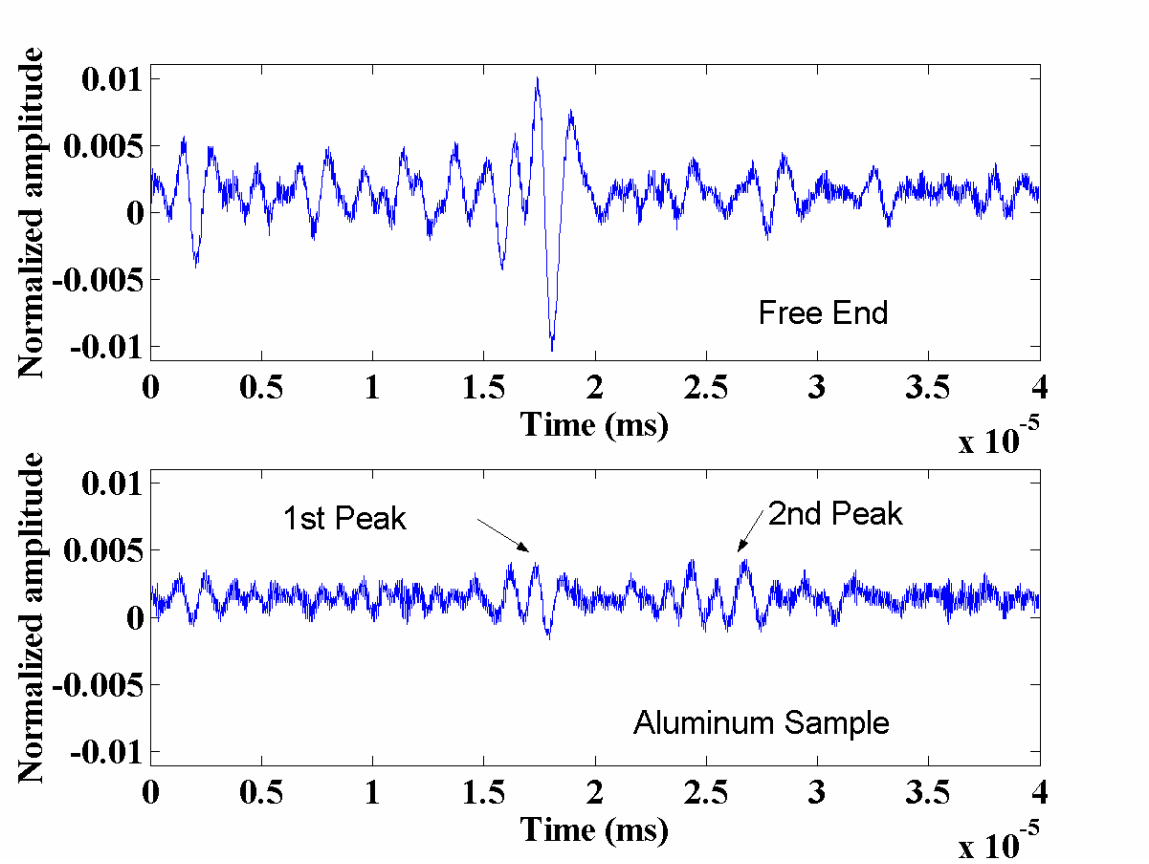

Figure 6. Comparison of received signals.

2.3.1.8 Conclusions

Results have been shown for the use of the thick solid cylindrical waveguides for the in-situ monitoring of the oxidation of carbon composites. The results demonstrate that this type of technique is useful for these measurements and that measurements of the samples are possible at temperatures up to about 1000ºC. However, the results also have shown that the signals that are acquired form the approach are quite complex. I the past extensive signal processing has been used to analyze the data. An alternative approach is shown that uses time reversal mirrors to produce simpler signals from the ultrasonic waveguides. This approach has the potential to produce a signal that is comparable to a simple experimental apparatus in a large and complex system such as the one shown. Future work will make use of multiple time reversal mirrors to

produce a set of six signals that are both simple to process and are usable for an in-situ tests system such as the one shown.

2.3.1.9 Acknowledgement

This research is sponsored by the Ballistic Missile Defense Organization through the Office of Naval research (ONR), Science Officer Dr. Y. D. S. Rajapakse.

2.3.1.10 REFERENCES

1 Peterson, M.L. "Prediction of longitudinal disturbances in a multi-mode cylindrical waveguide," Experimental Mechanics. 39, 1999, p. 36-42.

2 M. L. Peterson, S. Srinath and J. Murphy, "A Waveguide Based Acoustic Microscope", *Ultrasonics* Vol. 36, 1998, p. 855-863.

3 Peterson, M. L., "A Method for Increased Accuracy of the Measurement of Phase Velocity", *Ultrasonics* Vol. 35, No 1, p. 17-29, 1997.

4 Jen, C.K., de Heering, Ph., Sutcliffe, P., and Bussiere, J.F., 1991, "Ultrasonic monitoring of the molten zone of single-crystal germanium," Mater. Eval. 49, 1991, 701-705.

5 Jen, C.K., Z. Wang, A. Nicolle, J.F. Bussiere, E.L. Adler and K. Abe. Acoustic Waveguideing rods with Graded Velocity Profiles. Ultrasonics 30, No. 2, 1992, p 91-94.

6 Peterson, M.L. "A signal processing technique for measurement of multi-mode waveguide signals: an application to monitoring of reaction bonding in silicon nitride," Res. Nondestr. Eval. 5, 1994, p 239-256.

7 Telschow, K.L., J.B. Walter, G.V. Garcia, D.C.Kunerth, "Process monitoring using Optical Ultrasonic Wave Detection. *Review of Progress in Quantitative NDE*. New York: Plenum Press, 1989.

8 Jen, C.-K., Cao, B., Nguyen, K.T., Loong, C.A., and Legoux, J.-G. "On-line ultrasonic monitoring of a die-casting process using buffer rods," Ultrasonics. 35, 1997, p. 335-344.

9 Puckett, A.D. and Peterson, M.L. "Fidelity of an Analytical Time Reversal Mirror," to appear in *Review of Progress of Quantitative Nondestructive Evaluation*, (American Institute of Physics, New York), Vol. 21. (2002).

10 Jen, C.-K., Franca, D.R., Sun, Z., and Ihara, I. "Clad polymer buffer rods for polymer process monitoring," Ultrasonics. 39, 2001, p. 81-89.

2.3.2 Evaluation of Dynamic Properties of Composites in an Oxidizing Environment

M.L. Peterson, Shaun Bunker and Anthony Puckett, "Evaluation of Dynamic Properties of Composites in an Oxidizing Environment" Review of Progress of Quantitative Nondestructive Evaluation, Vol. 21, American Institute of Physics , Melville NY, 2002, p. 1038-1045.

Abstract. The development of methods for in-situ monitoring of high temperature composites materials during oxidation is important in a number of technological applications. This work is the development of methods that make use of solid cylindrical multi-mode waveguides to monitor the oxidation reaction in carbon-carbon composites. Results are shown for preliminary coupling studies that will be used to help in characterization of ultrasonic attenuation. A signal obtained during an oxidation of carbon composites is also shown. Future work will focus on the signal processing required to obtain quantitative information from the experimental apparatus described.

2.3.2.1 INTRODUCTION

Advancement of technologies such as those proposed for a number of new missile and satellite technology programs are pushing the thermal requirements of materials to new levels. Technological advancements proposed, as a part of these programs will require components to operate on high-maneuvering targets in a severe aero-thermal environment. Carbon-carbon composites are an ideal choice for these components. Carbon-carbon (C/C) composites are composite materials that consist of carbon fibers embedded in a carbonaceous matrix. Developed for aerospace applications, carbon-carbon composites exhibit low density, high thermal conductivity and excellent mechanical properties at elevated temperatures. The ability to provide good mechanical properties at temperatures in excess of 2000°C makes it an ideal material for rocket nozzles and re-entry nose tips. Due to their superior high-temperature properties, these materials have been used in the nose and leading edges of the NASA space shuttle along with a number of military applications. Commercial applications of this technology exist in areas such as aircraft brake systems. However, carbon readily reacts with oxygen at temperatures greater than 500°C. This reaction results in a rapid material loss (primarily matrix) and loss of the mechanical properties of the material. Consequently, C/C composites are often

coated with oxidation resistant coatings. Additionally, the material used is sufficiently thick to allow for the loss of material and strength as oxidation occurs at elevated temperatures.

Significant research effort has been directed at the oxidation resistant coatings. The coatings in use not only protect the material, but also have a limited capability to regenerate. The coatings are easily damaged due to their low ductility and fracture toughness. In many applications, however, the thickness of the material must be optimized in order to provide sufficient residual strength as oxidation occurs due to the loss of the coatings. In weight critical applications, design for finite life requires a thorough knowledge of the residual strength of the material. The system design must focus on the optimal use of the material in light of the expected life of the coating. Even given the demands of new applications, the opportunity may exist to use existing materials at very high temperatures if the residual mechanical properties can be accurately predicted. As the material oxidizes both the strength and the modulus of the material will change. With careful design, current-coating technologies may be sufficient even for use in some oxidizing environments. To allow system designers to make use of the remaining strength of these materials when used in an oxidizing environment, new in-situ monitoring methods are required. These new monitoring methods will also help materials researchers to better understand the mechanisms of oxidation and coating failure in these materials.

2.3.2.1.1 Objective of Work

The objective of this work is to develop methods that can be used in-situ to characterize the oxidation resistance of materials and to determine the residual strength of carbon-carbon materials when subjected to oxidation. The real time monitoring of oxidation will support both the basic materials research in the area, as well as potentially providing technologies for process monitoring of manufacturing processes. The approach that has been selected for this work, is the use of solid cylindrical waveguides that will be intermittently in contact with the sample. Conventional ultrasonic transducers will be used in the system. A primary focus of the larger effort will be on the modeling and characterization of the waveguides to facilitate signal interpretation.

2.3.2.1.2 Related Research

Researchers have considered the ultrasonic monitoring of materials using waveguides at high temperatures since at least the late 1940's. One of the earliest published accounts of an application of buffer rod techniques for measurement of elastic properties at elevated temperature is by J.R. Frederick [1]. Frederick used a discontinuity at the end of a buffer rod to measure the change in velocity over a short portion of the bar that was heated up to ~1000°C. Lynnworth [2] contains a summary of the various applications of buffer rods as high temperature sensors and for measurement of elastic moduli in a book. Various efforts to overcome the loss of energy due to sidewall echoes (mode conversion) are discussed and the problem is described as an important limitation on application of buffer rods to high temperature monitoring. In particular Lynnworth states that when "the buffer rod conveys longitudinal waves, sidewall reflections cause mode conversion to shear, resulting in energy lost from the initial pulse and generation of many spurious delayed echoes that become extremely troublesome in pulse-echo measurements." Some of the methods of limiting the mode conversion reviewed by Lynnworth are tapering, threading or grooving of the buffer rod or use of a non-circular cross section buffer rod to separate the trailing echoes in time. While reviewing a number of alternative methods of reducing the effects of mode conversion, Lynnworth continues his examination of high temperature methods with a discussion of alternatives to buffer rod methods. Methods such as EMAT and laser transduction avoid the problems encountered with buffer rods while introducing difficulties of their own. While the applications of buffer rods as process sensors has been limited by difficulties with the buffer rods, for more exact laboratory studies ultrasonic measurements are a standard method for measuring the high temperature elastic modulus of materials.

2.3.2.2 Single Crystal High Frequency Elastic Properties

Since the use of ultrasonic methods has become a standard method of measuring the elastic properties of materials at elevated temperatures, papers that describe these measurements for particular materials are numerous. Representative of these measurements is a paper by Fisher and Renken [3] in which single crystal elastic moduli are measured for three elements: titanium, zirconium and hafnium. These measurements are made at temperatures from -269 to 827°C. using an 18 mm diameter fused quartz buffer rod and radio frequency pulses of 35 to 50 MHz. for the ultrasonic measurements. Coupling between the buffer rod and the specimen was

achieved using high temperature cement. The velocity measurements are made by measuring the time between reflections that are resolved in time and show no apparent dispersion. As is typical when measurements of this type are performed two factors exist which make the measurement possible. The use of large diameter buffer rods allows the wave which travels with the velocity of longitudinal waves in an unbounded solid to be used, and allows the use of semi-permanent couplants between the buffer rods and the sample. A particularly effective couplant is necessary since shear as well as longitudinal wave measurements are required, usually in several crystal orientations, to get the full set of elastic constants for the single crystal material. In addition, the test specimen must be carefully prepared with smooth parallel faces. While this method is well suited to fundamental investigations into the behavior of materials at high temperature, they are impractical for most engineering applications. In particular the careful sample preparation makes the measurement unsuitable for process monitoring. Examples of work that makes use of similar techniques are papers by Leese and Lord [4] and Devers [5] which consider the behavior of single crystal iron at temperatures up to 900°C. The interest in single crystal behavior and the associated solid state physics problems has produced a significant quantity of information in this area. Investigators who are interested in the high temperature properties of engineering materials have required a somewhat different approach since lower frequencies must be used on polycrystalline materials because of attenuation due to grain scattering.

2.3.2.3 Low Frequency Investigations of Polycrystalline Materials

The measurement of high temperature elastic moduli of polycrystalline materials is quite similar to the measurement for a single crystal. This measurement is simpler in the absence of significant texture since it requires only two elastic moduli to describe the material. One method of making this measurement is to machine a stepped buffer rod of the material under investigation. Frederick [1] used this technique. Another approach by Papadakis et al. [6] & Papadakis [7] employs momentary contact between the buffer rod and the sample. The work by Papadakis also includes attenuation measurements. The attenuation measurements require that multiple resolvable echoes in the sample material be detectable after passing through a pressure dry coupling layer. As with the measurements in single crystals, the work by Papadakis relied on large diameter buffer rods. The buffer rod diameter is sufficient for the side wall echoes (other waveguide modes) to be resolved in time. Other work which is very similar but uses high purity

polycrystalline nickel was performed by Takahashi and Yamamoto [8] and is used for comparison to reference experiments in the present work. Takahashi and Yamamoto also make use of a second waveguide mode to obtain shear modulus measurements. The shear modulus is determined by accurately measuring the delay to the second signal arrival in the waveguide. Hughes et al. [9] to investigate a number of materials at room temperature used this method in an earlier paper. A summary of a large quantity of both single crystal and polycrystalline high temperature properties, many of which were acquired using ultrasonic methods, is contained in a book by Zinov'yev [10]. Two factors have made it possible for these measurements to become standard techniques. First is acceptability of large diameter buffer rods (or high frequency ultrasonic signals) with an acoustic impedance similar to the sample. Second is the existence of both low attenuation in the sample and efficient coupling between the buffer rod and the sample. Low attenuation allows back wall reflections to be of sufficient amplitude for use in measurements. Other opportunities exist for application of this sort of a waveguide as an acoustic sensor. The other applications require more flexibility in choice of waveguide diameter and the removal of the requirement that excellent coupling exist between the sample and buffer rod.

Recent introduction and popularization of time reversal mirrors presents a new approach to the use of waveguides in this buffer rod application. However, it is first necessary to show the applicability of buffer rod measurements to the monitoring of oxidation in carbon-carbon composites. This paper present preliminary results for a new system that allows intermittent contact between the buffer rod and the sample. The system also includes a controlled atmosphere to allow the oxidation of the specimen to be performed slowly and in a controlled manner so that the monitoring can be used to evaluate the residual properties of the material.

2.3.2.4 Alternative Methods to Measure Elastic Properties

In addition to buffer rod methods, a number of both new and old techniques exist for measuring the elastic properties of a solid in a high temperature environment. While static testing in mechanical fixtures is possible for larger specimens, significant cost and complexity is involved in developing even the basic elastic properties of an anisotropic sample. The other older dynamic method that is used are varieties of vibration testing. These methods range from the standard dynamic mechanical analysis (DMA) used in commercial instruments for

characterizing polymers to the more general resonance spectroscopy measurements. DMA has a broad range of applicability beyond the traditional applications such as the determination of the glass transition temperature in polymers. Using modern three or four point bend fixtures it is possible to obtain visco-elastic properties for small (less than 50 mm long) beams cut from composite materials. Resonance spectroscopy is a more general method than DMA since it is directly focussed on allowing the user to obtain the elastic properties in a general anisotropic material. Resonance spectroscopy makes use of a known geometry and excites resonance modes through the material thickness for a specific frequency range [11,12]. This approach differs from the method used in this work since it employs continuous wave excitation. The resonant peaks in a frequency sweep are then used to determine the velocity of the wave in the material. Like the system in this work, resonant spectroscopy uses transducers that are placed outside of the furnace. Older systems that are also referred to as resonance spectroscopy are more similar however to what is now considered to be a part of commercial DMA equipment that has used an increasing range of fixturing.

Another alternative to the buffer rod methods is laser generation and detection of ultrasound. This approach is very promising for high temperature applications. However, laser ultrasound, like the buffer rods, requires that more a fundamental understanding of the measurements at elevated temperature be developed. The buffer rod method is used in the current research effort, but future work is proposed that will make use of laser generation and buffer rod detection of the ultrasound. Laser detection of ultrasound on a black surface with significant particulate matter in the atmosphere as well as convective air currents promises to present significant technical challenges.

2.3.2.5 Experimental Apparatus

The furnace employed for this work is a conventional tube type furnace (Lindberg Model 55346, Watertown WI) with heating elements capable of producing sample temperatures of approximately 1100°C. The furnace used is a 3-zone furnace, however for the experiments performed the outer zones were not observed to differ significantly from the central zone regardless of settings. The furnace is evacuated using a medium vacuum pump (Marvac Scientific, Model #R-10, Concord CA) that is attached to the sealed furnace tube. The apparatus is also supplied with an inert gas atmosphere from bottled source. In the experiments shown on

coupling a nitrogen atmosphere was used, however argon would be used in oxidation studies. For the experiments, the system was purged with the vacuum pump and then back filled with nitrogen. This process was repeated several times in each experiment to eliminate oxygen from the furnace environment. Experiments are performed at a slight pressure about atmospheric. The pressurized furnace maintains the atmosphere even in the presence of leaks. A gas flow meter is used on the output of the pressure tank to monitor leakage from the system. Simultaneous measurement of the furnace temperature profile on the buffer rods is also possible for up to eight channels using a switchable thermocouple system.

The ultrasonic system used is a conventional pulser with standard low temperature transducers. The initial waveguide experiments were carried out using a spike pulser (Panametrics Model 5072PR, Waltham MA). For the higher amplitude required for monitoring samples in the furnace a square wave pulser is used (Ritec SSP-801, Warwick, RI). The receiving transducer uses a separate pre-amp (Panametrics 5660C) to improve the signal isolation due to low signal to noise ratio in the received signal. The transducers used are broadband nominal 1 MHz. central frequency units (Panametrics V103, Waltham MA) which are coupled to the end of the waveguides using High Vacuum Grease (Dow-Corning, Midland MI). Standard room temperature transducers are used since most “high temperature” transducers are significantly past their Curie temperatures at the temperatures of interest in these experiments. High temperature transducers are also significantly less efficient than the room temperature counterparts. In this application large signal amplitudes are required because of the attenuation that occurs in the sample, in the coupling between the buffer rods and the sample, and in the coupling between the buffer rods and the transducer. The cooling system associated with the waveguides is then sized to maintain the transducers at the lower temperature.

Thus the key to the apparatus is the design of the end-caps used in the system. The end cap configuration is shown in an exploded view in Figure 1. The ultrasonic transducer is designed to maintain continuous contact with the end of the waveguide. The waveguide and the transducers are withdrawn when measurements are not being made on the specimen in the furnace. Small, one inch diameter air cylinders, that are operated using the inert gas, are used to retract and extend the waveguides. A series of water cooling coils are wrapped around a double set of ball bearings. These ball bearings are the only contact between the furnace frame and the waveguides. This design allows the waveguides to be retracted as well as being cooled by the

water jacket. The entire system is air tight, with the only penetrations of the furnace end caps used for the ultrasonic cable and the thermocouples and other wiring. A spring-loaded fixture that holds the transducer provides constant pressure between the transducer and the waveguide.

Unlike the intermittent contact between the buffer rods and the sample, the buffer rods and transducers can be in continuous contact. In order to restrict movement of the transducers, they are clamped along with the buffer rods in a cylindrical housing. Set screws are used to secure the transducer and buffer rod into place. The quartz buffer rods however prove to be a bit more difficult due to the brittle nature of the quartz. Minimal pressure applied to the setscrews along with the use of a Nylon tip will decrease the chance of damaging the buffer rods.

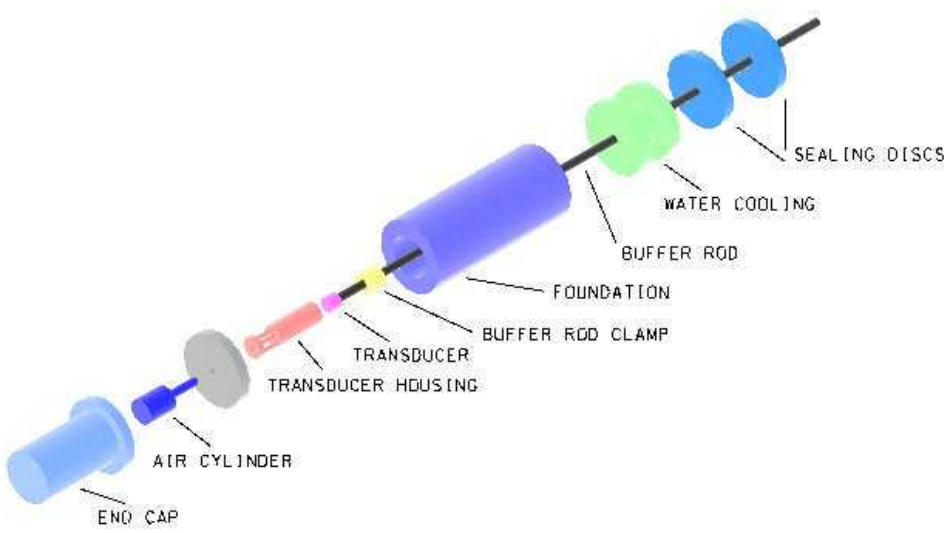

FIGURE 1. Exploded view of end cap and frame for housing the transducer, air cylinder, and buffer rod. The cooling system is also shown.

2.3.2.6 Experimental results

2.3.2.6.1 Coupling Studies

Intermittent contact between the sample and the buffer rods is used for several reasons. First, the buffer rod inhibits the flow of the atmosphere around the sample during the testing. When the buffer rod is withdrawn the influence on the atmosphere is reduced and any cooling associated with the contact of the buffer rod with the face of the sample is eliminated. Withdrawing the buffer rod also reduces contamination of the end of the buffer rod by material

from the sample. Even heating of the end of the buffer rod is also ensured. At the higher temperatures used in this testing the fused quartz buffer rods approach their softening point, which significantly changes the properties of the material. The softening may increase the coupling between the buffer rod and the sample. Finally, the buffer rod is withdrawn so that the ultrasonic signal from the free of the buffer rod may be acquired. This signal is used in the deconvolution of the signal. The effects of changes in the rest of the system make it necessary to obtain a number of signals in order to extract the material response of the sample [13].

The use of intermittent contact does however require that the transmission coefficient between the buffer rod and the specimen be well characterized. The first effort in the development of this system is the characterizing of the transmission coefficient and the development of a curve that can be used to determine the required ultrasonic excitation energy in order to obtain a usable received signal. Figure 2 shows the variation of time delay with temperature for fused quartz buffer rods in direct contact. The time delay and the amplitude were determined using a cross-correlation method with a semi-analytical model of the waveguides for the reference signal [14]. Vacuum grease was used as a couplant between the quartz rod. As the temperature increased, the couplant baked off decreasing the transmission coefficient and increasing the range of the time delay. At the highest temperature the softening of the quartz increased the transmission coefficient.

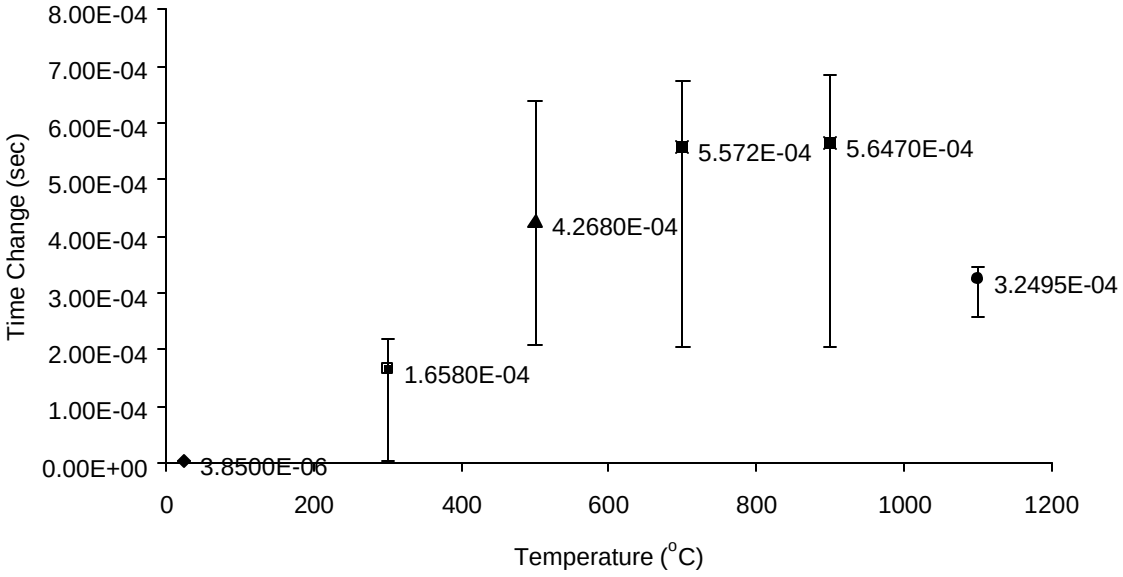

FIGURE 2. Change of time delay with temperature for fused quartz buffer rods in direct contact. Time delay calculated from reference signal. Error bars indicate range of time delay for four measurements.

The configuration of the carbon samples and the alumina support tooling is shown in Figures 3a & 3b. This configuration allows gas flow around the sample and withdrawal of the buffer rods during times at which measurements are not being taken. The buffer rods are shown in both a contact and a withdrawn configuration. An example of a signal that has been propagated through a carbon sample at 1000°C is shown in Figure 4. The signal to noise ratio in the signal is quite good and shows the effects of the complex signal which results from propagation through waveguides that propagate multiple modes.

2.3.2.7 Results and Conclusions

A new system has been built that uses ultrasonic testing to monitor the change in attenuation and velocity during oxidation of a carbon-carbon material.

- The system facilitates the nondestructive testing of samples at temperature in-situ.
- The ultrasonic velocity of the system has been demonstrated to be measurable from a coupling study.
- The system produced an acceptable signal to noise ratio in this configuration even for a highly oxidized carbon composite sample.

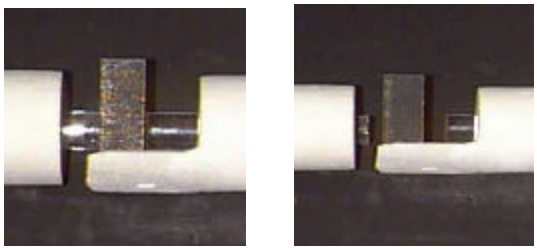

FIGURE 3a &3 b. Photographs show the intermittent contact between C/C sample and Quartz buffer rods.

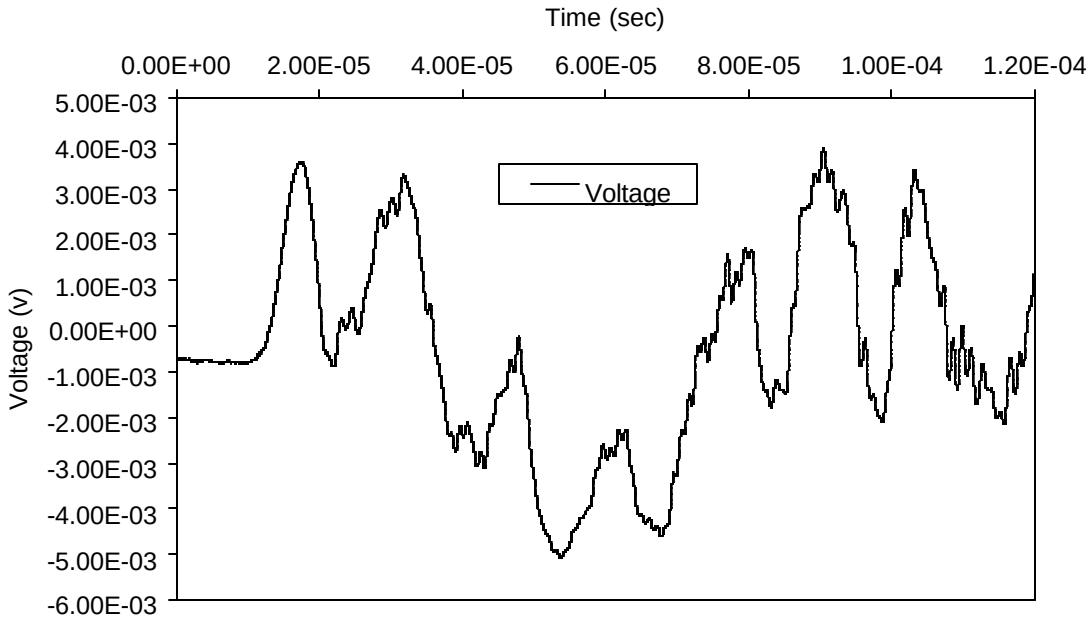

FIGURE 4. Received signal after propagating through the Quartz buffer rods (with NO sample) at 1000^{o}C.

2.3.2.8 references

Frederick, J.R., *Journal of the Acoustical Society of America*, **20**, 586 (1948)

Lynnworth, L.C., *Ultrasonic Measurements for Process Control*, Academic Press, Boston MA, 1989

Fisher, E.S. and Renken, C.J., *Physical Review*, **135**, no. 2A, A482-A494 (1964)

Lesse, John and Lord, A.E. Jr., *Journal of Applied Physics*, **vol. 39**, 3986-3988, (1968)

Devers, D.J., *Journal of Applied Physics*, **43**, 3293-3301, (1972)

Papadakis, Emmanuel P., Lynnworth, L.C., Fowler, Kenneth A. and Carnevale, E.H., *Journal of Acoustic Society of America*, **52**, 850-857, (1972)

Papadakis, Emmanuel P., *Journal of Acoustic Society of America*, **44**, 724-734, (1968)

Takahashi, Sennosuke and Yamamoto, Eiji, *Journal of the Japan Institute of Metals*, **37**, 373-375, (1973)

Hughes, D.S., Pondrom, W.L. and Mims, R.L., *Physical Review*, **75**, no. 10, 1552-1556 (1949)

Zinov'yev, V.E., *Metals at High Temperatures*, trans. Itkin, V.P., Hemisphere Publis hing Co., New York, 1990

Demarest, H. H., *Journal of Acoustic Society of America*, **49**, 768, (1971)

Ohno, I., *Journal of Physical Earth*, **24**, 355, (1976)

Peterson, M. L., *Research in Nondestructive Evaluation*, **5**, 239-256, (1994)

Puckett, A. D. and Peterson, M. L., to appear *in Review of Progress of Quantitative Nondestructive Evaluation*, "Fidelity of an Analytical Time Reversal Mirror", Vol. 26 American Institute of Physics, (2002)